Stress and Deformation of Biological Membranes during Cellular Outgrowth and Cell and Liposome Injection: A Numerical and Experimental Study

A Thesis

Submitted to the Faculty

of

Drexel University

by

Kathleen Bridget Allen

in partial fulfillment of the

requirements for the degree

of

Doctor of Philosophy

August 2008

Dedication

This work is dedicated to my parents,
Jerry and Kathleen Allen.

Mom and Dad, thank you so much for your love, confidence, and encouragement throughout my scholastic endeavors. Dad, thank you for teaching me the value of hard work and for always offering to help out in any way you could, and Mom, thank you for always being there to cheer me on during the pursuit of my goals.

Acknowledgements

First and foremost, I would like to thank my advisor, Dr. Bradley Layton, for instilling in me the excitement and satisfaction that accompanies the world of research. Dr. Layton's willingness to help his students, diligent work ethic, and positive attitude has made him an excellent role model. As a mentor, he has allowed me to be creative in my approach to problem solving, but he has always been available to provide guidance and a fresh perspective whenever I needed help. His mentorship has allowed me to grow as both a student and a researcher. Additionally, I'd like to thank Dr. Layton for his dedication in establishing a collaboration with the National Nanotechnology Laboratories in Lecce, Italy. It was this collaboration that provided me with the opportunity to perform research abroad, an experience that was extremely rewarding from both a professional and personal standpoint.

I would also like to thank Dean Selçuk Güçeri. Dean Güçeri first introduced me to Biomechanical Research at Drexel University while I was still an undergraduate, and ever since, he has been instrumental in all that I have accomplished here at Drexel. The strong support that I received from Dean Güçeri has opened doors for me in terms of funding, research opportunities, and future career endeavors. I can not thank Dean Güçeri enough for all that he has done. Furthermore, Dean Güçeri's philosophy on Engineering education and his dedication to the students in the College of Engineering has been an inspiration.

Furthermore, I'd like to acknowledge Dr. Mun Choi, former Mechanical Engineering Department Head at Drexel University, as well as the entire faculty in the Mechanical Engineering and Mechanics Department. Dr. Choi's loyalty and dedication to the

students, and the friendly, helpful environment that he created in the Mechanical Engineering Department has made my time at Drexel most fulfilling.

I would also like to acknowledge my committee members, Dr. Abrams, Dr. Baas, Dr. Capaldi, Dr. Lau, and Dr. Tan. I thank Dr. Abrams for his insightful comments and careful eye proofreading this document, Dr. Baas for offering a different perspective to my research work, a perspective that I may not have considered without his guidance, Dr. Capaldi for providing me with a broad range of ideas to consider in order to improve the quality of my work, Dr. Tan for his help with Finite Element Analysis and for offering ideas and solutions to the analytical and modeling problems that I've encountered along the way, and finally, Dr. Lau for always taking the time to ask how things were going and for his genuine interest in my development as a student and a professional during both my undergraduate and graduate years at Drexel.

Additionally, I'd like to thank my labmates: Mert Sasoglu for his willingness to help, Andrew Bohl for helping me to come up with creative solutions to the experimental road bumps, and Ben Legum for manufacturing the nanopipettes that I've used in my experiments. I'd also like to thank Kivilcim Buyukhatipoglu for her help with endothelial cell culture and Keith Sevcik for his help machining the micromanipulator adapter and for all his technical support along the way. I'd also like to acknowledge Keith for being a dedicated study partner, and Keith and Kivilcim for being loyal lunch and coffee break companions.

I'd like to acknowledge the other labs in which I have worked during my time at Drexel. In particular I'd like to thank Dr. Aladin Boriek from Baylor College of Medicine in Houston, Texas. Dr. Boriek first introduced me to Biomechanical Research,

and it was my experience in his lab that first got me excited about a research career. I would also like to thank Dario Pisignano from the National Nanotechnology Laboratories in Lecce, Italy for allowing me the opportunity to work in his lab. I also thank Dr. Bahram Nabet from Drexel University for first recommending me to Dr. Pisignano. Finally, I'd like to thank Dr. Gianluca Gallo from the Neurobiology and Anatomy Department at Drexel University College of Medicine for allowing me the use of his lab for neuronal cell culture, and I thank Lee Silver from this lab for teaching me these procedures.

I would also like to acknowledge Dr. Yury Gogotsi, Dr. Tony Lowman, Dr. Wei Sun, Dr. Alisa Morss, and Dr. Eli Fromm for taking an interest in my future career endeavors and for their advice and guidance along the way. Additionally, I'd like to thank my professors at Drexel whose classes I thoroughly enjoyed and therefore have helped shape my academic path, Dr. T.S. Venkataraman, Dr. Donald McEachron, and Dr. Cecile Goodrich.

For administrative support I'd like to thank Kathie Donahue, and for help with outreach and various other activities I'd like to thank Joanne Ferroni, Colleen Rzucidlo, Amy Campbell, Katie Gibson, Christine Haas, Elizabeth Brachelli, Ashley Myers, and Lydia Kokolskyj.

Most importantly, thanks to my family and friends for their unconditional love and support. Thanks to my parents for their guidance and encouragement, and thanks to my brother, Greg Allen, for his comic relief and for all his "big brother" insight and advice along the way. I'd especially like to thank Brian Rodowicz for allowing me the freedom

and encouragement to pursue my goals but all along providing me with the assurance and confidence that I won't have to tackle them alone.

I'd also like to acknowledge the National Science Foundation Graduate Research Fellowship Program for funding my graduate school education as well as the William M. Keck Foundation for supporting my research endeavors.

Table of Contents

List of Tables

List of Figures

Abstract

Stress and Deformation of Biological Membranes during Cellular Outgrowth and Cell and Liposome Injection: A Numerical and Experimental Study
Kathleen B. Allen
Bradley E. Layton, Ph.D.

Revealing the molecular events of neuronal growth is critical to obtaining a deeper understanding of nervous system development, neural injury response, and neural tissue engineering. Central to this is the need to understand the mechanical interactions between the cytoskeleton and the cell membrane, and how these interactions affect the overall growth mechanics of neurons. Using finite element analysis, the normal contact stress produced by a protein filament that is acting against a deformable membrane was modeled, and the deformation, stress, and strain were computed for the membrane. The model predicts that a single actin filament is able to produce a normal contact stress on the cell membrane that is sufficient to cause membrane deformation, but not rupture.

During single-cell and single-organelle injection, damage to the cell will often result. By first determining the mechanical properties of the cell, and then quantifying the amount of force that is required for cell membrane puncture, the use of excessive force during injection can be avoided. This will serve to minimize the damage done to the cell during these procedures. Using micropipette-deformation-based methods and an image-processing based algorithm for measuring deformation, the mechanical properties of spherical DOPC:DOPS liposomes, model cells, were measured. From these values, the forces that injection pipettes of various sizes exert onto liposomes during manipulation were determined. Forces ranged from ~1 - 6 pN, and these forces increased as the pipette size decreased.

Chapter I: Introduction

Motivation

This thesis has two main objectives: The first is to quantify the stresses and strains in the membranes of peripheral nerve cells as the cytoskeleton of the cell pushes against the membrane during cell growth and development. The "safety factor" imposed by nature that allows for the cell membrane to be deformed by its cytoskeleton without the cytoskeleton causing damage to the cell was explored. The second goal is to quantify the forces and deformations that are required to puncture aspirated cells with micro and nanopipettes during the injection of these cells with pharmaceuticals, macromolecules, and genetic information. During single-cell and single-organelle injection, damage to the cell will often result. By first determining the mechanical properties of the cell, and then quantifying the amount of force that is required for cell membrane puncture, the use of excessive force during injection can be avoided. This will serve to minimize the damage done to the cell during these procedures.

Overview of the Peripheral Nervous System

At the organism scale, the peripheral nervous system is comprised of axons that may extend for meters, with diameters six orders of magnitude smaller. Maintenance of these high-aspect-ratio structures depends on their mechanical integrity and a reliable transport mechanism (Dennerll, Joshi et al. 1988; Ingber 1993; Baas 2000; Tuszynski, Luchko et al. 2005). Axons grow to reach their target tissues during embryogenesis and continue to grow into adulthood to maintain connections between the cell body and the target tissues (Lertmanorat and Durand 2004).

At the cellular scale, axonal growth and maintenance also depend on attachments and interactions with other cells and elements of the extracellular matrix (Zheng, Buxbaum et al. 1994). In this way, nerves are similar to any other mechanical structure, subjected to mechanical stresses and forces such as tension, compression, bending and torsion.

At the sub-cellular scale, axons require internal dynamic protein struts called the cytoskeleton. The cytoskeleton includes microtubules, actin filaments and intermediate filaments, and working together, these protein struts permit the axons to grow, and subsequently to maintain their shape once growth is complete. However, rather than existing in a static state as an artificial macroscopic structure might, these living structures are genetically "programmed" for self-assembly via mobile protein subunits, and these protein struts generate mechanical forces between and among one another (Hotani and Miyamoto 1990). The dynamic equilibrium of forces on the cytoskeletal elements integrate the cytoskeleton into a structure with mechanical integrity and stability as well as mechanical and metabolic plasticity to respond to biological cues such as stretch or injury. The cell's mechanical properties (e.g. stiffness, resting tension, etc.) also result from the interactions of these structural proteins (Ingber 2003).

Microtubules and actin filaments are the main internal structural supports for the axon. Microtubules polymerize and depolymerize in the growth cone region, and thereby "explore" growth cones by extruding into the growth cone region during polymerization, and backing out during depolymerization (Dent and Gertler 2003). Similarly, actin filaments polymerize and depolymerize in the growth cone region of the neuron, and it is the interactions between the actin filaments and the neuronal membrane that are responsible for mechanically moving the growth cone forward during development

(Andersen and Bi 2000). The prediction of cell morphology and how cells respond to the forces of microtubules and actin filaments acting against their membranes has only recently been explored (Fygenson, Elbaum et al. 1997; Hotani, Inaba et al. 2003; Atilgan, Wirtz et al. 2006).

Overview of Bio-Nanotechnology and Cellular Injection

Recent advancements in nanotechnology have lead to developments in the diagnosis and treatment of diseases. Nanoparticles are currently being used to target biomarkers of different diseases, e.g. cancer and atherosclerosis, distinguish between healthy and cancerous cells in the liver, increase the effectiveness of various pharmaceuticals, such as chemotherapy drugs, and increase the efficiency of targeted drug delivery when incorporated into liposomes (Caruthers, Wickline et al. 2007).

Additionally, nanosurgeries, or surgeries performed on single-cells and single-organelles, are becoming increasingly popular as a means of gaining a better understanding of biology at the cellular level. Nanosurgeries are used for targeted drug delivery, e.g. the delivery of pharmaceuticals to individual cells or organelles (Han, Nakamura et al. 2005), gene therapy, e.g. the dissection of single chromosomes (Obataya, Nakamura et al. 2005; Leary, Liu et al. 2006), and cell tracking, e.g. the monitoring of a cell to gain a better understanding of single-cell behavior (Lee, Stainier et al. 1994). Additionally, by altering or enhancing the performance of single-cells or single-organelles, unhealthy cells, or even stem cells, can be programmed to perform specific functions (Ebbesen and Jensen 2006).

Nanosurgeries often entail the successful delivery of drugs, genetic information, and other macromolecules into individual cells or organelles. However, the cell and its

organelles (nucleus, mitochondria, lysosomes, etc.) are surrounded by highly selective membranes, and one of the challenges during nanosurgeries is to ensure that the intended material is able to penetrate these membranes and arrive at its target. There are numerous ways to introduce various substances into the cell. Intracellular delivery techniques include biological methods, e.g. viral vectors (Walther and Stein 2000) and the gene gun (Lin, Pulkkinen et al. 2000), chemical methods, e.g. lipid fusion (Laffafian and Hallett 1998) and cell penetrating peptides (Trehin and Merkle 2004), and physical methods, e.g. electropermeabilization (Rols 2006), ultrasound (Sundaram, Mellein et al. 2003), optoinjection (Clark, Hanania et al. 2006), and penetration of the membrane by use of a capillary (Ansorge 1982; Pepperkok, Schneider et al. 1991; Davis, Yannariello-Brown et al. 2000; Miller, Holtzman et al. 2002; Viigipuu and Kallio 2004; Matsuoka, Shimoda et al. 2007). Biological and chemical methods need to be specialized for each cell type, unlike physical methods, which can be utilized for a wide range of cell types. Physical methods are therefore more versatile, making them generally more favorable (Sundaram, Mellein et al. 2003).

Of all of the physical methods for cellular injection, the glass micropipette has been shown to be the most effective on the basis of cell survival, successful delivery of molecules, and range of applications (Wang, Liu et al. 2007). Examples of injection by a micropipette include injection of a single LA7 cell to determine if an individual cell can initiate tumor growth (Zucchi, Sanzone et al. 2007), injection of an individual neuron to determine specific protein expression and morphology (Kao and Sterling 2003), injection of a mutant protein into a single cell to observe its response (Storrie 2005), and

intracytoplasmic sperm injection (ICSI) into an oocyte to treat infertility (Varghese, Goldberg et al. 2007).

Although the glass micropipette is commonly used, there are several setbacks to this technology. During ICSI, the cytoplasm of an oocyte is aspirated into the pipette until the membrane is broken. This is "proof" that the membrane has been penetrated. However, it has been suggested that damage to the oocyte can occur during the aspiration process, decreasing fertilization rates (Dumoulin, Coonen et al. 2001). Additionally, when a micropipette is inserted into a cell, physical damage can result to the membrane, cytoplasm, and/or the organelles of the cell, and the extent of the damage increases as the size of the cell decreases (Laffafian and Hallett 1998; Han, Nakamura et al. 2005; Freedman, Mattia et al. 2007). In a study done by Wang et al. (2007) using zebrafish embryos (diameters ~ 1200 μm), the survival rate of the cells was ~98% (Wang, Liu et al. 2007). In a different study by Davis et al. (2000), hematopoietic stem cells (diameters ~ 6 μm) were injected by a micropipette, and their survival rates ranged from 50% to 95% (Davis, Yannariello-Brown et al. 2000). The larger percentage of cell volume and membrane surface area that is affected during the injection of the smaller cells may be the cause for their lower survival rates. Another reason for the lower survival rate may be that the force required to penetrate the membranes of the smaller cells is less than that for the larger cells. If an excessive amount of force is used to penetrate the cell membrane during injection, unnecessary and potentially fatal damage to the cell may result.

There are several ways to alleviate the mechanical damage done to the cell during the injection process. One way is to decrease the size of the injection device, which can be done by using smaller pipettes, or by using carbon nanotubes (CNT) to create carbon

nanopipettes (CNP) (Han, Nakamura et al. 2005; Chen, Kis et al. 2007; Freedman, Mattia et al. 2007; Schrlau 2007). CNP are favorable as injection devices because they are small and flexible, yet still strong enough to puncture cell membranes (Schrlau 2007). However, although the use of CNP for injection purposes is less intrusive to the cell, it cannot be assumed that the damage caused by these pipettes is negligible.

An understanding of cellular mechanics is essential in order to quantify the amount of force and deformation cells experience during injection. If the forces and deformations required for membrane penetration are known, the pipette can be inserted into the membrane far enough so that it goes through the membrane of the cell, but not further into the contents of the cell where it may cause additional damage. Additionally, injection devices can be designed so that the forces required to perform specific cellular manipulations are not exceeded during these procedures. Avoiding the use of excessive force during manipulation will increase the success rates of nanosurgeries.

Organization of the Thesis

Chapter II reports the deformations, stresses, and strains in neuronal membranes as cytoskeletal proteins exert forces against these membranes, as in the case of neuronal development. This chapter also determines the rupture forces of these membranes.

Chapter III reports the determination of the area expansion modulus and Young's modulus of DOPC:DOPS liposomes using a micropipette-aspiration technique.

Chapter IV expands upon the work of Chapter III and uses liposome bending energy calculations to determine the forces exerted onto aspirated liposomes during the probing of these liposomes with micro and nanopipettes.

Chapter V reports the injection capabilities of both the micro and nanopipettes, as well as the ability of aspirated liposomes and cells to be punctured by these injection devices. A relationship between injection speed, pipette size, and the injectability and deformation of the liposomes and cells is determined.

Chapter VI reports the development of a computer model to predict the forces and deformations that are required to puncture aspirated liposomes. The parameters of this model can be adjusted to predict the forces necessary to puncture a multitude of different cell types using a variety of injection devices.

Chapter II: Cytoskeleton-Membrane Interactions in Neuronal Growth Cones: A Finite Analysis Study

Abstract

Revealing the molecular events of neuronal growth is critical to obtaining a deeper understanding of nervous system development, neural injury response, and neural tissue engineering. Central to this is the need to understand the mechanical interactions between the cytoskeleton and the cell membrane, and how these interactions affect the overall growth mechanics of neurons. Using finite element analysis, the normal contact stress produced by an actin filament or a microtubule that is acting against a deformable membrane was modeled, and the deformation, stress, and strain were computed for the membrane. Parameters to represent the flexural rigidities of the well-studied actin and tubulin cytoskeletal proteins as well as the mechanical properties of cell membranes were used in the simulations. The model predicts that a single actin filament is able to produce a normal contact stress on the cell membrane that is sufficient to cause membrane deformation, but not growth. The model also predicts that under clamped boundary conditions, a filament with a buckling strength equal to or smaller than an actin filament would not cause the areal strain in the membrane to exceed 3%, and therefore the filament is incapable of causing membrane rupture or puncture to a safety factor of ~15-25. Decreasing the radius of the membrane upon which the normal contact stress is acting allows an increase in the amount of normal contact stress that the membrane can withstand before rupture. The model predicts that a 50 nm radius membrane can withstand ~4 MPa of normal contact stress before membrane rupture whereas a 250 nm radius membrane can withstand ~2.5 MPa. Understanding how the mechanical

properties of cytoskeletal elements have coevolved with their respective cell membranes may yield insights into the events that gave rise to the sequences and superquaternary structures of the major cytoskeletal proteins. Additionally, numerical modeling of membranes can be used to analyze the forces and stresses generated by nanoscale biological probes during cellular injection.

Introduction

In the peripheral nervous system, axons can grow to be a meter in length, with diameters of only one to ten micrometers. Peripheral neurons, and some neurons within the central nervous system, such as those of the optic tract, with their enormous aspect ratios, actively push forth into growing, developing, or healing tissue. Maintenance of these million-to-one aspect ratio structures requires internal dynamic protein struts. The primary proteins include microtubules, comprised of polymerized tubulin, microfilaments, comprised of polymerized actin, and intermediate filaments, comprised of polymerized neurofilament light (NFL), neurofilament middle (NFM), and neurofilament heavy (NFH) subunits. These cytoskeletal proteins are the most abundant proteins in neurons (Yu, Son et al. 2006), with actin comprising up to 15% of the total protein in the cell (Pollard and Earnshaw 2002). The polymerization and interactions of these proteins drives cell growth and maintains the morphology of adult cells (Dennerll, Joshi et al. 1988; Ingber 1993; Baas 2000; Tuszynski, Luchko et al. 2005).

Microtubules are typically regarded as the primary compressive structural elements. Additionally, they act as force sensors, detecting the magnitude and direction of the force causing them to compress (Karafyllidis and Lagoudas 2007). Actin networks, which are typically regarded as supporting tensile forces in cells, also sustain compressive loads in

the growth cone region of the axon where an actin cortex is maintained (Dennerll, Joshi et al. 1988; Dent and Kalil 2001). These two internal compression-sustaining structures are responsible for maintaining neuronal membrane tension (Sheetz and Dai 1996). Previous work that has focused on determining the flexural rigidity of these isolated cytoskeletal proteins includes observation of thermal fluctuations (Gittes, Mickey et al. 1993), hydrodynamic flow (Kurz and Williams 1995), optical tweezers (Dupuis, Guilford et al. 1997), and microneedle manipulation (Kojima, Ishijima et al. 1994).

Living cells have been described as having a tensegrity architecture, with their cytoskeletal elements forming a lattice support structure that flattens when the cell is adhered to a surface and rounds to a spherical shape when the cell is unattached (Ingber 1993). If cells were true tensegrity structures, the protein filaments within the cell would always seek a minimal energy confirmation, with all of the protein filaments sustaining equal strain energy-densities. Microtubules in the growth cones of neurons and in fibroblast cells have been observed to buckle, bend, or break at the leading edge of the cell, indicating that stress is not always evenly distributed throughout the cytoskeleton (Odde, Ma et al. 1999; Schaefer, Kabir et al. 2002; Gordon-Weeks 2004). A dynamic balance of forces must therefore exist between the cytoskeleton and the neuronal membrane that allows the cytoskeleton to not only support the stress of the membrane, but also to push the membrane forward during development, and then sustain this shape after growth is complete. An understanding of this balance is important for determining how nerves will respond to injury, e.g. the re-growth of peripheral nerve cells through scar tissue, to the application of various pharmaceuticals, and to forces and stresses endured during tissue engineering applications.

Recently, Atilgan, Wirtz, and Sun (2006) used an energy-based membrane-cytoskeleton interaction model to predict that the polymerization energy of a single actin filament is insufficient to initiate the formation of a filopodium (Atilgan, Wirtz et al. 2006). Rather, two to three are required. Their model predicts that at an intracellular concentration of 500 μM, the amount of free energy reduction caused by actin polymerization of a single actin filament is sufficient to overcome the concomitant rise in free energy caused by the resulting elastic membrane deformation. Using models employing uniform stress distributions throughout the cytoskeleton, finite element methods have been used to determine the strain on the nucleus of an endothelial cell caused by cytoskeletal deformation during cell rounding (Jean, Chen et al. 2005). Other work on force generation through actin polymerization studied the elastic Brownian ratchet model (Mogilner and Oster 2003). In this model, the elastic forces of growing actin filaments push the cell forward. While these models are valuable in predicting the coalescence of nearby actin filaments into filament bundles, explaining filopodia growth rates through a thermal ratchet model, and understanding the mechanism in which bacteria migrate, they do not consider the stress state within the membrane as it is deformed under natural or artificial growth conditions, or under similar externally induced cell probing conditions.

This chapter thus has a two-fold goal. The first is to introduce the concept that there exists a “natural mechanical safety factor” built into the mechanical relationship between the cell membrane and the cytoskeleton, such that the growth rate and forces of the cytoskeletal elements do not rupture the cell. The second is to quantify the stress and strain state of the membrane as it undergoes contact and penetration by nanopipettes e.g.

(Freedman, Mattia et al. 2007; Schrlau 2007). By using boundary conditions that represent either a naturally or artificially constrained membrane, the stress state within a patch of membrane when it is acted upon by a single actin filament or microtubule is investigated.

The results are thus also two-fold: one scientific and one technological. The scientific point of interest is in investigating the limits imposed by nature upon the relative mechanical strengths of the cytoskeleton versus the cell membrane. For example, if the cell membrane were to have evolved as a structure that was incapable of flexibility, this would not allow for cell motility. Flexibility implies a thin structure, which typically implies a weak structure. However, if the cell membrane were too weak to sustain either environmental or growth and movement loads, this would compromise the cell's integrity, leading to a reduced fitness. Using similar reasoning, a cytoskeletal element such as actin or tubulin that was too weak to maintain cell shape would result in an unviable cell as it would be incapable of growth or movement at a rate sufficient to compete with sister cells or other cells occupying a similar ecological niche. If on the other hand the cytoskeletal actin or tubulin formed structures that were so strong as to rupture a cell membrane, this would also lead to an unfit species.

The results obtained through computer simulations can be used to not only better understand the force balance necessary for cell growth, motility, and mechanotransduction, but also to determine the forces and stresses required to puncture a biological membrane. This has potential for single cell injection and *in vitro* fertilization applications.

Methods

Model Parameters

In the present model it is assumed that the membrane is homogeneous, ignoring the effects of inhomogeneities caused by membrane proteins. It is also assumed that under quasi-static loading conditions, the membrane may be modeled as a transversely isotropic material, with the membrane normal serving as the axis of symmetry. A transversely isotropic material requires that five elastic constants be specified. Since the cell membrane has been observed to behave as a two-dimensional fluid with the two layers of the membrane flowing smoothly past each other and with individual phospholipid molecules diffusing freely and exchanging locations (Dai and Sheetz 1995; Fygenson, Elbaum et al. 1997), both the in-plane and out-of-plane Poisson's ratios have been chosen to be 0.49. Indeed Charras et al. (2004), previously assumed a Poisson's ratio of 0.49 for the cell membrane (Charras, Williams et al. 2004). This ratio was based on a paper by Hamill and Martinac (2001) in which the cell membrane is assumed to be incompressible (Hamill and Martinac 2001). To our knowledge, this is yet to be experimentally verified or theoretically predicted. The in-plane Young's moduli, $Y_{r\theta}$, was set equal to 128 MPa. This was computed by dividing the area expansion modulus of a lecithin:cholesterol (SOPC:CHOL) lipid vesicle, which is representative of a neuronal growth cone, by the thickness of the membrane, ~4.5 nm (Kas, Strey et al. 1993; Dent, Callaway et al. 1999; Dong, Arai et al. 2004). The area expansion modulus of the membrane is related to the bending modulus, κ_B, used by Atilgan et al. (2006) through,

$$\kappa_B = \frac{K_A t^2}{24}, \tag{1}$$

where K_A is the area expansion modulus of the membrane and t is the thickness of the membrane (Evans and Rawicz 1990; Boal 2002). The bending modulus is then related to the Young's modulus through,

$$\kappa_B = \frac{Yt^3}{24}. \tag{2}$$

The bending modulus calculated for the SOPC:CHOL membrane is 4.9×10^{-19} Nm (1), greater than the bending modulus used by Atilgan, 8.6×10^{-20} Nm. The greater bending modulus of the SOPC:CHOL membrane is likely caused by its cholesterol content (Evans and Rawicz 1990). Note that Atilgan et al. (2006) did not use an explicit membrane thickness, thus discrepancies may also lie in the third-order relationship between thickness and bending modulus. Circular patches of membrane with radii of 50 nm and 250 nm, a range over which a single actin filament or microtubule is expected to act, were modeled (Lewis and Bridgman 1992; Atilgan, Wirtz et al. 2006).

For an isotropic material with a Poisson's ratio of 0.5, the shear modulus is equal to $Y/3$, and therefore 43 MPa. This value was chosen for the through-plane shear moduli, G_{rz} and $G_{\theta z}$. However, because the layers of the membrane flow freely over one another, the in-plane shear modulus, $G_{r\theta}$, must be lower. This was taken to be 1.28 MPa, two orders of magnitude smaller than the out-of-plane shear modulus.

In addition to the membrane properties, a quantification of the amount of force that the cytoskeleton can exert against a membrane is needed to understand the stress state of the cell membrane. Generally this force, F_{crit}, is taken to be the amount of force that a straight filament can withstand in compression before first-mode buckling,

$$F_{crit} = \frac{EI\pi^2}{L^2}, \tag{3}$$

where *EI* is the flexural rigidity, and *L* is the length of the cytoskeletal filament.

The maximum deformation of the membrane will occur under the maximum force prior to cytoskeletal buckling. Once the buckling force is reached, additional force will cause the filament to bend, but with only minimal additional membrane deformation. Instead, a continued increase in force will result in filament deformation and eventually filament collapse (Stamenovic, Mijailovich et al. 2002). This phenomenon has been demonstrated by aspirating liposomes containing microtubules (Fygenson, Elbaum et al. 1997). Thus, to determine the maximum stress in the membrane, forces only up to the filament buckling is considered.

A transverse loading of the cytoskeletal element will also occur due to the force generated as the membrane of the growth cone slides along the tip of the protein during membrane extension. This force is dependent on the viscosity of the membrane and the extension rate of the growth cone, via

$$F = \eta v, \tag{4}$$

where viscosity, η is approximately 0.00021 dynes-sec/cm and velocity, v is 0.003 – 0.25 μm/s, resulting in a force of 0.0063 – 0.053 pN (Dai and Sheetz 1995), or ~1 – 3 orders of magnitude smaller than the normal load on the cytoskeletal element. These forces are therefore not considered in the model. Dai and Sheets (1995) also stated that the viscous forces are too small to cause a significant effect on growth rate and extension rates (Dai and Sheetz 1995). Therefore, to determine the maximum stress in the membrane, only a force up to the filament buckling force is considered, since it is likely to be ~ 99.9% of the total force experienced by filament bending and compression (Stamenovic, Mijailovich et al. 2002).

In general, the axis of a cytoskeletal element will interact with the surface of the membrane at an angle, Figure 1.

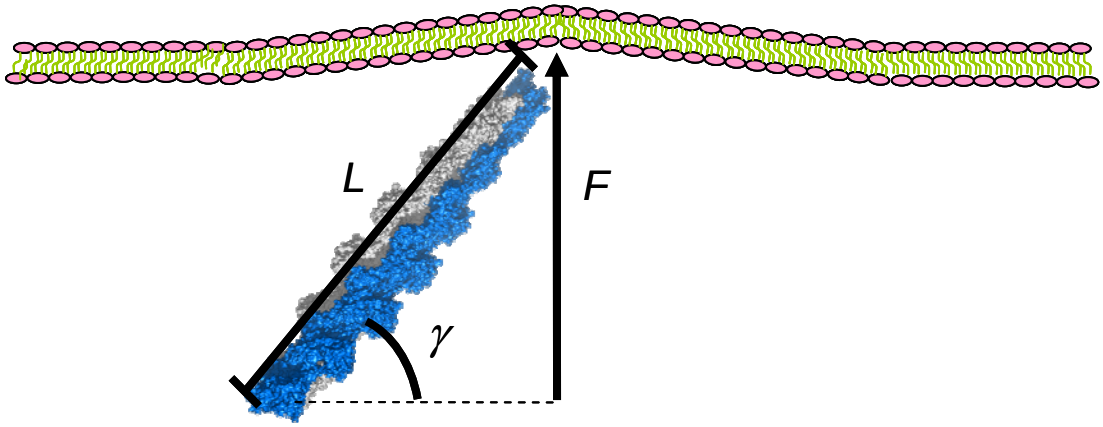

Figure 1: *Scale schematic of an actin filament (blue and white) with a diameter of approximately 8 nm impinging on the inner surface of a phospholipid bilayer membrane with a thickness of approximately 4.5 nm. Hydrophilic regions of the membrane are shown in pink, and hydrophobic portions are shown in yellow.*

This is demonstrated in neuronal and mobile cells that contain the protein complex Arp2/3, which causes actin filaments to branch from mother actin filaments at angles of 70° (Pollard and Earnshaw 2002; Pollard and Borisy 2003). This results in a meshwork of cortical actin filaments acting at a wide range of angles to the surface of the membrane. When the protein and membrane are not aligned normally, the magnitude of force that can be exerted against the membrane before the protein deforms is,

$$F = F_{crit} \sin \gamma \,, \tag{5}$$

where γ is the angle between the filament and the surface of the membrane.

After the amount of force that a filament can support was computed, the normal contact stress exerted on the membrane due to this force was calculated. This normal contact stress is $s = F / A$, where s is the normal contact stress of the filament acting on

the membrane and A is the area of the protein that acts against the membrane. An actin filament was treated as a solid cylinder with area, $A_a = \pi r_a^2$, where r_a is the radius of an actin filament, ~4 nm (Boal 2002; Pollard and Earnshaw 2002). The microtubule was taken as a hollow cylinder, and the area of the microtubule that acts against the membrane is then $A_{MT} = \pi r_{MTo}^2 - \pi r_{MTi}^2$, where r_{MTo} is the outer radius of the microtubule, ~12.5 nm, and r_{MTi} is the inner radius of the microtubule, ~8.5 nm (Boal 2002; Pollard and Earnshaw 2002).

Reported values for the flexural rigidities, EI, of actin filaments range from 10^{-27} to 10^{-26} Nm^2 (Kojima, Ishijima et al. 1994; Schaefer, Kabir et al. 2002; Jean, Chen et al. 2005; Atilgan, Wirtz et al. 2006; Ermilov, Murdock et al. 2007). Two extremes of these values reported for actin flexural rigidity, 0.40×10^{-26} and 7.3×10^{-26} Nm^2 were used in the simulations (Gittes, Mickey et al. 1993; Kas, Strey et al. 1993). By contrast, the flexural rigidity of individual microtubules is ~5.0×10^{-24} Nm^2 (Odde and Renn 2000; Brangwynne, MacKintosh et al. 2006; Kerssemakers, Munteanu et al. 2006), and for multiwalled carbon nanotubes with a diameter of ~50 nm the flexural rigidity is ~2.1×10^{-19} Nm^2 (Dong, Arai et al. 2004).

Since we are interested in the interaction of single filaments with the membrane, such as may be found in a neuron at the inception of axon or dendrite development, or in an actively growing lamellipodial or filopodial region where a new branch may be forming, we chose to simulate an actin filament with a length of 300 nm. By contrast, aligned actin filaments within the lamellipodia and filopodia, which are actively contributing to filopodial growth are ~0.5 to 5 μm in length, and filaments found in the

branched networks tend to be shorter (Timoshenko, Woinowsky-Krieger et al. 1959; Charras, Williams et al. 2004; Ergenc and Olgac 2007).

Using 0.40×10^{-26} and 7.3×10^{-26} Nm^2 for the actin flexural rigidities and 300 nm for the filament length, two different values for F_{crit} were determined (3). Next, F was computed for filament angles ranging from 10˚ to 90˚, in increments of 10˚ (5). This gave us a total of 18 forces, ranging from 0.0763 to 8.01 pN. This range of forces corresponds to a microtubule with a flexural rigidity of $5.0x10^{-24}$ Nm^2 and length between 2.5-25 μm and a multiwalled carbon nanotube with a flexural rigidity of $2.1x10^{-19}$ Nm^2 and a length between 509-5000 μm, both acting perpendicularly to the membrane (3).

The areas in which the protein filaments will act against the membrane for an actin filament and a microtubule are ~50 nm^2 and 263 nm^2, respectively (Boal 2002; Pollard and Earnshaw 2002). Given the calculated range of forces, the normal contact stresses exerted on the membrane by an actin filament is then 0.0015-0.1602 MPa. These normal contact stresses acting in the center of a membrane were modeled, and the deformations and strains of the membrane were determined. All modeling work was performed using ANSYS, Appendix A.

Table 1: *Model parameters*

parameter	description	value	reference
a	membrane diameter	100 nm, 200 nm, 500 nm	(Lewis and Bridgman 1992)
A_a	area in which actin filament can exert force	~50 nm^2	(Boal 2002; Pollard and Earnshaw 2002)
EI_a	flexural rigidity of actin filament	0.40×10^{-26}, 7.3×10^{-26} Nm^2	(Gittes, Mickey et al. 1993; Kas, Strey et al. 1993)
F	filament force acting on membrane	0.0763 – 8.01 pN	(Lewis and Bridgman 1992; Gittes, Mickey et al. 1993; Kas, Strey et al. 1993)
$G_{r\theta}$	in-plane shear modulus of membrane	1.28 MPa	(Evans and Rawicz 1990)
G_{zr} and $G_{\theta z}$	out of plane shear moduli of the membrane	43 MPa	-
r_a	radius of actin filament	4 nm	(Boal 2002; Pollard and Earnshaw 2002)
s	normal contact stress acting of membrane	0.0015-0.1602 MPa	(Lewis and Bridgman 1992; Gittes, Mickey et al. 1993; Kas, Strey et al. 1993)
t	thickness of neuronal membrane	4.5 nm	(Boal 2002)
Y_{rr}, Y_{zz}, $Y_{\theta\theta}$	Young's modulus of membrane	128 MPa	(Evans and Rawicz 1990)
γ	angle in which filament acts	10˚ – 90˚	-
$\upsilon_{r\theta}$, υ_{zr}, $\upsilon_{\theta z}$	Poisson's ratio membrane	0.49	(Elbaum, Fygenson et al. 1996; Dimova, Dietrich et al. 1999; Helfer, Harlepp et al. 2001)

Boundary Conditions

Simulations with two different boundary conditions (BCs) were performed, Figure 2. For BC_1, the edge of the membrane was clamped and immoveable: Dirichlet BCs at the boundary, $\delta\Omega$. This BC represents a bounding case that may be similar to what a cell might encounter if were loaded very quickly, such that the membrane had insufficient time to "flow into the boundary", as in the case of a cell injection. Indeed, such practice is used by modern cell injectors that use a very fast jabbing or hammering motion to inject a neuronal growth cone once the pipette tip has been brought into close proximity (Dent, Callaway et al. 1999) (personal observation). To our knowledge, no such boundary condition has been observed *in vivo*, but might represent a condition wherein the cell membrane was under osmotically induced tension and unable to flow freely or if it were tightly constrained by integral proteins interacting with both the cytoskeleton and the extracellular matrix, thereby restricting membrane flow. For BC_2, the Neumann-Dirichlet conditions were employed by constraining movement in the through-plane and by specifying the slope, $\delta w/\delta r = 0$ at the boundary. Two additional boundary conditions were supplied at the center of the membrane as a mixed BC wherein the slope $\delta w/\delta r = 0$ due to symmetry, and the loading force was specified. The clamped-moveable condition of BC_2 is equivalent to that used by Atilgan (Atilgan, Wirtz et al. 2006).

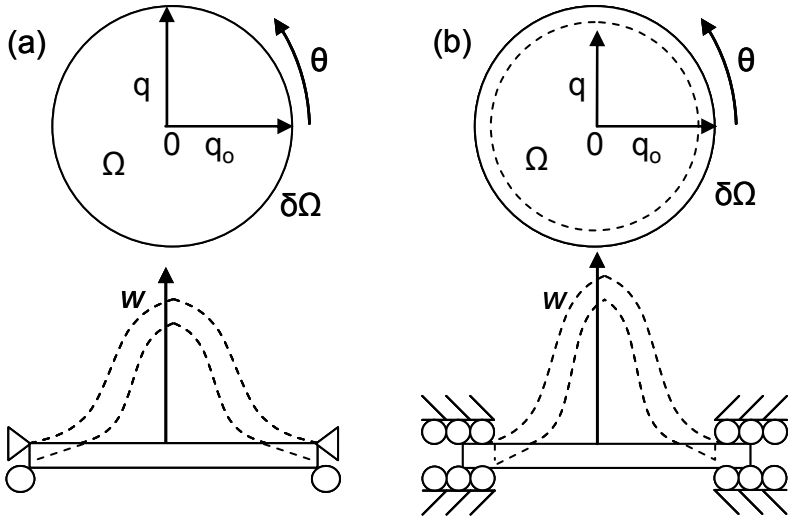

Figure 2: *Schematic of a circular membrane deforming under a point force acting at the membrane center. The membrane is represented by Ω, and the edge of the membrane by δΩ. Polar coordinates, r, z, θ were used. The top view and side view, respectively, of a clamped and immoveable membrane along δΩ, where* $\left.\frac{dw}{dq}\right|_{\delta\Omega} = 0$ *and* $q = q_o$ *(a). The top view and side view, respectively, of a membrane clamped along δΩ but free to move in q,* $\left.\frac{dw}{dq}\right|_{\delta\Omega} = 0$*, but* $q \neq q_o$ *(b). Dashed lines depict the deformed membrane (not to scale).*

Both BC_2 and that of Atilgan allow the membrane to flow freely in the radial direction. However, BC_2 allows the boundary to move in as the membrane is deformed. BC_1 on the other hand, restricts the in-plane flow of the membrane, and therefore when a force acts on the membrane it will produce a greater areal strain. Without providing any restrictions, the membrane can essentially be pulled to infinity, as modeled by Atilgan. In living cells, the flow and the growth of the membrane is restricted by integral proteins and their numerous interactions with both the cytoskeleton and the extracellular matrix. These interactions and inhomogeneities will therefore affect the stress state in the

membrane when a load is applied. These complexities, however, are reserved for future work.

Since the diameter-to-thickness ratio of the simulations ranged from ~20 – 200, a large deflection analysis was used to account for the stresses in the middle plane of the membrane as the membrane deformed.

Numerical vs. Analytical Solution

The Timoshenko membrane model (Timoshenko, Woinowsky-Krieger et al. 1959) was used to validate the numerical model. A comparison of the finite element analysis with the analytical solution was performed to ensure that ANSYS is capable of accurately modeling the geometries and boundary conditions used in the model. The analytical solutions for the simulations were performed for an isotropic membrane with a Poisson's ratio of 0.3 and an elastic modulus of 128 MPa. For validation purposes, a point force at the center of the membrane, as opposed to a normal contact stress, was applied to the membranes. The analytical solution includes the deformation and stresses caused by membrane bending and stretching. It utilizes the following equations to solve for the maximum deflection of the membrane, w_o, bending stresses at $\delta\Omega$ in the r and θ directions, σ_{rr} and $\sigma_{\theta\theta,}$ respectively, and mid-plane tensile stresses at $\delta\Omega$ in the r and θ directions, σ_{rr}' and $\sigma_{\theta\theta}$', respectively,

$$\frac{w_o}{t} + A\left(\frac{w_o}{t}\right)^3 = B\frac{Fa^2}{Yt^4}, \tag{6}$$

$$\sigma_{rr} = \beta_{rr} Y \frac{w_o t}{a^2}, \tag{7}$$

$$\sigma_{\theta\theta} = \beta_{\theta\theta} Y \frac{w_o t}{a^2}, \tag{8}$$

$$\sigma_{rr}' = \psi_{rr} Y \frac{w_o^{\,2}}{a^2}, \tag{9}$$

$$\sigma_{\theta\theta}' = \psi_{\theta\theta} Y \frac{w_o^{\,2}}{a^2}, \tag{10}$$

where t is the thickness of the membrane, F is the applied force, a is the radius of the membrane, Y is the elastic modulus of the membrane, and A, B, β_{rr}, $\beta_{\theta\theta}$, ψ_{rr}, and $\psi_{\theta\theta}$ are constants derived from the approximate solution using the Galerkin equations.

In determining the most appropriate failure criteria for assessing the stress value at which the membrane ruptures, several stress formulations were considered. Among these include the maximum principal stress, the areal strain, the Tresca stress, and the von Mises stress. We decided upon the areal strain, defined as the sum of the in-plane strains, since it is the only known failure criterion previously considered for membrane rupture. We also report the von Mises stress criterion for the following reasons: 1) the von Mises stress offers a means of comparing the stress states of any stress condition to that of a tensile stress, 2) the Tresca stress is primarily for modeling plastic flow and lies within the von Mises ellipse, 3) the von Mises stress represents the energy per unit volume that a material may sustain prior to failure, and it gives a field of the scalar equivalent of the stress state, which in this case is a compound loading condition: bending and tension. There are also precedents for using von Mises stress to quantify membrane stress (Smith, Moxham et al. 2000; Volokh 2007; Xing, Pan et al. 2007). The von Mises stress, σ_e, at the edge of the membrane under plane stress conditions was determined from σ_{rr} and $\sigma_{\theta\theta}$ by,

$$\sigma_e = \sqrt{\frac{((\sigma_{rr} + \sigma_{rr}') - (\sigma_{\theta\theta} + \sigma_{\theta\theta}'))^2 + (\sigma_{rr} + \sigma_{rr}')^{\,2} + (\sigma_{\theta\theta} + \sigma_{\theta\theta}')^2}{2}}. \tag{11}$$

A comparison of the numerical solution and analytical solution was made for the maximum membrane deflection and von Mises stress along the edge of the membrane. The results of 108 total simulations were compared: three different diameter membranes (100 nm, 200 nm, 500 nm), BC_1 & BC_2, and nine calculated forces (0.076 pN – 8.01 pN).

Element Type

Because the membrane was modeled as a circular section, with symmetric boundary conditions, only axisymmetric element types were considered for our model. Atilgan also assumes symmetric boundary conditions. The use of axisymmetric elements allowed us to model only one section of the membrane, but was representative of the entire membrane. This permitted us to use fewer elements, resulting in faster computation times. Preliminary simulations run with 3D tetrahedral elements resulted in identical results to those found with the 2D axisymmetric. However, once a radius of 50 nm was surpassed, the 32,000-node limit of the ANSYS license was exceeded. Since the structure is very high aspect ratio, and since 3D elements must maintain an aspect ratio close to unity, adding more elements of a different shape was not possible.

The membrane modeled in the simulations had a large diameter-to-thickness ratio, similar to a shell structure. Two different shell element types, SHELL208 and SHELL209, as well as a 2D, plane element type PLANE183 were used to model the membrane. SHELL208 and SHELL209 are typically used to model thin to moderately thick, shell structures. SHELL208 elements contain two nodes, and SHELL209 elements contain three nodes. The nodes in each of the shell types contain three degrees of freedom: two translational and one rotational. PLANE183 is an eight-node element, with each node having two translational degrees of freedom.

The deformation resulting from the use of three element types were compared to the analytical solution, (6), for a clamped-immoveable membrane with a radius of 250 nm. The von Mises stresses as calculated from (11) were also compared. Using element type PLANE183, deflection errors ranged from 0.11 to 2.20% and errors in von Mises stress along $\delta\Omega$ ranged from 26.49 to 35.45%. For these membrane dimensions and boundary conditions, SHELL208 elements produced deflection errors ranging from 1.63 to 3.74% and stress errors along $\delta\Omega$ from 0.81 to 7.88%. The larger errors in von Mises stress made PLANE183 an unfavorable element type.

Comparisons were then made between the two shell element types and the analytical solution for a clamped-immoveable membrane with a 250 nm radius and a force of 1.39 pN acting at the membrane center. This force was chosen because it is an intermediate of the forces considered in the simulations. Deflection errors at the center of the membrane and error in von Mises stress along $\delta\Omega$ were compared for the two shell types with a varying number of elements. Element types SHELL208 and SHELL209 yielded similar results, with similar percent errors from the analytical solution (Table 2 and Table 3).

Table 2: *Percent error of the numerical solution compared to the analytical solution for the maximum deflection of a clamped-immoveable, 250 nm radius membrane with a force of 1.39 pN acting at its center.*

element type	# elements	% error
SHELL208	4	21.01
	10	7.35
	25	2.80
	50	2.15
	100	1.50
SHELL209	4	13.86
	10	6.70
	25	3.45
	50	2.15
	100	1.50

Table 3: *Percent error of the numerical solution compared to the analytical solution for the von Mises stress along $\delta\Omega$ for a clamped-immoveable, 250 nm radius membrane with a force of 1.39 pN acting at its center.*

element type	# elements	% error
SHELL208	4	10.82
	10	4.18
	25	1.20
	50	0.17
	100	0.34
SHELL209	4	12.09
	10	4.38
	25	1.23
	50	0.17
	100	0.38

The trend for percent error in the deflection and von Mises stress calculations showed a decrease in error as the number of elements increased. The percent errors for membranes composed of ten or more elements for both shell types within 1% of each

other. The element type SHELL208 was chosen because it had fewer nodes and therefore a faster computational time than SHELL209.

Convergence Study

A strain convergence study was performed to determine the number of elements needed to model the membranes given the largest normal contact stress, 0.1602 MPa, acting against the membrane. Preliminary studies demonstrated that the larger the normal contact stress, the greater the number of elements needed for the maximum strain in any element of the membrane to converge. The convergence study was performed for both BC_1 and BC_2 on membranes with 50 nm and 250 nm radii. The maximum strain in the radial direction on the outer surface of the membrane was determined numerically, and the results were compared for membranes comprised of 100, 1000, and 2500 elements for the 50 nm radii membranes and 500, 1000, and 10,000 elements for the 250 nm radii membranes. The 2500-element solution was used as the convergence criterion for the 50 nm radii membranes, and the 10,000-element solution was used as the convergence criterion for the 250 nm radii membrane. Increasing the number of elements in the simulation beyond these numbers resulted in high-aspect-ratio elements with radial dimensions approaching zero.

The convergence study indicated that a 1000-element mesh was sufficient to model a membrane with a radius ranging from 50 to 250 nm. Using 1000 elements, the membranes with radii of 250 nm, under a normal contact stress of 0.1602 MPa, converged within ~2% of the 10,000-element solutions. For the 50-nm radii membranes, the 1000-element membranes converged to a solution within ~3.5% of their 2500-element solution, Figure 3.

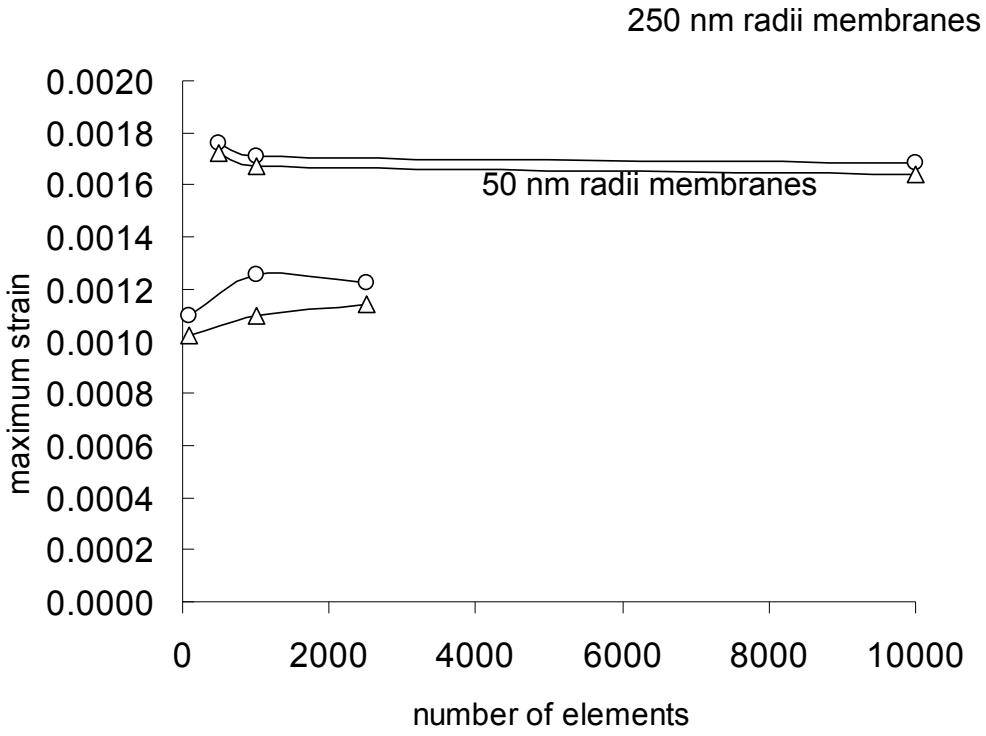

Figure 3: *Numerical solution for the maximum membrane strain for clamped-immoveable and clamped-moveable membranes with radii of 50 and 250 nm vs. the number of elements used to create the membranes. The clamped-immoveable membranes are represented by circles, and the clamped-moveable membranes are represented by triangles.*

Deformations and Stresses in Neuronal Membranes

After verifying that ANSYS is capable of solving the simulation given the geometries and boundary conditions, the deflections and stains of neuronal clamped-immoveable membranes, BC_1, and clamped-moveable membranes, BC_2, of 50 and 250 nm radii were computed. Neuronal membranes were modeled as transversely isotropic with the values listed, Table 1.

ANSYS was also used to determine the areal strain in the membrane. If the areal strain in a single element of the membrane exceeded ~3 %, the membrane was considered

to have ruptured (Nichol and Hutter 1996; Heidemann and Wirtz 2004). The areal strain of an element is the sum of its in-plane strains such that,

$$\varepsilon_{areal} = \varepsilon_r + \varepsilon_\theta , \tag{12}$$

where ε_{areal} is the areal strain, ε_r is the radial in-plane membrane strain, and ε_θ is the circumferential in-plane strain.

In addition to simulation data, the normal contact stresses that a buckling (Schaefer, Kabir et al. 2002) and a breaking (Odde, Ma et al. 1999) microtubule can exert on the membrane were calculated, and these values were included in the simulations. The flexural rigidity of the microtubules used for these calculations was estimated to be 5×10^{-24} Nm^2 (Venier, Maggs et al. 1994; Felgner, Frank et al. 1996; Kikumoto, Kurachi et al. 2006). The length of the breaking microtubule was determined visually from Odde *et al.,* (1999) to be 4 μm, and the length of the bending microtubule was listed in the Schaefer *et al.,* (2002) as 20 μm.

Results

Numerical vs. Analytical Solutions

The percent error for deformation and maximum von Mises edge stress were computed for three different membrane sizes with both boundary conditions. A comparison was made between the analytical solution and the numerical solution for an isotropic membrane with a Poisson's ratio of 0.3, Young's modulus of 128 MPa, and shear modulus of 43 MPa subjected to a point force. The clamped-immovable, BC_1, 50-nm membrane had an error in the deformation calculation of about 18%, Figure 4, and an error in von Mises edge stress ranging from 0.00% to 1.49%, Figure 5. Using these same boundary conditions, a membrane with a 100-nm radius had a deformation error ranging

from 5.40% to 7.86% and an edge stress error of 0.00% to 1.29%. The error for the 250-nm radius membrane had a deformation error range of 1.63% to 3.74% and an edge stress error ranging from 0.00% to 7.89%. For the 250 nm radius membrane, as the force increased, the error tended to increase as well.

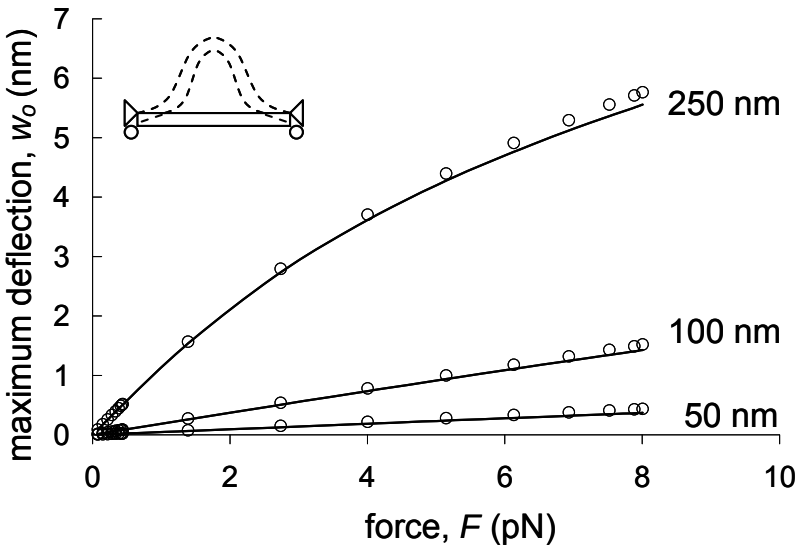

Figure 4: *Maximum membrane deflection in the z direction vs. applied force for clamped-immovable membranes of sizes 50, 100, and 250 nm in radii with Poisson's ratio 0.3. The analytical solution is represented by the solid line and the ANSYS solution with the open circles.*

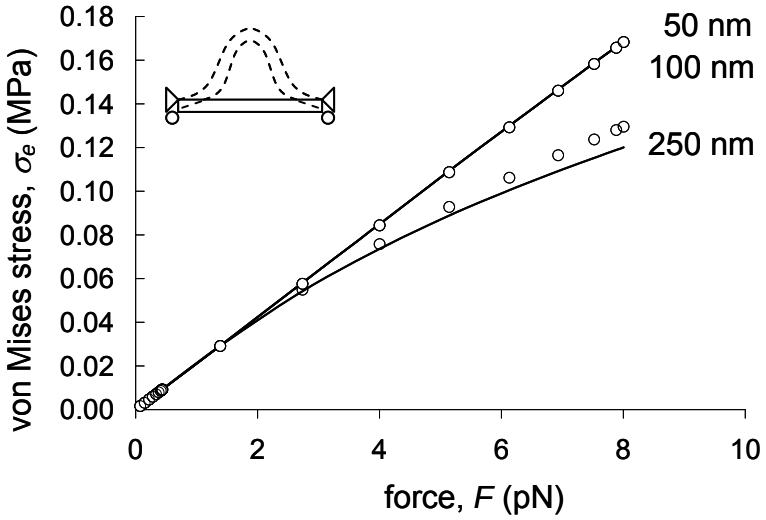

Figure 5: *von Mises stress along $\delta\Omega$ vs. applied force for clamped-immovable membranes of sizes 50, 100, and 250 nm radii with Poisson's ratio 0.3. The analytical solution is represented by the solid line and the ANSYS solution with the open circles. The 50 nm and 100 nm stresses were nearly identical.*

When the edge of the membrane was moveable, BC_2, the percent errors for the membrane deformation and edge stress were similar to when the membrane was immoveable, Figure 6 and Figure 7. For these boundary conditions, the 50 nm membrane had a deflection error ~18%, with an error in edge stress ranging from 0.00% to 2.17%. The 100 nm membrane had a deflection error from 5.40% to 7.86% with a stress error from 0.00% to 2.17%. Finally, the 250 nm membrane had a deflection error from 1.89% to 3.52% and a stress error from 0.00% to 13.06%. For the 250 nm radius membrane, as the force increased, the error tended to increase as well.

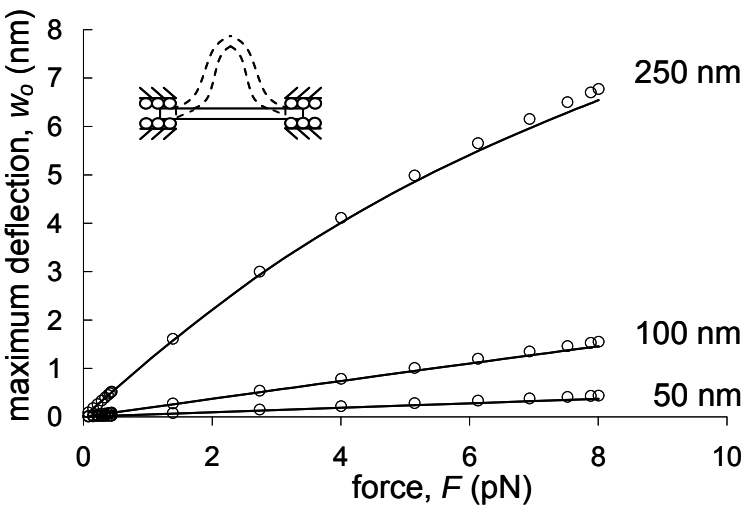

Figure 6*: Maximum membrane deflection in the z-direction vs. applied force for clamped-movable membranes of sizes 50, 100, and 250 nm radii with Poisson's ratios of 0.3. The analytical solution is represented by the solid line and the ANSYS solution with the open circles.*

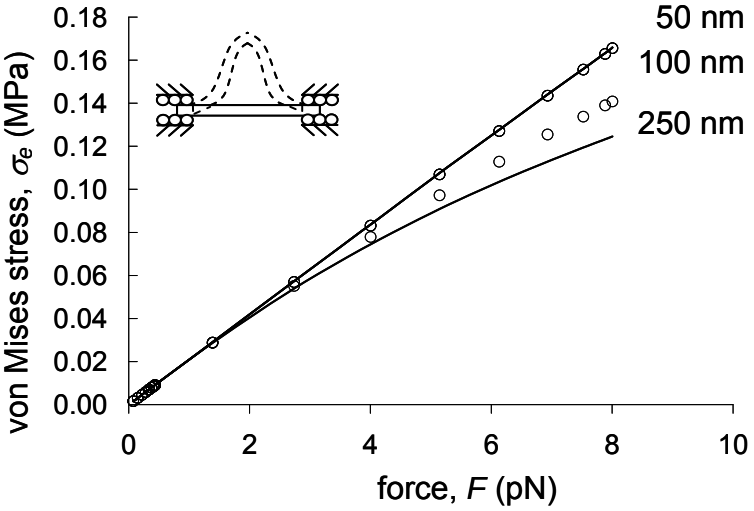

Figure 7: *von Mises stress along $\delta\Omega$ vs. applied force for clamped-movable membranes of sizes 50, 100, and 250 nm radii with Poisson's ratios of 0.3. The analytical solution is represented by the solid line and the ANSYS solution with the open circles. The 50 nm and 100 nm stresses are nearly identical.*

Deformations and Stresses in Neuronal Membranes

The low percent error computed when comparing the analytical solution to the numerical solution for an isotropic membrane demonstrates that the model is accurate for the given forces and geometries. The membrane model was then changed to represent the transversely isotropic neuronal membrane. A normal contact stress distributed over the area in which an actin filament would act, 50 nm^2, was substituted for the point load. Since ANSYS does not have a transversely isotropic material type, an orthotropic material type was chosen. Of the nine constants necessary to define an orthotropic material, five unique values were entered as summarized, Table 1. The low in-plane shear modulus was selected to simulate a fluid incapable of supporting shear load. Although the static in-plane shear modulus of the membrane is unknown, the ability of the layers of the membrane to flow freely across one another indicates that the membrane has a low in-plane shear modulus. The membrane strains and deformations were then reported for three surfaces of the membrane: inner (the inner surface of the membrane in which the filament acts), outer (the surface of the membrane outside the cell), and the midplane of the membrane.

Boundary Condition 1. The bending and breaking microtubules taken from the experimental data were modeled as exerting forces of 0.17 and 3.1 pN, respectively (3). The force in which a polymerizing microtubule was measured to exert against a barrier is within this range, ~2.5 pN (Kerssemakers, Munteanu et al. 2006). Forces of 0.17 and 3.1 pN correspond to normal contact stresses of 0.00065 and 0.012 MPa, respectively, given the geometry of the microtubule. The maximum normal contact stress the experimentally observed microtubule can exert is therefore within the values tested in our simulations.

For a 250 nm cell membrane with a clamped-immovable edge, BC_1, a normal contact stress of 0.1602 MPa acting on a 8 nm diameter circular area at the center of the membrane deflected the membrane 5.81 nm. The maximum areal strain in the membrane under this force was ~0.17% (12). This maximum strain occurred at the element in the center of the stress distribution on the outer surface of the membrane. To prevent rupturing of the membrane, the maximum normal contact stress that can be applied to a membrane under these boundary conditions is ~2.55 MPa, many times greater than that expected to be exerted by the cytoskeleton, but less than that imposed by a glass micropipette or nanopipette e.g. (Freedman, Mattia et al. 2007; Schrlau 2007). The maximum normal contact stress before rupture was determined by dividing the maximum allowable areal strain, 0.03, by the maximum strain in the membrane when 1 MPa of normal contact stress is applied, Figure 8. The results predict that rupture will first occur in the center of the stress distribution, on the outer surface of the membrane.

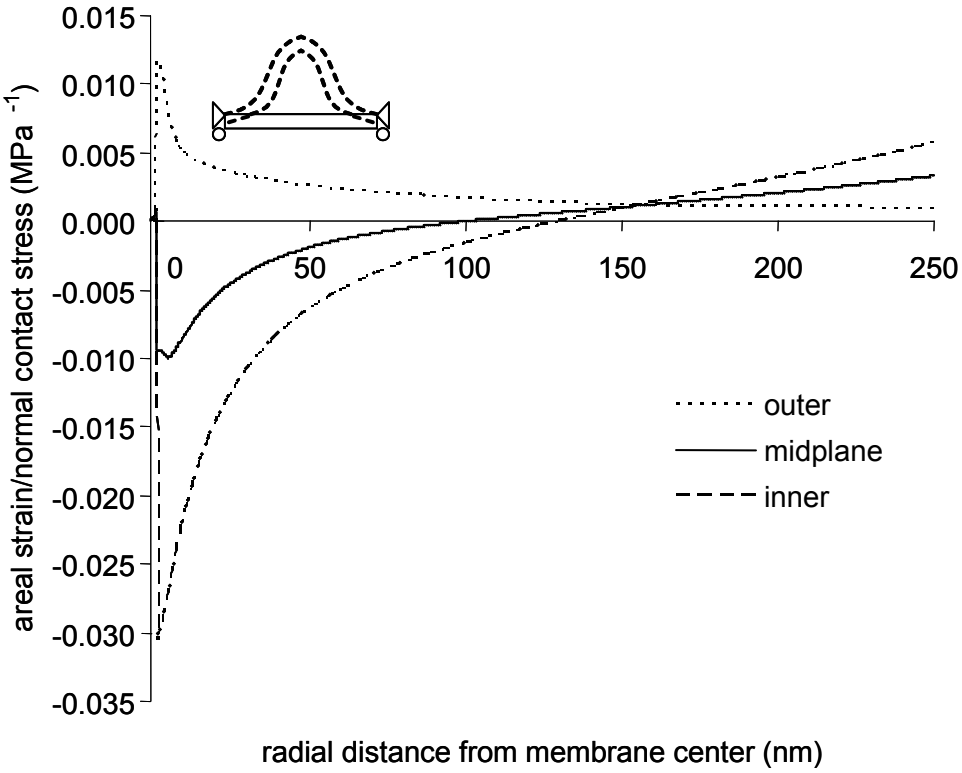

Figure 8: *Areal strain (ε_{areal}) /MPa vs. radial distance from the center of the membrane for a clamped-immoveable membrane with a radius of 250 nm. Membrane rupture will occur when the tension in the membrane causes the areal strain to exceed 3%. This will occur at center of the membrane on its outer surface if the normal contact stress applied exceeds ~2.55 MPa.*

For the 50 nm membrane, a 0.1602 MPa normal contact stress displaced the membrane 1.05 nm. The maximum areal strain in the membrane given these conditions is ~0.13%. The model predicts that rupture will first occur at the center of the stress distribution on its outer surface at a force of approximately 3.74 MPa, Figure 9.

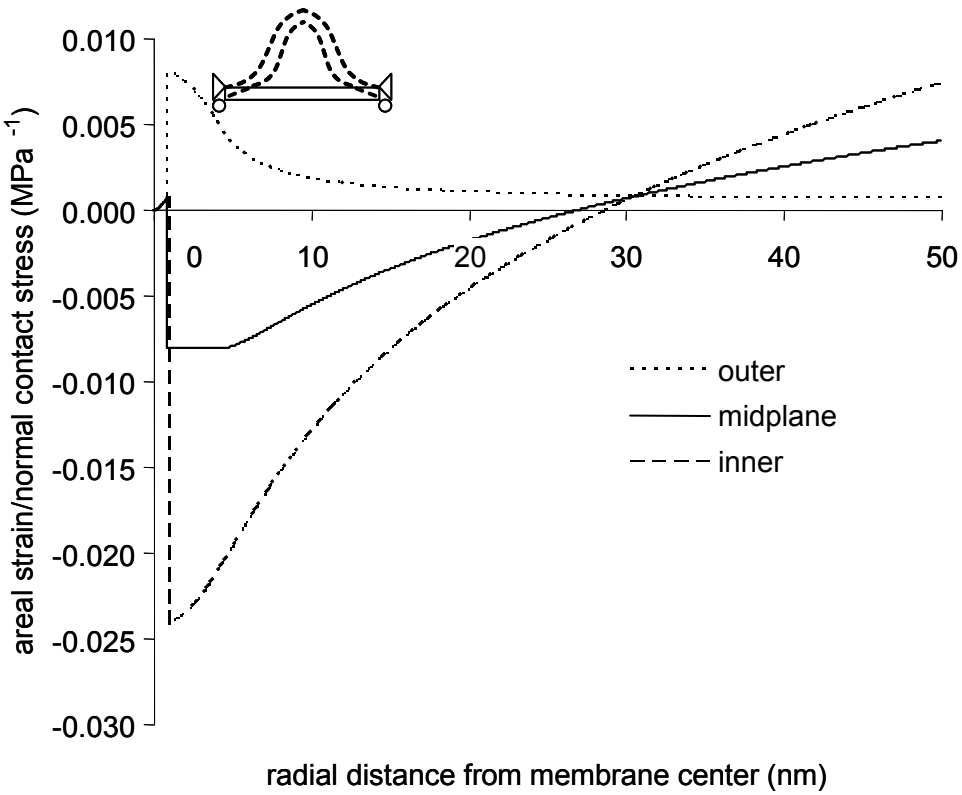

Figure 9: *Areal strain (ε_{areal}) /MPa vs. radial distance from the center of the membrane for a clamped-immoveable membrane with a radius of 50 nm. Membrane rupture will occur at center of the stress distribution on its outer surface if the normal contact stress applied exceeds ~3.74 MPa.*

Boundary Condition 2. A 250 nm membrane with a clamped-movable edge, BC_2, under a normal contact stress of 0.1602 MPa caused membrane deflection of 6.87 nm. The greatest areal strain in the membrane under this force is ~0.17%. The maximum normal contact stress that can be applied to this membrane without the membrane rupturing is ~2.61 MPa. Rupture will first occur at the center of the normal contact stress distribution on its outer surface, Figure 10.

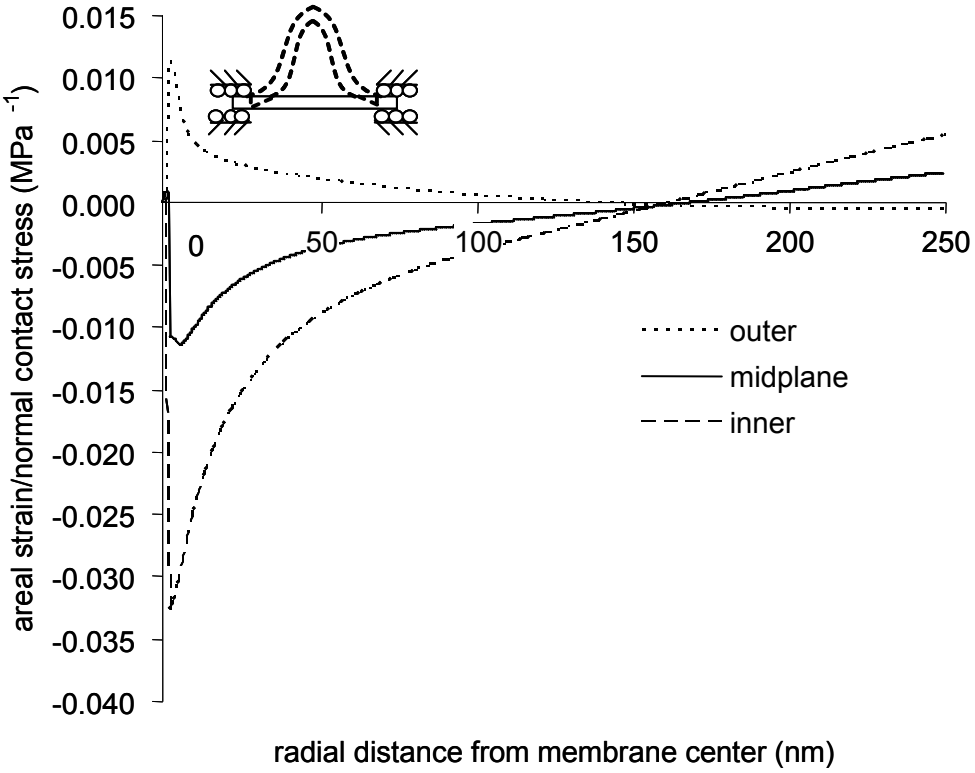

Figure 10: *Areal strain (ε_{areal}) /MPa vs. radial distance from the center of the membrane for a clamped-moveable membrane with a radius of 250 nm. Membrane rupture will occur at the center of the normal contact stress distribution on its outer surface if the normal contact stress applied exceeds ~2.61 MPa.*

For the 50 nm membrane, a 0.1602 MPa normal contact stress displaced the membrane 1.08 nm. The maximum areal strain in this membrane given the moveable boundary conditions is ~0.11%. The normal contact stress exerted on this membrane can not exceed ~4.09 MPa without membrane rupture occurring on its outer surface at the center of the normal contact stress distribution, Figure 11.

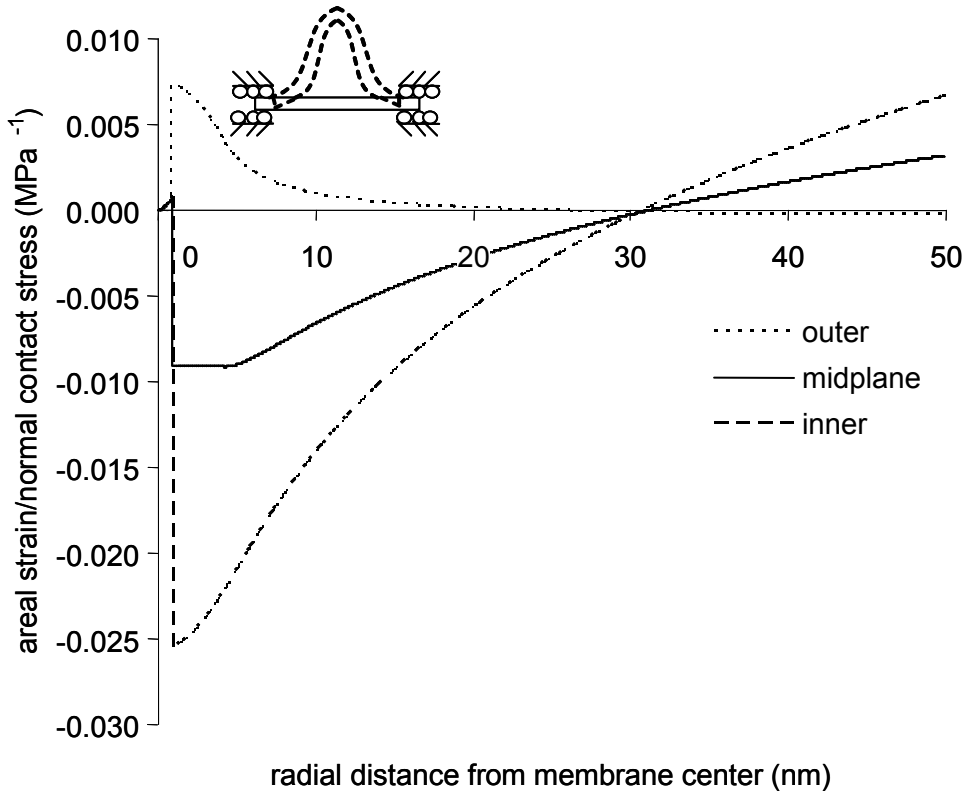

Figure 11: *Areal strain (ε_{areal}) /MPa vs. radial distance from the center of the membrane for a clamped-moveable membrane with a radius of 50 nm. Membrane rupture will occur at the center of the normal contact stress distribution on its outer surface if the normal contact stress applied exceeds ~4.09 MPa.*

Discussion

The stress distribution in a neuronal membrane under localized contact force was modeled. This model represents the loading conditions likely to occur under a variety of conditions. One is the interaction between the cell membrane and a single actin filament, as in the case of lamellipodial extension. Two is the interaction of the cell membrane with a single microtubule. The third loading case is one in which a nanopipette impinges upon the cell membrane during an injection. We conclude similarly to Atilgan et al. (Atilgan, Wirtz et al. 2006), that a single actin filament with a length of ~300 nm is incapable of deforming the membrane into a filopodial shape prior to its buckling, and therefore

multiple actin filaments must be present in order for a filopodia to form. Furthermore, we conclude that the membrane stresses likely to be generated by microtubules loaded axially as they impinge upon a cell membrane, as computed from the experimental data of Odde et al. (1999) (Odde, Ma et al. 1999), will not cause the membrane to exceed the areal strain failure criterion given for phospholipid bilayers by Boal (2002) (Boal 2002). The 0.00065 MPa normal contact stress estimated from a bending microtubule and the 0.0120 MPa normal contact stress estimated for the buckling microtubule are too small to rupture a membrane ranging from 50-250 nm in radius under the constrained boundary conditions. Therefore, we predict that both a 100-nm diameter patch of membrane and a 500 nm diameter patch of membrane have "natural mechanical safety factors" of ~15 – 25. It has been shown that the lateral reinforcement of microtubules can allow them to sustain forces of ~30-100 pN (Stamenovic, Mijailovich et al. 2002; Brangwynne, MacKintosh et al. 2006). However, even at this force, the maximum normal contact stress on the membrane is only ~0.380 MPa. This increase in normal contact stress would still not cause the membranes to rupture, but it would reduce the safety factor to be within ~7 – 10. The implication is that natural selection phenomenon early in life's history may have "found" this mechanical relationship between cytoskeleton and cell membrane.

While the strain energy contained in a single actin filament or microtubule is insufficient to cause membrane rupture or puncture, this is not the case with micropipettes or nanopipettes. Since the load was applied on an area with a diameter of 8 nm, representative of an actin filament, it is noted that the forces necessary to cause a local areal expansion of 3% are likely to be lower than those imposed by larger structures

such as those used in typical tethering experiments. In an experiment performed by Dai and Sheetz (1995) (Dai and Sheetz 1995), using 0.5 μm microspheres, the tether force, or the force required to produce and maintain a tether in a DRG growth cone was determined to be 6.7 pN. However, using much larger microspheres, 4.0 μm, another group found a steady-state tether pulling force of 246.3 pN for human embryonic kidney cells (Ermilov, Murdock et al. 2007). Thus, from these two papers alone we may conclude that the tether forces calculated are dependent on the size of the microspheres, and thereby the radius of membrane being pulled. In the simulations the load is applied on an 8-nm diameter circular area, thus simulating a much greater strain gradient and resulting stress gradient within the membrane, leading to a smaller force to produce deformation and, under the right conditions, rupture or puncture.

An understanding of the magnitude of forces between cytoskeletal proteins and the cell membrane is necessary for basic science, as well for cell and tissue engineering applications. A cytoskeleton structure that is too stiff, either by nature, disease, or human design, could potentially rupture a cell membrane. If the support structure is too compliant however, it will not be able to drive and maintain the morphology of the cell. Additionally, a change in the deformation of the cytoskeleton, which could occur due to a change in the mechanical properties of the cytoskeleton or cell membrane, may lead to cell damage (Takamatsu and Kumagae 2002).

As cytoskeletal proteins and membranes co-evolved, and indeed continue to evolve, presumably an optimization did occur and continues to persist wherein the material strength of the cytoskeletal filaments are sufficient to deform the cell membrane at a rate capable of generating cell growth, but insufficient to cause membrane rupture. Likewise,

the phospholipids responsible for maintaining cell integrity must remain compliant enough to allow transmembrane proteins to populate the membrane with adequate frequency and density to sustain cell metabolism, but must also remain strong enough to resist rupture from either externally or internally generated forces. This line of investigation brings new possibilities and imposes limits on what may be achievable with cellular and tissue engineering projects as well as artificial life efforts.

Additionally, this work is a precursor to quantifying the normal contact stresses required to penetrate a cell membrane during cellular injection, single cell surgeries, and organelle injections. Knowledge of these normal contact stresses is necessary to ensure that minimal damage is done to the cell during these procedures. BC_2 represents a boundary condition identical to that used by Atilgan. On the other hand, BC_1 represents a case where the membrane is undergoing rapid loading, whereby the membrane flow response time is inadequate to respond to the load. Both boundary conditions produced deflection and stress results within the same order of magnitude. While this is surprising considering that the membrane is allowed to flow radially under BC_2 conditions, the results are consistent with the Timoshenko solution. However, further experimental verification with probes on the same scale as actual cytoskeletal elements is warranted.

There are a number of technological applications that would benefit from a better understanding of the response of a membrane to an applied force. Specifically, the amount of normal contact stress required to puncture a membrane for drug injection or *in vitro* fertilization can be determined using simulation (Roth, Howard et al. 1994; Ergenc and Olgac 2007). This would enable application of a force from a microfluidics device or nanofluidics device to permeate the membrane of a cell, while minimizing the chance of

cell or organelle injury e.g. (Freedman, Mattia et al. 2007; Schrlau 2007). This knowledge would allow for the automation of a force-controlled injection system. When implementing haptic feedback into an injection device, a feedback 'target', generated through simulation, would benefit device calibration.

Future work will include modeling an aspirated, spherical cell, and then determining the normal contact stresses required to puncture the membrane. Additionally, future work could include making the current model dynamic by incorporating the polymerization of the cytoskeletal filaments against the membrane. The amount that the cytoskeletal filament can grow, and thereby the amount of force the filament will be able to exert on the membrane, will be dependent on the tautness, or the size of the undulations, of the membrane. The more taut the membrane, the less accessible the end of the cytoskeletal element is to an additional protein subunit (Hill 1987).

Chapter III: Determination of the Mechanical Properties of Liposomes: A Precursor to the Numerical Quantification of the Forces Imposed by Micro and Nanopipettes during Liposome Manipulation

Abstract

Using micropipette-deformation-based methods, a numerical implementation of the Evans membrane model, and an image-processing based algorithm for measuring deformation, the mechanical properties of spherical DOPC:DOPS liposomes were measured. Liposomes were aspirated to pressures of -10 mmHg (~ -1333 Pa) and the area expansion modulus and Young's modulus of the liposomes were found to be 0.067 $N \cdot m^{-1}$ (67 ± 4 dynes/cm) and 15 ± 1 MPa, respectively. Quantification of the mechanical properties of liposomes is critical in determining the behavior of liposomes during various activities, e.g. how drug-encapsulated liposomes will diffuse through pores during targeted drug delivery, or how liposomes will respond to probing during imaging and injection.

Introduction

An understanding of membrane mechanics is essential in determining how liposomes and cells respond to stimuli. These stimuli include shear stresses caused by fluid flow (Chen, Niu et al. 2008; Li, Liu et al. 2008), pressures due to aspiration or injection (Henriksen and Ipsen 2004; Ohashi, Hagiwara et al. 2006), and contact forces as liposomes or cells are either squeezed through pores or vessels, or probed by an atomic force microscope or injection device (Cevc, Schatzlein et al. 2002; Chen, Kis et al. 2007; Brochu and Vermette 2008).

For the past twenty years, liposomes have been used as drug-encapsulating, transportation vesicles that diffuse through the pores of the skin in order to reach their

target tissues (El Maghraby, Barry et al. 2008). An understanding of liposome mechanics is essential in order to quantify the diffusion rates of these liposomes, determine the damage that these liposomes may incur during diffusion, and calculate the drug-encapsulation efficiency of these liposomes during their manufacture (Gompper and Kroll 1995; Cevc, Schatzlein et al. 2002; Ramachandran, Quist et al. 2006).

Additionally, the mechanical properties of liposomes and cells are responsible for the amount of force and deformation that these vesicles undergo when they are probed or injected by various devices. The injection of drugs, genetic information, and macromolecules into single-cells or single-organelles is currently being used to modulate and monitor individual cell activity (Han, Nakamura et al. 2005; Obataya, Nakamura et al. 2005; Leary, Liu et al. 2006). Examples of single-cell injection include injection of a single LA7 cell to determine if an individual cell can initiate tumor growth (Zucchi, Sanzone et al. 2007), injection of an individual neuron to determine specific protein expression and morphology (Kao and Sterling 2003), injection of a mutant protein into a single cell to observe its response (Storrie 2005), and intracytoplasmic sperm injection (ICSI) into an oocyte to treat infertility (Varghese, Goldberg et al. 2007). Although these procedures, often referred to as nanosurgeries, show great promise in improving health care, damage to the cell often results, and this damage can be fatal (Laffafian and Hallett 1998; Han, Nakamura et al. 2005; Freedman, Mattia et al. 2007).

We have created spherical liposomes, and the mechanical properties of these liposomes were determined using the micropipette-aspiration technique developed by Evans and Rawicz (1990) (Evans and Rawicz 1990). By first determining the mechanical properties of a liposome or cell, the amount of force and deformation necessary to

perform a specific manipulation to the liposome or cell can be quantified. Once this information is known, measures can be taken to ensure that these forces and deformations are not exceeded during manipulation, thereby minimizing damage. Additionally, injection and probing devices can be created based on the amount of force and deformation that they will need to withstand during probing, injection, or other manipulation.

Methods

Theory

The most important mechanical property for determining the morphology of a liposome or cell under mechanical load is the in-plane Young's modulus. The Young's modulus of the DOPC:DOPS liposomes has been determined using the micropipette aspiration technique developed by Evans and Rawicz (Evans and Rawicz 1990). This technique involves slowly aspirating a liposome into pipette, measuring the geometry of the liposome and the pressure inside the pipette during aspiration, and then calculating the liposome's surface tension and areal (in-plane) strain to determine its mechanical properties, Figure 12.

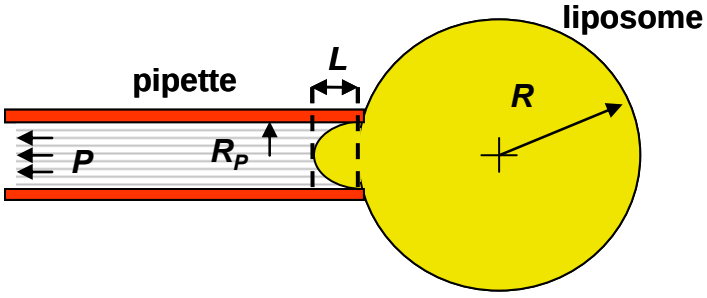

Figure 12: *Schematic of spherical liposome being aspirated inside a pipette.*

The liposome membrane, like any material, can deform in three fundamental modes: bending, dilatation (stretching), and shearing. When subjected to bending, the outer surface of the membrane is subjected to a tensile load, and the inner surface of the membrane to a compressive load. When the liposomes were free to float in solution, their membranes were free to fluctuate, and their behavior was primarily governed by their bending rigidity. However, when a liposome was aspirated into the holding (aspiration) pipette, its membrane appeared to tighten, indicating the presence of an additional tensile load on both the inner and outer layers of the bilayer. Membrane tightening was associated with the portion of the membrane outside the holding pipette having a spherical, visually clear edge. As the aspiration pressure applied to the liposome was increased, the liposome was pulled further into the pipette, but the portion of the liposome that was outside the holding pipette did not appear to change shape or size. The membrane of the liposome was being stretched during aspiration, and therefore its primary deformation mode during this time was dilatation. By measuring the change in aspiration pressure and the change in geometry of the membrane, the area expansion modulus, and thus the in-plane Young's modulus, can be determined by first computing the surface tension and areal strain of the membrane. The surface tension of the membrane of a liposome during aspiration and release is determined using Laplace's law,

$$\tau = \frac{\Delta P \, R_P}{2(1 - R_P / R)}, \tag{13}$$

where τ is the surface tension of the liposome, ΔP is the difference in pressure inside the pipette from its current state to when it was just being held by the holding pipette (reference state), R_P is the radius of the pipette, and R is the radius of the liposome outside the pipette. As the aspiration pressure increases, the surface area of the liposome

increases, and therefore the areal strain of the membrane increases as well. The areal strain is computed using,

$$\alpha = \frac{1}{2}[(\frac{R_P}{R})^2 - (\frac{R_P}{R})^3]\frac{\Delta L}{R_P}, \quad (14)$$

where α is the areal strain of the membrane and ΔL is the difference between the length of the liposome inside the pipette from its current state to the length of the liposome inside the pipette at its reference state.

Liposome Creation

Hollow, spherical liposome vesicles were created from a phospholipid membrane based on the method of Fygenson et al. (1997) (Fygenson, Elbaum et al. 1997). Liposomes were produced from a synthetic phospholipids blend, 1,2-dioleoyl-*sn*-glycero-3-phosphocholine (DOPC):1,2-dioleoyl-*sn*-glycero-3-[phospho-L-serine] (DOPS) (7:3, w/w), purchased from Avanti Polar Lipids, Inc. The lipids were stored in a chloroform solution. To create liposomes, a roughened, Teflon™ disk was placed inside a 20 mL glass vial, and 150 μL of the phospholipid solution was deposited onto this disk. The vial was then left on the bench top, with its cap off, for approximately one hour to allow the chloroform to evaporate. After the chloroform had appeared to have fully evaporated, the cap to the vial was placed loosely onto the vial, and the vial was placed into a vacuum desiccator for four hours. The vacuum desiccator was used to ensure that all traces of the chloroform had been removed. Next, the phospholipids were placed into an incubator, set at 49˚C, for 2 hours. This was done to hydrate the phospholipids. The cap of the vial remained loose during hydration. The phospholipids were then removed from the incubator, and 4 mL of 0.9% (w/v) saline solution was added to the vial. The 0.9% saline solution is representative of physiological osmolality, the environment a cell would

experience *in vivo*. The cap of the vial was then tightened, and the phospholipids were placed back into the incubator for 4 hours where they swelled to form liposomes (Lasic 1988). During this process, phospholipid bilayers were created as the hydrophilic heads of the phospholipids become exposed to the saline solution, and the hydrophobic tails of the phospholipids become sequestered within the heads. The phospholipid bilayers then encapsulated the saline solution, minimizing the electrostatic energies between the phospholipid and salinated water phases of matter, Figure 13. Liposomes appeared as a whitish cloud floating on top of the Teflon™ disk. The liposomes created were ~10-50 μm in diameter with a thickness of ~4.5 nm (Boal 2002; Kucerka, Pencer et al. 2007). Using a 50 μL pipette, the liposomes were harvested from the Teflon™ disk and placed into a clean vial.

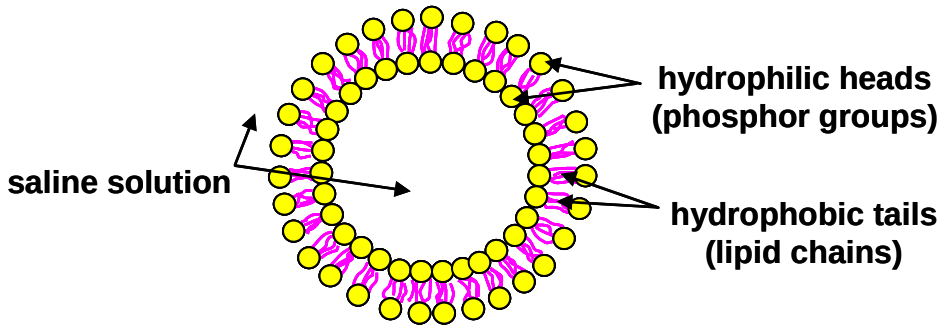

Figure 13: *Schematic of a cross-sectional slice of a liposome. Liposomes form when phospholipids encapsulate the saline solution, exposing their hydrophilic heads to solution but preventing contact between the solution and their hydrophobic tails. Liposome diameters ranged from ~10-50 μm. Image is not drawn to scale.*

Experimental Setup

The liposome aspiration experiments were performed on an inverted light microscope (Olympus IX-81) with a total magnification of 400×. To reduce background

vibrations, the microscope was floated on a TMC 63-500 vibration table. Liposomes were aspirated with a CellTram air pressure transmitter (Eppendorf), and pressure measurements were recorded using a Traceable® pressure meter (Control Company), with a resolution of 2 mmHg (~ 267 Pa). The holding pipettes used to apply pressure to the liposomes had an inner diameter of ~ 15 μm (Eppendorf Vacutips), and all pipette manipulations were controlled using an Eppendorf NK-2 micromanipulator (B&B Microscopes, Ardmore, PA). A bubble test was performed to ensure that there were no leaks in the connections between the pressure transmitter, pressure transducer, and pipette holder. Images of the liposomes during aspiration were taken using SPOT Advanced software (Sterling Heights, MI).

A coverslip was placed on the microscope stage and 100 μL of 0.9% (w/v) saline solution was deposited onto the coverslip. Next, 10 μL of liposome solution was added to the center of the saline droplet. The holding pipette was then inserted into the grip head of the pipette holder that was connected to the CellTram pressure transmitter, and the pipette holder was then attached to the left micromanipulator so that the tip of the pipette was directly above the solution, Figure 14.

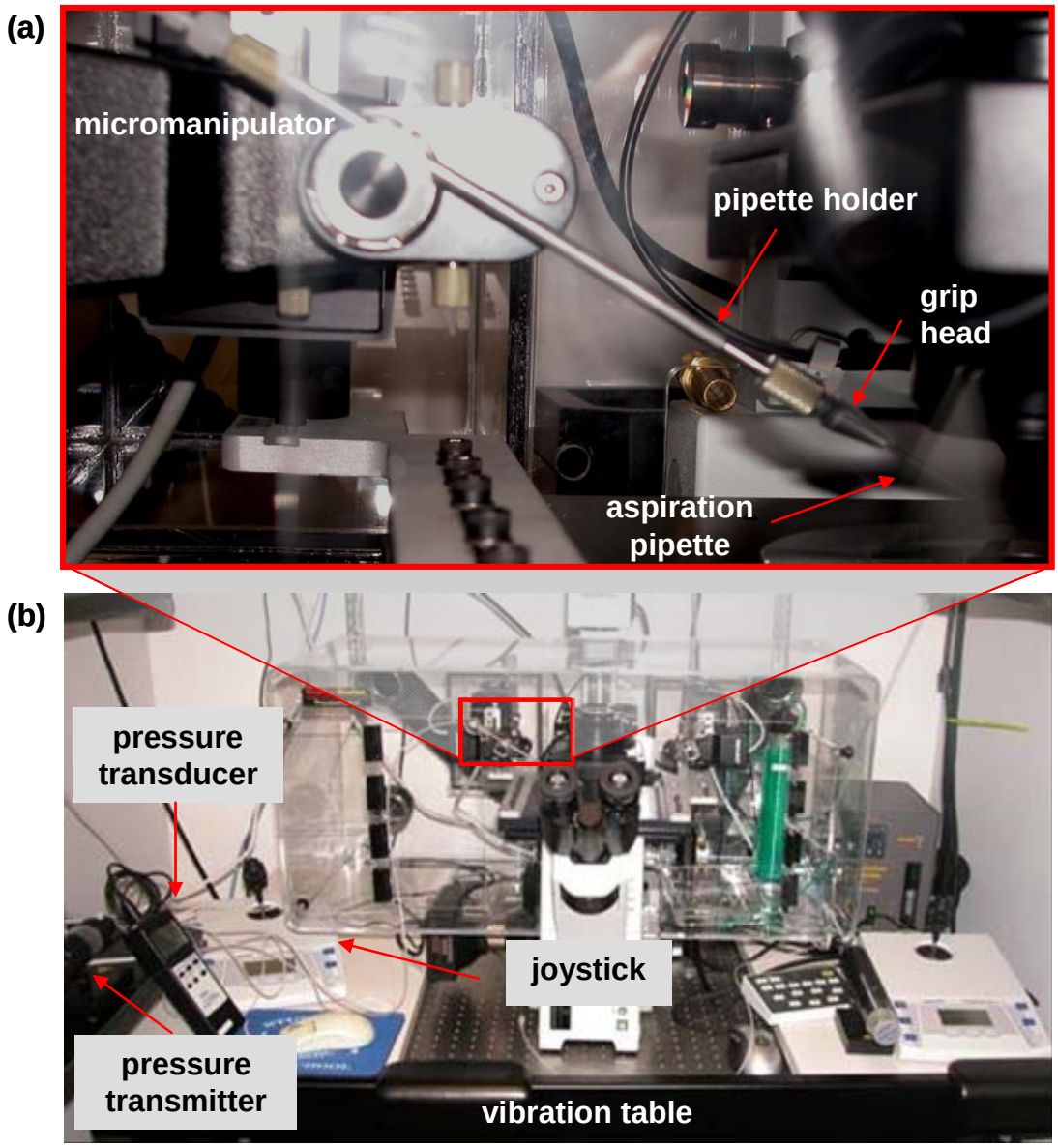

Figure 14: *Photo of the experimental setup (b) with a close up of the manipulator and pipette holder (a). The holding pipette is inserted into the grip head of the pipette holder, and the pipette holder is attached to the left micromanipulator.*

Once the setup was complete, the micromanipulator joystick was used to position the tip of the holding pipette into the microscope field of view. To do this, the *x* and *y* positions of the manipulator were adjusted using the course control of the manipulator (manipulator speed 4000 µm/sec). The height of the pipette above the coverslip (*z*

position) was not adjusted at this time. When the light from the microscope could be seen on the tip of the pipette, the pipette was considered to be within the microscope field of view. Next, the 10× objective was used to focus on the liposomes that were floating within the saline solution. While looking through the eyepiece of the microscope, the joystick was used to move the manipulator fore and aft (*y* direction). A shadow from the pipette could be observed through the eyepiece, and when the pipette shadow was in the center of the field of view, the manipulator was locked in the *y* direction. Next, the joystick was used to lower the pipette tip into the saline solution (*z* direction). When the pipette tip had entered the solution, the manipulator was switched to fine control (manipulator speed 450 μm/sec), and the tip of the pipette was slowly brought into focus. The manipulator was then adjusted in the *x* direction to center the pipette tip in the microscope field of view.

After the pipette tip and the liposomes were in focus, the *y* direction of the manipulator was unlocked, and the pipette tip was manipulated in the *x* and *y* directions until it was next to a liposome that appeared to be ~45 μm in diameter. Suction was created by increasing the piston volume of the CellTram pressure transmitter until the chosen liposome was "caught" by the holding pipette. The aspiration pressure was then decreased slowly until the smallest pressure necessary to hold the liposome inside the pipette was applied to the liposome. At this time, the aspiration pressure inside the pipette was smaller than the resolution of the pressure transducer, but the membrane of the liposome that was inside the pipette had conformed to the walls of the pipette, and the membrane of the liposome that was outside of the pipette appeared to be taut. This was considered to be the reference state of the liposome, and an image of the liposome in this

state was taken using the 40× objective (resolution of 177 nm/pixel). All of the pressure and geometry changes during the aspiration and release of the liposome were compared to this reference state.

Next, aspiration pressure was slowly applied to the liposome until the transducer read -2 mmHg. An image of the liposome was taken at this aspiration pressure. It was assumed that the there was a tight seal between the holding pipette and the liposome. To ensure this was in fact the case, approximately 5 minutes were allowed to pass before the aspiration pressure was adjusted again. The ability of the setup to hold the applied pressure confirmed that there were indeed no leaks in the system. Once this was confirmed, the aspiration pressure continued to be increased slowly, and images were collected at pressure increments of 2 mmHg until four of five data points had been collected (aspiration pressure reached -8 mmHg or -10 mmHg). Once the final aspiration pressure had been reached and an image had been taken, the aspiration pressure was slowly decreased, releasing the liposome from the pipette. Images were also collected during the release of the liposome in increments of 2 mmHg. However, during the release of the liposome, images were taken just before the pressure reading was 4 mmHg greater than the last. For example, as the aspiration pressure was decreased from -6 mmHg to -4 mmHg, the image of "-4 mmHg" was taken just before the pressure transducer read "-2 mmHg". This was done to ensure that the volume of the air inside the pressure transmitter for each of the pressure readings was the same for both the aspiration and release of the liposome.

Once all of the images of the aspiration and release of the three different liposomes were collected, they were imported into MATLAB in TIF format (size 1024 x 1024

pixels). A MATLAB algorithm was written that would perform the following manipulations to each image: crop the image to isolate the liposome from the background, perform histogram equalization to the image to enhance its contrast, and convert the grayscale image to a binary image based on a user-specified threshold, Appendix B. The threshold value chosen ranged from 0.3 - 0.5, and the same threshold value was used for each image taken during the aspiration and release of a liposome. Changes in the focus and brightness of the three liposomes required that the threshold value be adjusted for each liposome. The processed, binary image was saved as a bitmap, and then Paint Shop Pro was used to manually remove pixels from the image. This was done in two steps. First, the binary image was rotated to be aligned with its primary axes vertical. Next, the pixels from the image that did not represent the edges of the liposome were removed using the Magic Wand tool. The Magic Wand tool selects all neighboring pixels that have the same threshold value as the selected pixel, threshold value 0. The "cleaned" images were then imported into another MATLAB algorithm where the diameter of the liposome outside the pipette, D, and the total length of the liposome, L_T, were determined for all of the images, Appendix C. The distance between the leftmost and rightmost pixels with a threshold value of 1 was taken as D, and the distance between the uppermost and lowermost pixels with a threshold value of 1 was computed as L_T, Figure 15.

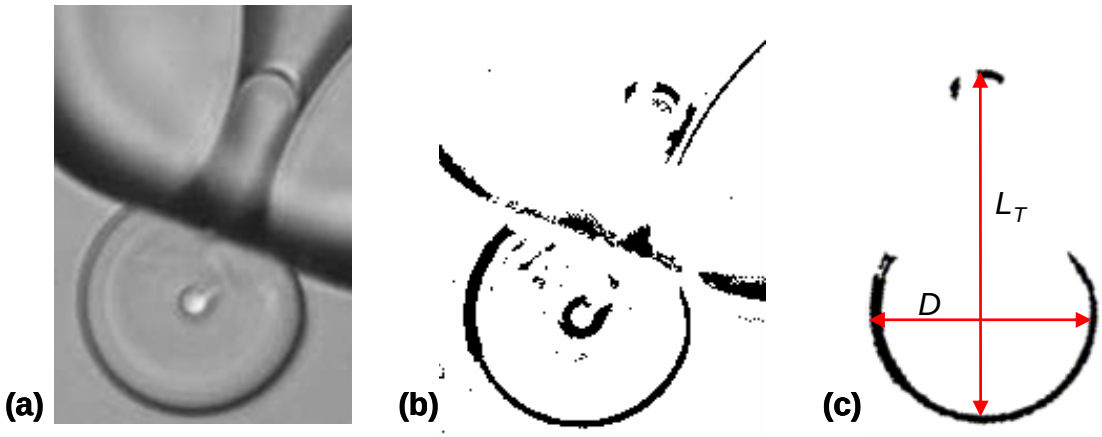

Figure 15: *Image taken of an aspirated liposome (a). The grayscale image was converted into a binary image (b). The binary image was then cleaned and rotated, and the diameter of the liposome outside the pipette, D, and the total length of the liposome, L_T, were computed for each of the liposomes at each stage during the experiment (c).*

Once D and L_T were known for each of the pressures during the aspiration and release of the liposome, the radius of the liposome outside the pipette, R, was determined from $R = D/2$, and the length of the liposome inside the pipette, L, was determined from $L = L_T - D$.

Next, the surface tension and areal strain of the liposomes at each stage of the experiment were calculated using (13) and (14). The surface tensions vs. areal strains were plotted for the liposomes, and the slopes of these plots were determined. These slopes represent the area expansion moduli of the liposomes. The average value for these slopes was taken to be the area expansion modulus for the DOPC:DOPS liposomes.

After the area expansion modulus was calculated, the in-plane Young's modulus of the liposome membrane was determined using,

$$E = \frac{K_A}{t}, \tag{15}$$

where E is the in-plane Young's modulus of the membrane, K_A is the area expansion modulus of the membrane, and t is the thickness of the membrane, which has been measured to be approximately ~4.5 nm by the X-Ray scattering technique (Boal 2002; Kucerka, Pencer et al. 2007).

The remaining material properties, in-plane and through-plane Poisson's ratios and in-plane and through-plane shear moduli, necessary to model the liposome membrane were calculated from the in-plane Young's modulus, as well as from a literature review on cell membrane behavior, Chapter VI.

Table 4: *List of Parameters*

parameter	description
independent	
P	pressure inside the holding pipette
ΔP	difference in aspiration pressure from reference state
R_P	radius of the holding pipette
t	liposome membrane thickness
measured/derived	
D	diameter of the portion of the liposome outside the holding pipette
E	in-plane Young's modulus of the liposome
K_A	area expansion modulus of liposome
L	length of liposome inside holding pipette
ΔL	difference in length of liposome inside holding pipette from its reference state
L_T	total length of aspirated liposome
R	radius of the portion of the liposome outside the holding pipette
α	areal strain of liposome
τ	surface tension of liposome

Results

Liposome Creation

The diameters of the liposomes ranged from ~10-50 μm, and both unilamellar (composed of only one bilayer) and multilamellar (composed of multiple bilayers)

liposomes were created. Liposomes with diameters of ~45 μm were used for all of the experimental work, Figure 16.

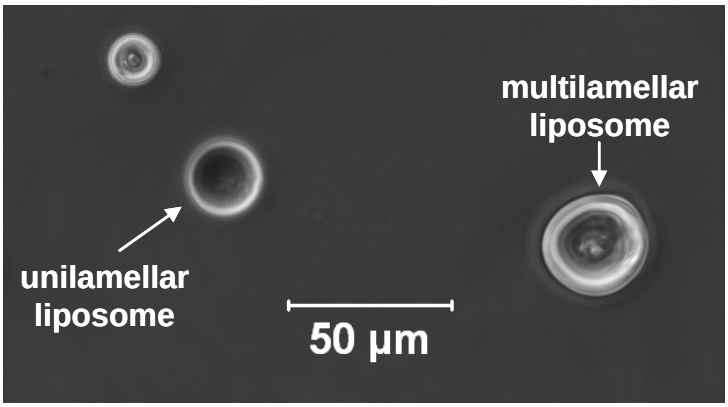

Figure 16: *Image of liposomes taken using phase contrast with a 40× objective. Both unilamellar and multilamellar liposomes are observed.*

Liposome Mechanical Properties Determination

Three different liposomes with an average diameter during aspiration of 46.3 μm were used to determine the Young's modulus of the DOPC:DOPS liposomes. Images were taken for pressures increments of 2 mmHg and compared to the reference state for each of the liposomes (ΔP = 0 mmHg), Figure 17, Figure 18, Figure 19.

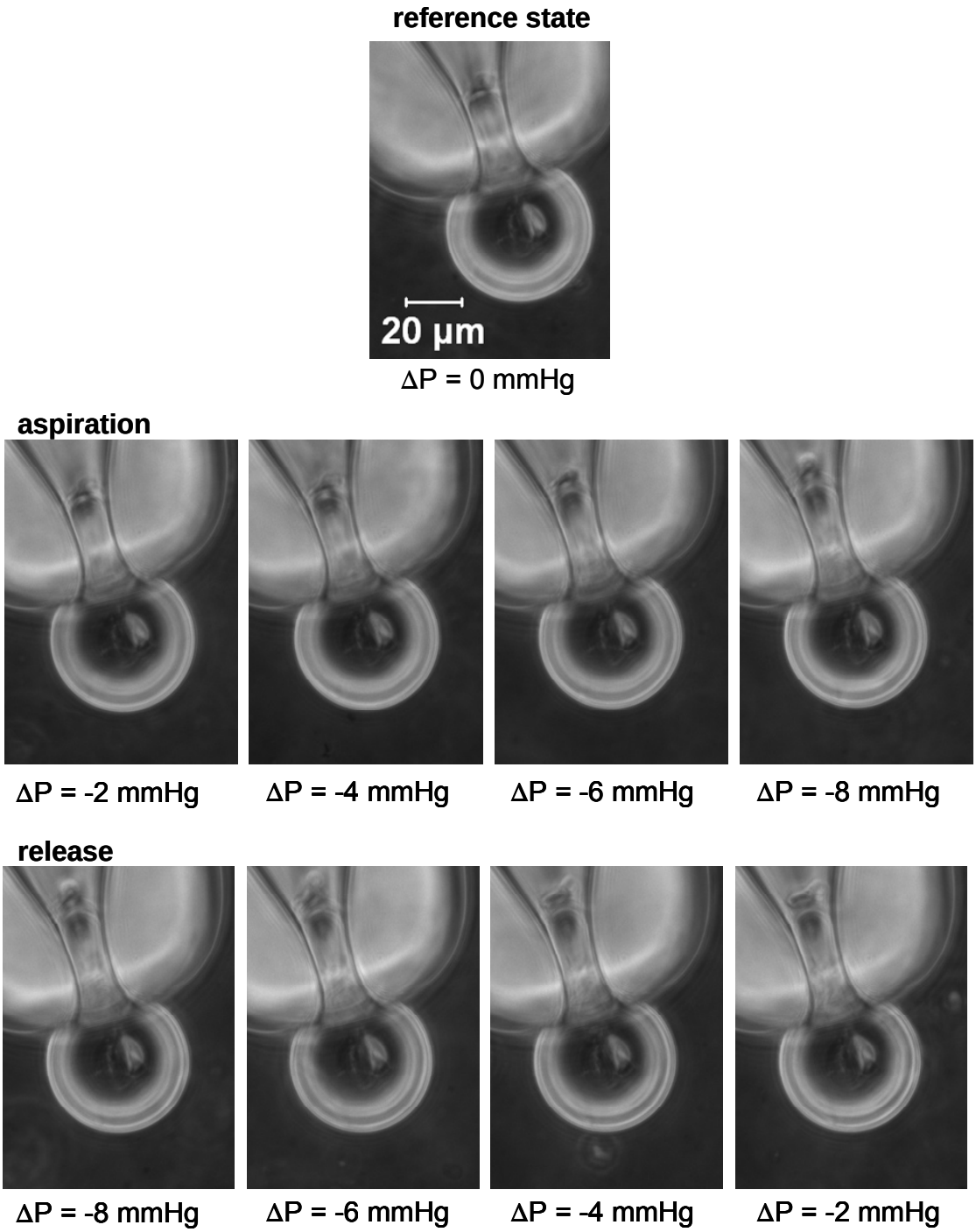

Figure 17: *Images of the aspiration and release of liposome 1, 019-059-01.*

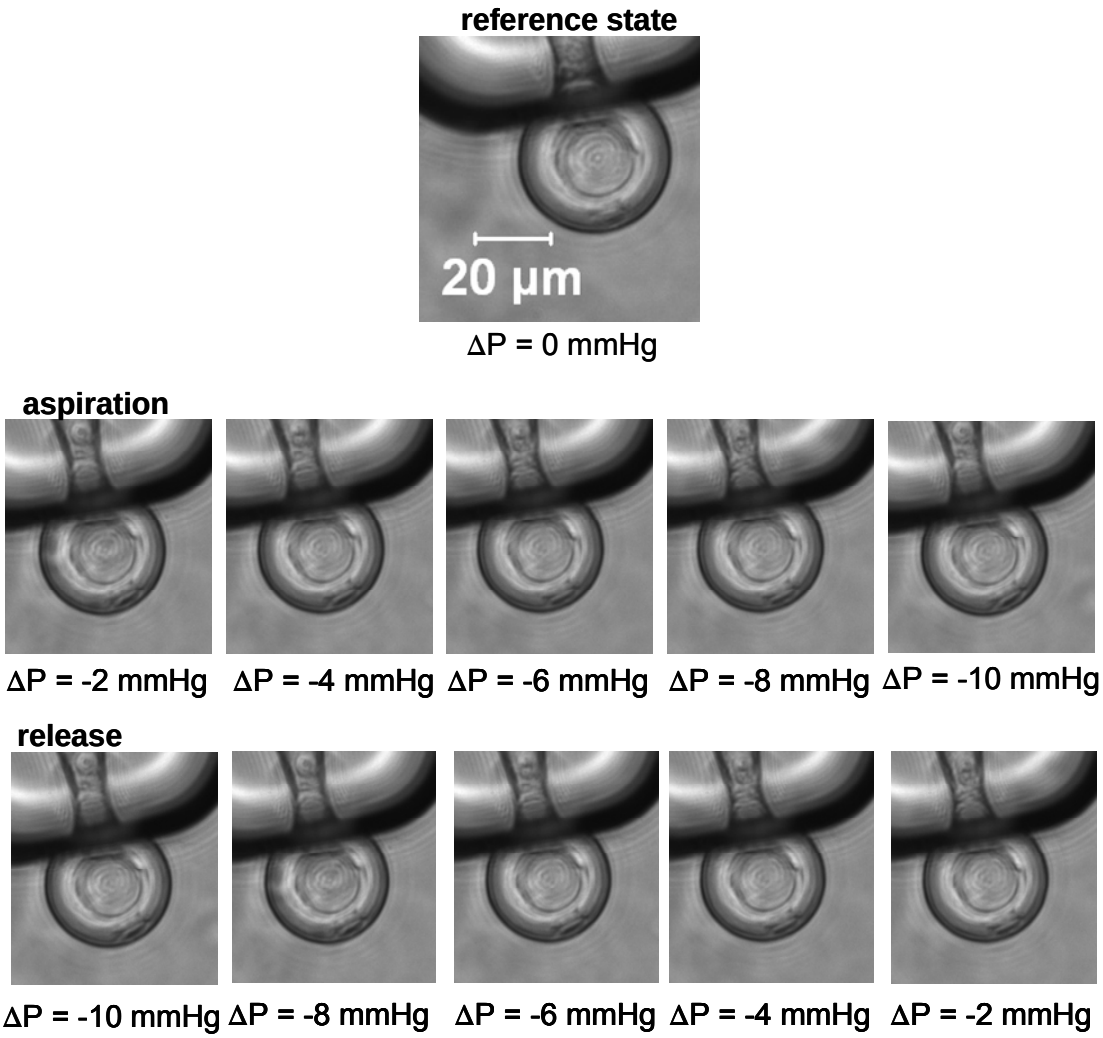

Figure 18: *Images of the aspiration and release of liposome 2, 019-060-02.*

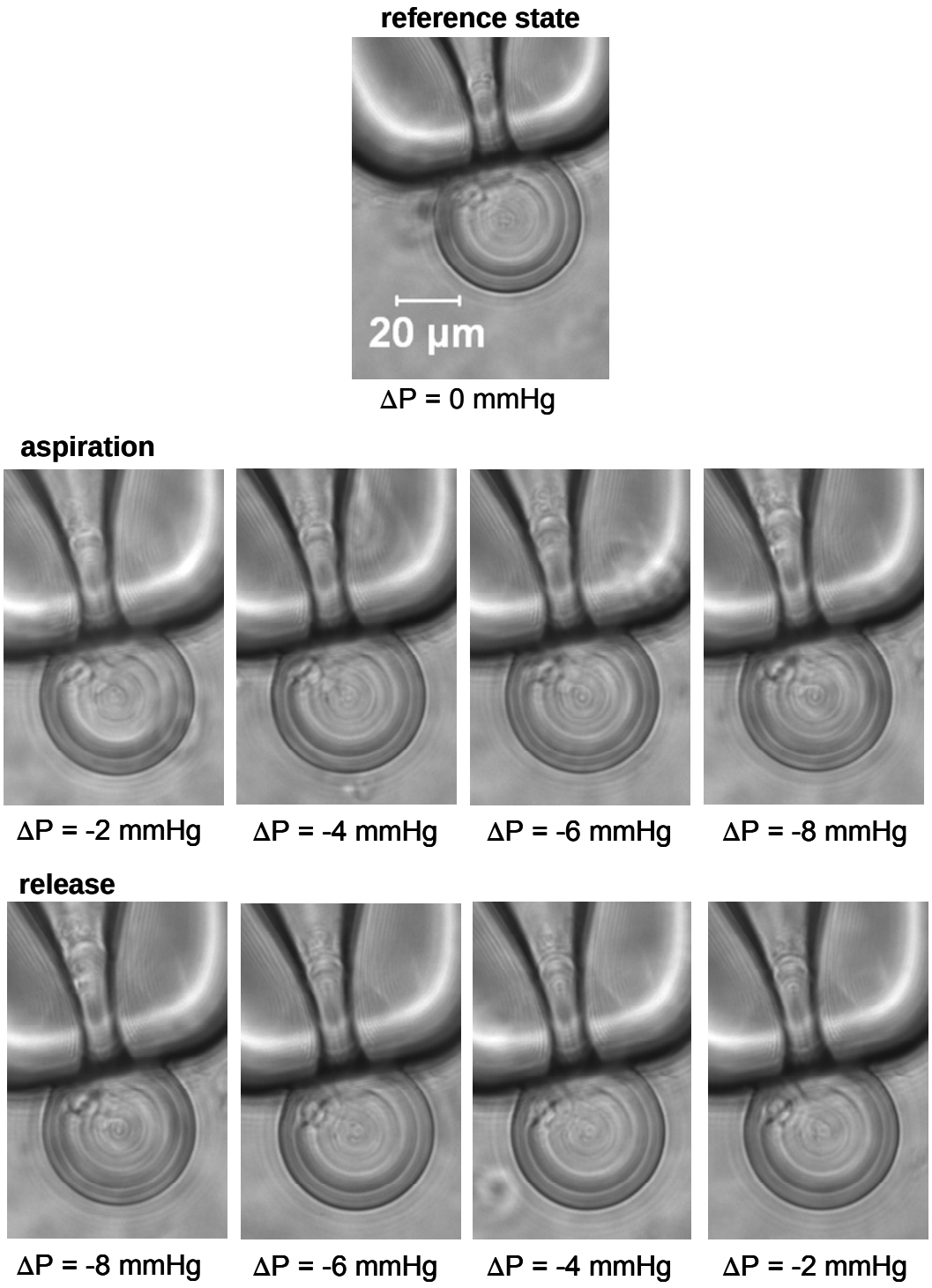

Figure 19: *Images of the aspiration and release of liposome 3, 019-060-04.*

After all of the images during the aspiration and release of the liposomes were collected, they were converted to binary images, and the geometries of the liposomes at each stage of the experiment were determined, Figure 20, Figure 21, Figure 22.

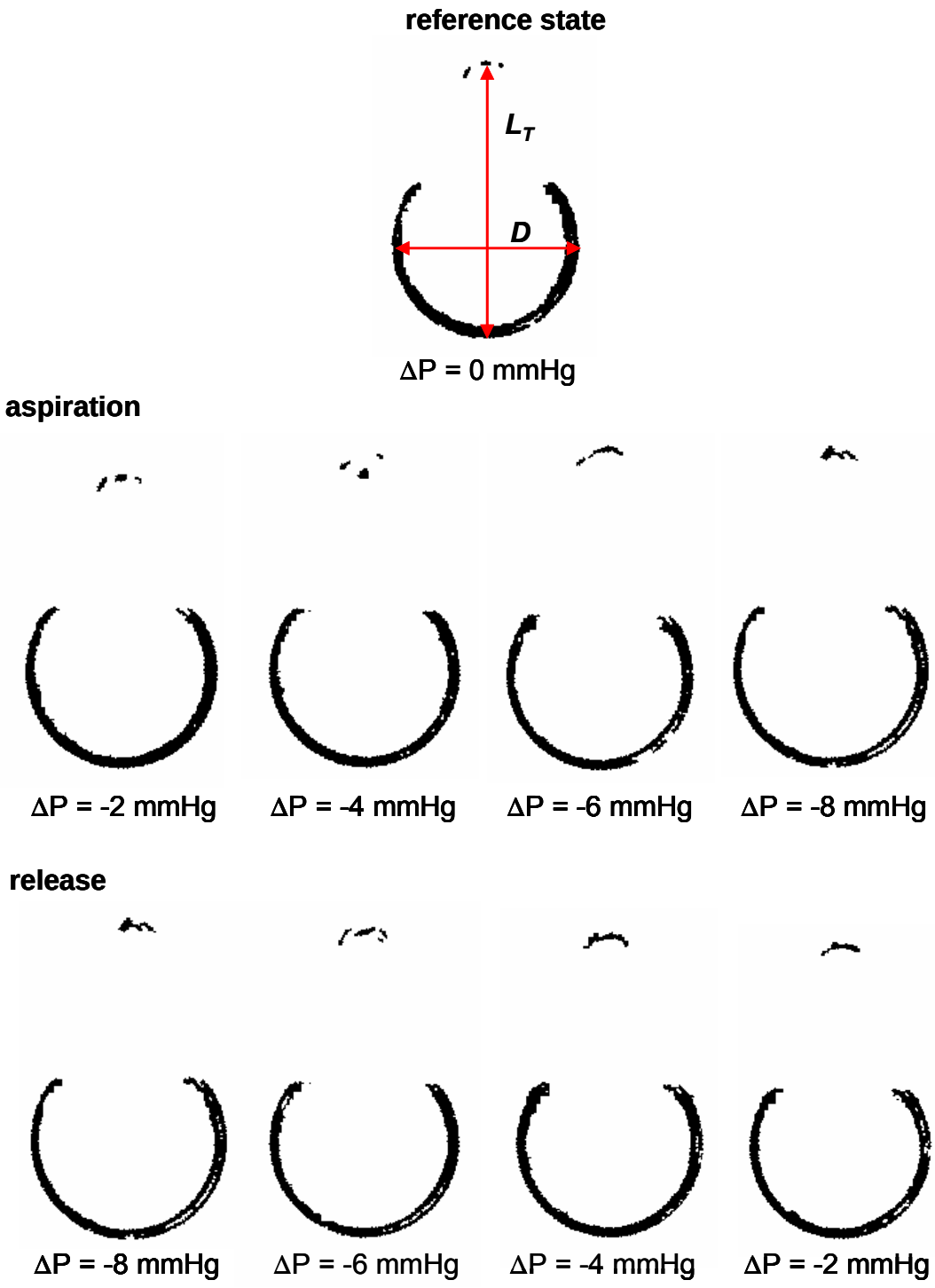

Figure 20: *Binary images of liposome 1 during aspiration and release. The geometry of the liposome at each stage of aspiration was computed using MATLAB.*

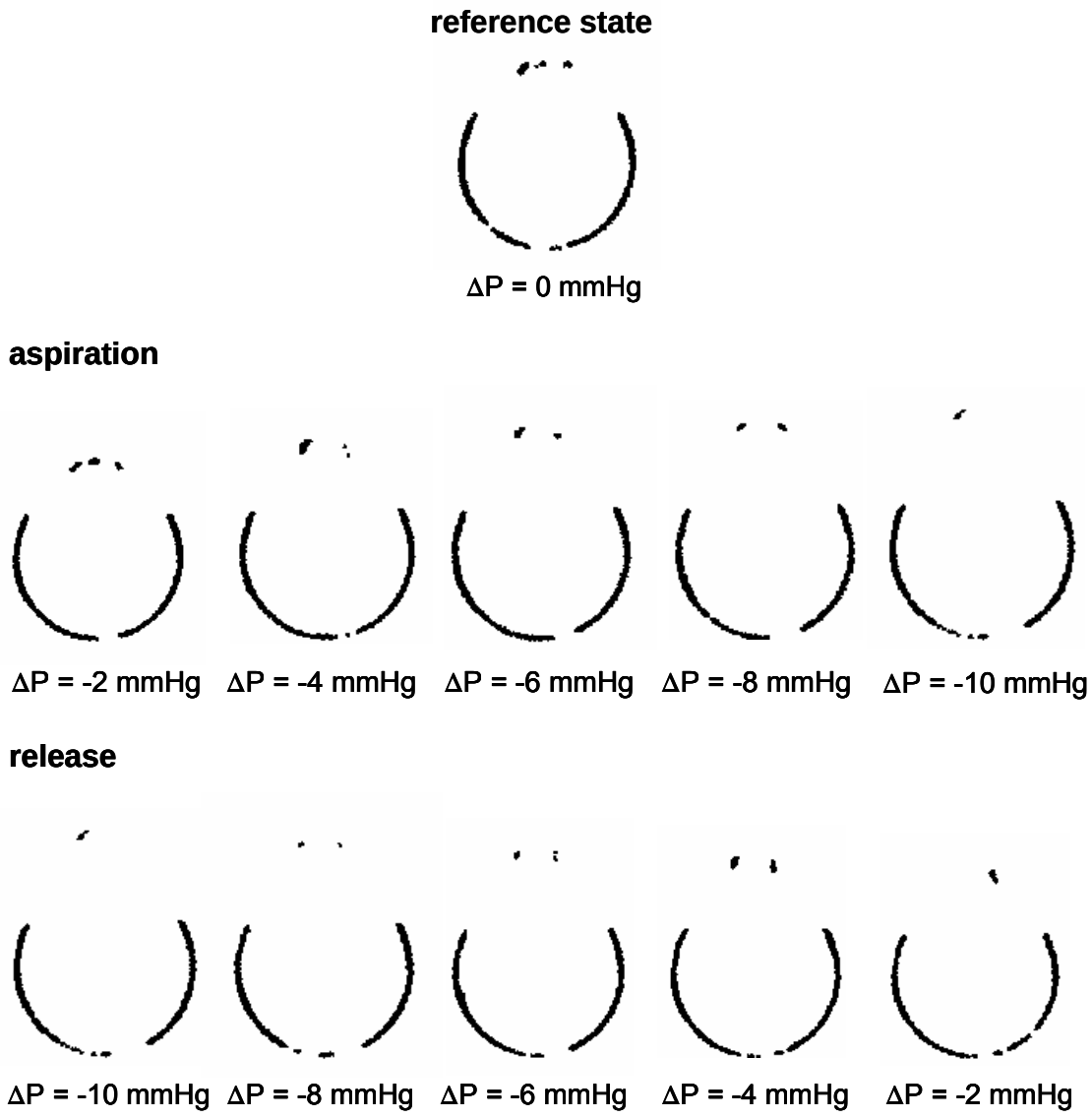

Figure 21: *Binary images of liposome 2 during aspiration and release.*

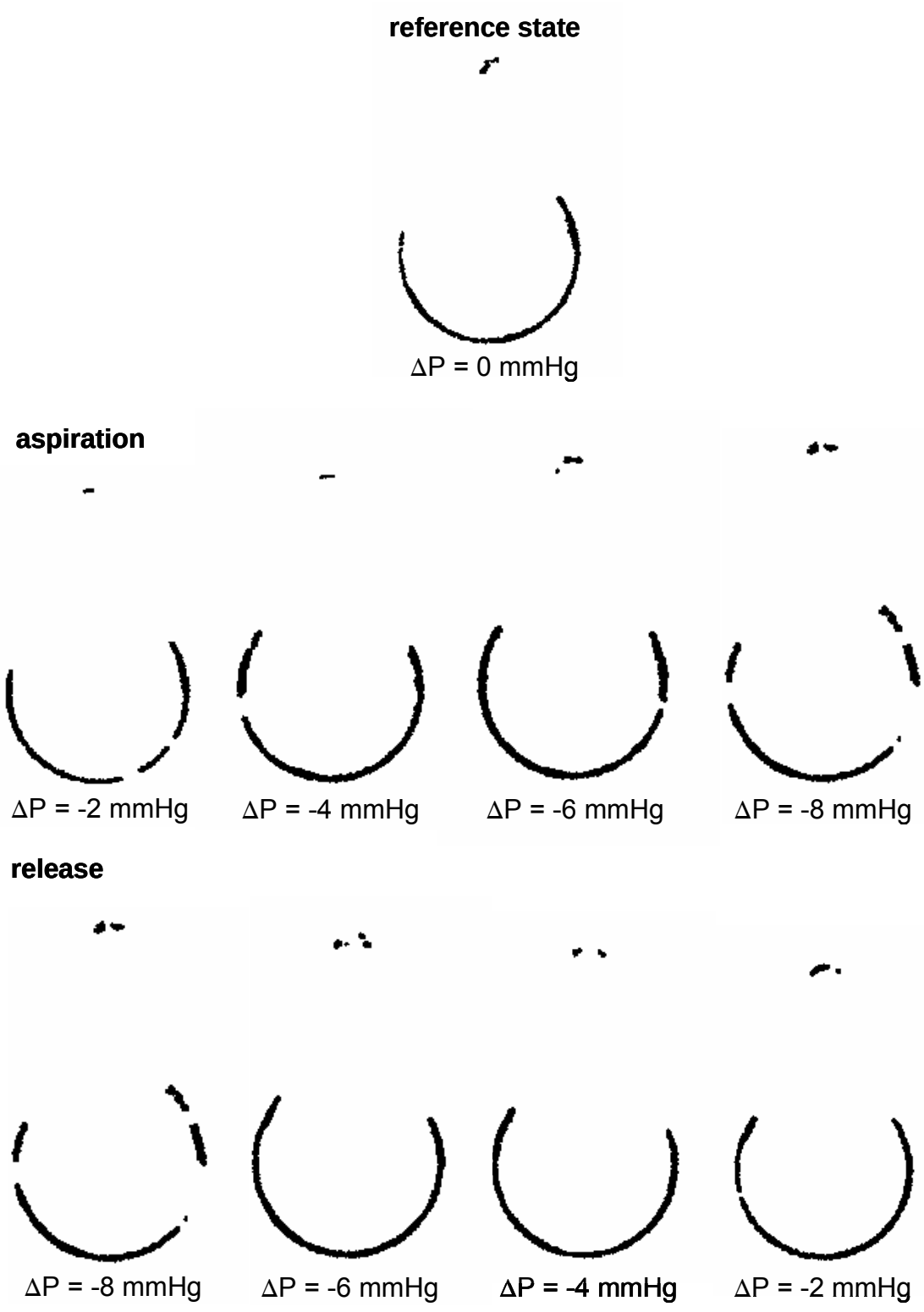

Figure 22: *Binary images of liposome 3 during aspiration and release.*

The changes in pressure, ΔP, and length of the liposome inside the pipette, ΔL, from the liposome's reference state, along with the radius of the liposome, R, at each stage during the experiments were used to calculate the surface tensions, τ, and areal strains, a, for each of the liposomes during their aspiration and release (13) and (14), Table 5. The surface tensions vs. areal strains were then plotted for the aspiration and release of each of the liposomes, Figure 23.

Table 5: *Calculated $\Delta L, \tau$, and α for each pressure differential during the aspiration and release of the liposomes.*

	ΔP (*mmHg*)	ΔL (*μm*)	τ (*N/m*)	α
liposome 1				
aspiration	-2	1.8	0.0007	0.007
	-4	3.9	0.0014	0.015
	-6	6.4	0.0022	0.024
	-8	9.6	0.0029	0.037
release	-8	9.6	0.0029	0.008
	-6	4.1	0.0022	0.017
	-4	4.3	0.0014	0.018
	-2	2.1	0.0007	0.037
liposome 2				
aspiration	-2	0.7	0.0006	0.004
	-4	3.9	0.0013	0.023
	-6	6.0	0.0019	0.035
	-8	6.4	0.0025	0.038
	-10	7.5	0.0031	0.044
release	-10	7.5	0.0031	0.008
	-8	6.4	0.0025	0.027
	-6	6.0	0.0019	0.035
	-4	4.6	0.0013	0.038
	-2	1.4	0.0006	0.044
liposome 3				
aspiration	-2	2.5	0.0007	0.012
	-4	4.2	0.0013	0.020
	-6	5.3	0.0020	0.026
	-8	8.5	0.0027	0.042
release	-8	8.5	0.0027	0.017
	-6	1.0	0.0020	0.019
	-4	3.9	0.0013	0.023
	-2	3.6	0.0007	0.042

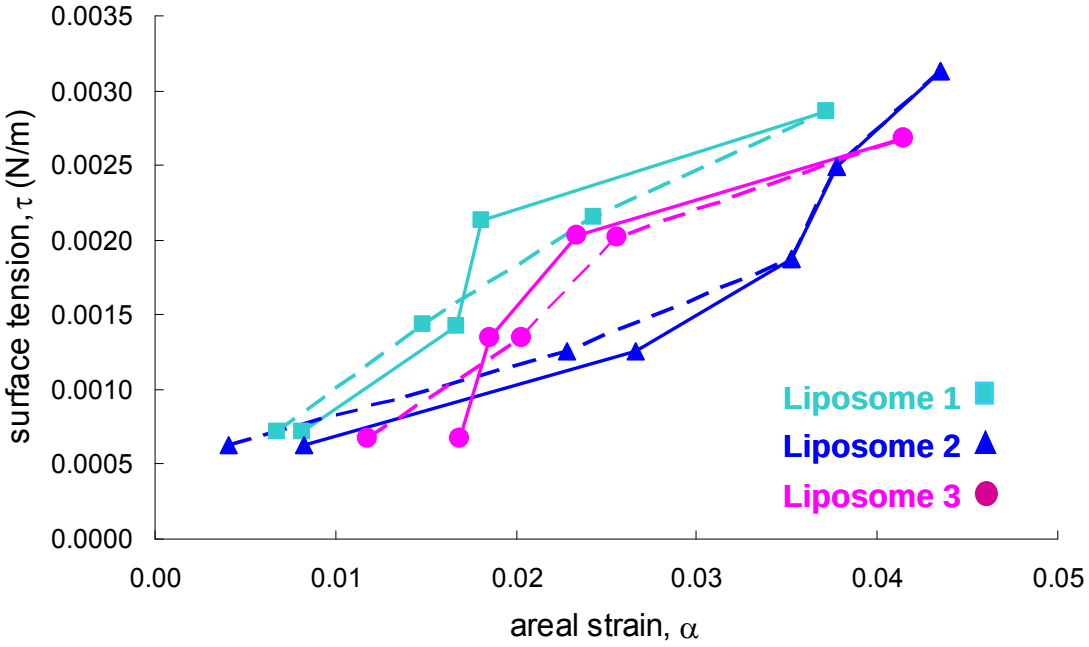

Figure 23: *Liposome surface tension, τ, vs. areal strain, α, for three different liposomes as they were being aspirated and released by the holding pipette. The aspiration of each liposome is represented by the dotted line, and the release of each liposome is represented by the solid line.*

The average slope of the surface tensions vs. areal strains represents the area expansion moduli for the DOPC:DOPS liposomes, 0.067 ± 0.004 N/m (67 dyn/cm), Figure 24. The average area expansion modulus corresponds to an in-plane Young's modulus of 15.0 ± 1.0 MPa (15).

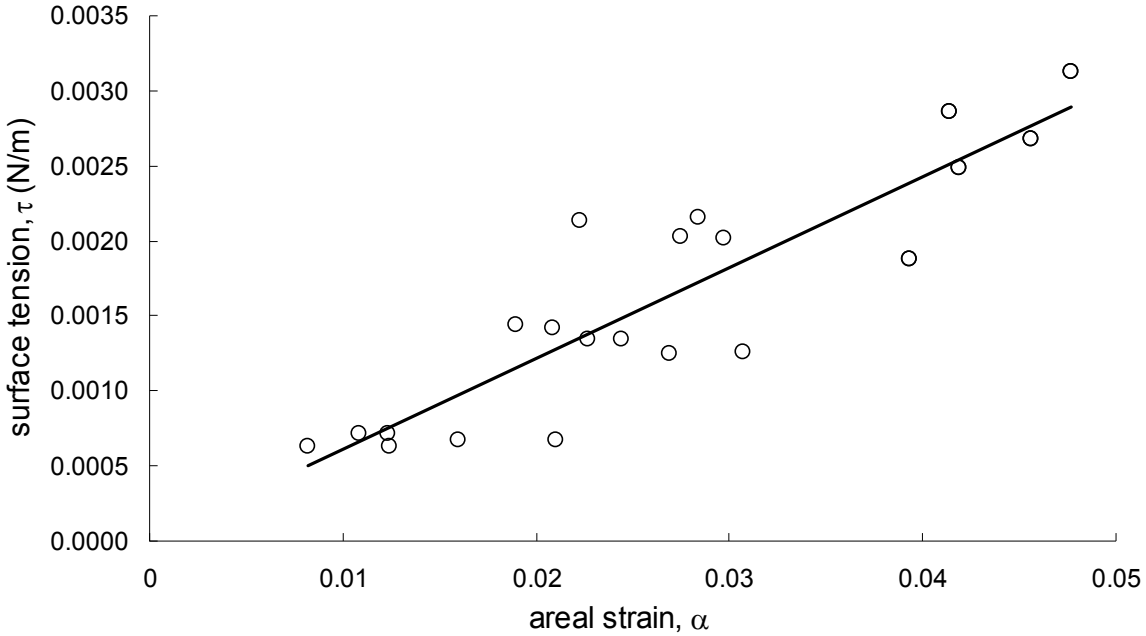

Figure 24: *Surface tensions, τ, vs. areal strains, α, for three liposomes during their aspiration and release. The circles represent the data points, and the solid line represents a linear regression average slope, or area expansion modulus of 0.067N/m.*

Discussion

The lipid composition of a membrane bilayer varies among different species as well as among different cell types within a species (Hulbert 2003). It has been suggested by Hulbert (2003) that the physical characteristics of membrane lipids are important in order for cells to perform their specific functions and thus maintain the overall fitness of an organism. The quantification of the mechanical properties of membranes with different lipid compositions may therefore become increasingly important.

The area expansion modulus of the DOPC:DOPS liposomes was determined to be 0.067 ± 0.004 N/m. This value is within an order of magnitude of the area expansion moduli computed for liposomes composed of other phospholipids (Evans and Rawicz 1990). The area expansion modulus for the DOPC:DOPS liposomes was expected to be

lower than these other phospholipids. The lowest area expansion modulus determined by Evans et al. (1990) was for the 1,2-diarachidoyl-*sn*-glycero-3-phosphocholine (DAPC) liposomes, and this value was computed to be 0.135 ± 0.020 N/m. It had been demonstrated by Evans et al. (1990) that the area expansion modulus decreases as the degree of saturation of the lipids decreases. Unsaturated bonds will cause lipid chain-packing irregularities and increase chain flexibility, and this will lead to less rigid membranes (Lehninger, Nelson et al. 2005). DOPC:DOPS membranes contain unsaturated bonds, whereas DAPC membranes do not, Figure 25. Additionally, shorter-chain fatty acyl groups cause chain packing irregularities as well, resulting in more flexible membranes (Lehninger, Nelson et al. 2005). DOPC and DOPS phospholipids have fatty acyl chains that are eighteen carbons in length, whereas DAPC phospholipids have fatty acyl chains that are twenty carbons long. The unsaturated bonds and shorter chain lengths of the DOPC:DOPS liposomes may account for the lower area expansion modulus.

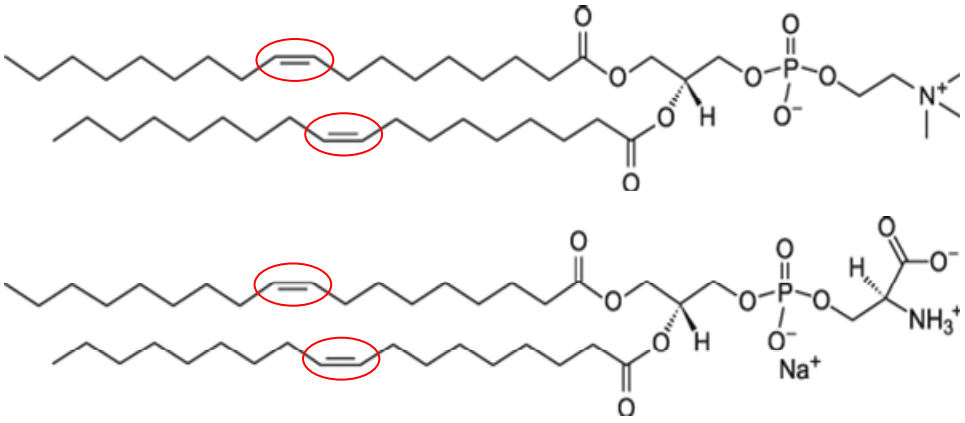

DOPC:DOPS: K_A = 0.067 ± 0.004 N/m

DAPC: K_A = 0.135 ± 0.020 N/m (Evans et al. 1990)

molecular structures of lipids were taken from Avanti Polar Lipids website

Figure 25: *Molecular structure of DOPC, DOPS, and DAPC lipids. The unsaturated bonds in the DOPC and DOPS phospholipids (circled) may account for the smaller area expansion modulus,* K_A*, of the DOPC:DOPS liposomes in comparison to the DAPC liposomes.*

When a liposome was aspirated into a holding pipette at the lowest pressure necessary to “catch” the liposome (a pressure smaller than the resolution of the pressure transducer), the membrane appeared to be taut. Membrane tautness was associated with the spherical, clear edge of the liposome outside the holding pipette. It was assumed that a liposome in this state (reference state) had an areal strain of 0%, and as the aspiration pressure was increased from this state, the areal strain increased as well. Under these assumptions, the calculated areal strain in these experiments exceeded 4%. However, a strain of 3 - 4% would cause membrane lysis (Nichol and Hutter 1996; Boal 2002; Heidemann and Wirtz 2004). Therefore, even though a slightly aspirated

liposome did not appear to contain membrane fluctuations, these undulations most likely existed. Membrane undulations for the DOPC:DOPS liposomes have an estimated amplitude of ~1.4 nm (Marsh 1997), approximately two orders of magnitude smaller than the resolution of the microscope, and they are therefore optically undetectable. The behavior of an undulating membrane is governed by its bending modulus. Since it was not possible to determine when the membrane first became taut during aspiration, the behavior of the aspirated liposome at low pressure was most likely due to a combination of the membrane bending and area expansion moduli. This may have resulted in an error in our calculations.

Experimental uncertainty needs to be considered in order to ensure the validity of the results obtained from our experiments. The measured values in our experiments include the aspiration pressures (via a pressure transducer) and the geometries of the liposomes inside the pipette (measured optically). The pressure transducer has a resolution of 2 mmHg and an accuracy of 1%. The maximum error in the calculated surface tensions of the liposome due to the pressure transducer is therefore ± 0.00004 N/m (Taylor 1994), ~0.06% of our determined area expansion modulus.

The resolution of the 40× objective is 177nm/pixel. However, it was difficult to visually decipher the individual pixels that made up the edge of the liposome. The image processing code may have enhanced the accuracy of our results by standardizing the process in which the pixels that created the edge of the liposomes were determined. The same code was run for all of the images collected during the experiments. Therefore, even if the length measurements themselves were not accurate, the differences in the measurements as the liposomes were aspirated should be accurate,

and it was the differences that were used to calculate our results. The enhanced accuracy of our results due to the use of the image processing algorithm is supported by the small standard deviation of our data, 0.004 N/m, or a dispersion of 6% from the average value. In comparison, Evans et al. (1990) reported an average standard deviation of 15% for their data (Evans and Rawicz 1990). The accuracy of the measurements, standardized analysis, low standard deviation, and literature support of our results reinforce the validity of our findings.

This work serves as a precursor to the numerical quantification of the forces and deformations that liposomes and cells experience during probing and injection. A continuation of this work is detailed in Chapter IV, and together these two chapters are intended to serve as a protocol for determining the forces and deformations associated with single-liposome and single-cell manipulation. Once these forces and deformations are known, a relationship between force, deformation, and liposome or cell damage can be established. This relationship is useful in developing the best practices for single-liposome and single-cell procedures.

Chapter IV: Determination of the Forces Imposed by Micro and Nanopipettes during Liposome Manipulation

Abstract

Using micropipette-deformation methods and an image-processing algorithm for measuring deformation, the bending energies of aspirated DOPC:DOPS liposomes were measured both before and during manipulation of these liposomes with an injection pipette. Using these energy calculations, the forces that injection pipettes of various sizes can exert onto liposomes during probing were determined. Forces ranged from ~1 - 6 pN, and these forces increased as the pipette sizes decreased. The quantification of the amount of force exerted on liposomes or cells during manipulation can assist in minimizing the damage done to these liposomes or cells during single-liposome, single-cell, or single-organelle injections and surgeries.

Introduction

Recent advances in nanotechnology have shown promise in improving healthcare through surgical, tissue engineering, and drug delivery applications (Ebbesen and Jensen 2006). In particular, nanosurgeries, or surgeries on single-cells or single-organelles, are currently being used to modulate and monitor individual cell activity to gain a better understanding of cell behavior (Han, Nakamura et al. 2005; Obataya, Nakamura et al. 2005; Leary, Liu et al. 2006). These nanosurgeries often involve the injection of the cell or its organelles with pharmaceuticals, genetic information, and/or other macromolecules. Although nanosurgeries show great promise, damage to the cell can result during the injection process, and this damage is often fatal to the cell (Laffafian and Hallett 1998; Han, Nakamura et al. 2005; Freedman, Mattia et al. 2007).

For the past twenty years, liposomes have been used as transport vesicles during targeted drug delivery (Gompper and Kroll 1995; Cevc, Schatzlein et al. 2002; Ramachandran, Quist et al. 2006). It has been shown that liposomal vincristine formulations can deliver fifty to one hundred times the amount of drug to a tumor site than when the free drug is injected into the system (Fenske and Cullis 2005). However, the percentage of a drug that is encapsulated into the liposomes during their manufacture is dependent on several factors. These include the composition of the liposomes, the size of the liposomes, and the composition of the drug. These factors combined result in liposome drug encapsulation efficiencies that range from 5% to 95%, where the encapsulation efficiency is equal to the amount of drug inside the liposomes divided by the total drug used during preparation (Semple, Klimuk et al. 2001; Fenske and Cullis 2005; Manojlovic, Winkler et al. 2008; Qiu, Jing et al. 2008). If the encapsulation efficiency of a drug is low, or if only a limited number of liposomes are required for delivery, injecting the drug into the liposomes could be an alternate method of encapsulating the drug into liposomes.

We have created spherical liposomes, determined their mechanical properties, Chapter III (Evans and Rawicz 1990; Allen 2008; Brochu and Vermette 2008), and then measured the change in energy that aspirated liposomes experience during probing with various-sized injection devices. From there, we determined the amount of force that these injection devices exerted onto liposomes during manipulation. Knowing the amount of force that is required for liposome and cell manipulation is essential to minimizing the damage done to liposomes and cells during single-liposome and single-cell injections. By establishing an upper bound for the force that is used during these

procedures, the use of excess force, which can potentially cause damage to the liposome or cell, can be avoided. Additionally, injection and probing devices can be created based on the amount of force and deformation that they will need to withstand during probing, injection, or other manipulation.

Methods

Theory

The liposome membrane can deform in three fundamental modes: bending, dilatation (stretching), and shearing. However, the primary deformation mode for biological membranes is bending (Gompper and Kroll 1995; Hotani, Nomura et al. 1999). When subjected to bending, such as in the formation of a spherical liposome, the outer surface of a membrane bilayer is subjected to a tensile load, and the inner surface to a compressive load.

Hollow, spherical liposome vesicles composed of phospholipid molecules have zero resting tension and therefore experience thermal induced bending fluctuations when they are free to float in solution (Evans and Rawicz 1990; Gompper and Kroll 1995; Marsh 1997). When a liposome is aspirated into a holding pipette (inner diameter ~15 μm) at the lowest pressure necessary to "catch" the liposome, these thermal undulations likely still exist, but at lower wavelengths and higher frequencies. This phenomenon was demonstrated and explained in Chapter III. Furthermore, if a slightly aspirated liposome is probed with an injection pipette (outer diameters ~ 25 nm to 2000 nm), the portion of the liposome outside the holding pipette bends around the injection pipette and conforms to the walls of the injection pipette. The behavior of a liposome when it is free to float in solution, is slightly aspirated into a holding pipette, or when it bends to conform to the

walls of an injection pipette are all governed by the bending modulus of the liposome, Figure 26.

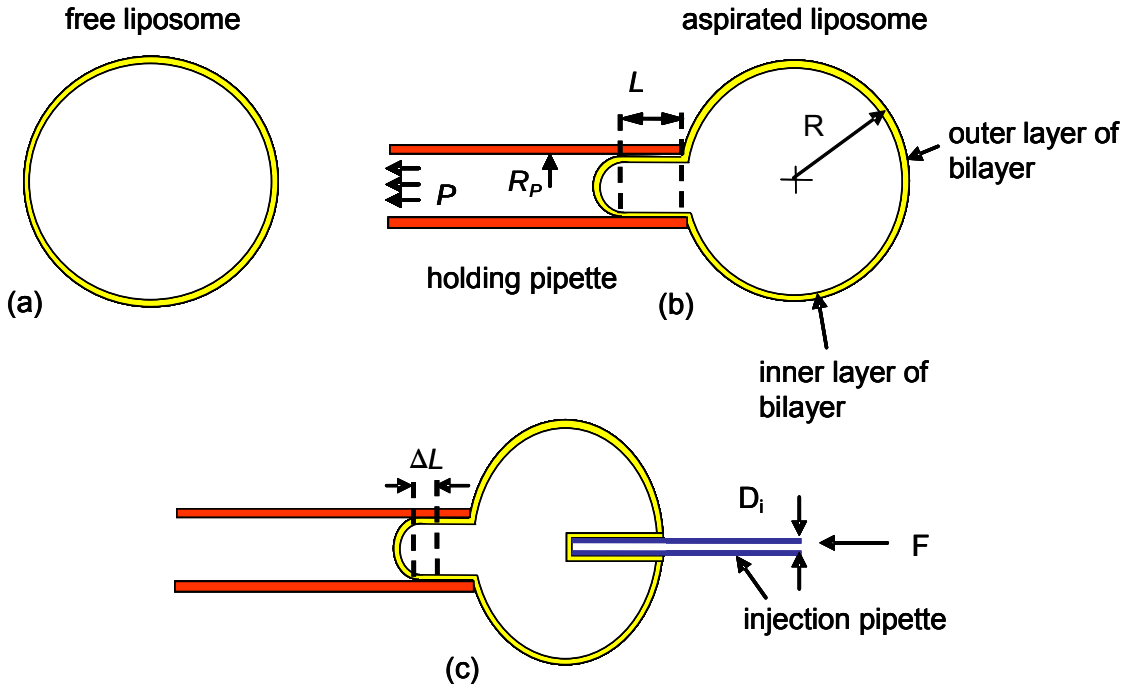

Figure 26: *Cross sectional schematic of a liposome floating freely in solution (a), a liposome aspirated into a holding pipette (b), and an aspirated liposome being probed by an injection pipette with force, F (c).*

A 3% increase in surface area (3% areal strain) has been observed to cause membrane rupture (Nichol and Hutter 1996; Boal 2002; Heidemann and Wirtz 2004). However, the membrane does not rupture when it is probed with the injection pipette, Chapter V. Instead, the length of the liposome inside the holding pipette, *L,* decreases, and the spherical portion of the liposome outside the holding pipette conforms to the walls of the injection pipette. This conformation is due to the translocation of the lipid molecules from areas of the liposome that are not being stressed (inside the holding pipette) to the areas that are being stressed (at the location of the injection pipette),

minimizing the strain on any one molecule in the membrane. This is similar to the translocation of lipid molecules that occurs when microtubules polymerize inside spherical vesicles, creating vesicles that have a spherical center and long tubular projections. In this situation, lipid molecules move from the spherical portion to the tubular portion of the liposomes (Hotani and Miyamoto 1990). The surface area of the membrane is assumed to remain the same during the probing of the liposome with the injection pipette. The surface areas of the liposomes both before and after probing with the injection pipette have been estimated, and the results support this assumption.

The total energy of the liposome includes both its local and non-local bending energies (Morikawa *et al.*, 1999; Jung *et al.*, 2002; Svetina and Zeks, 2002; Majhenc *et al.*, 2004). The non-local bending energy is due to the bending of the two layers of the bilayer in the relationship to each other. This relationship has shown to be particularly important in determining the shape behavior of liposomes during tether pulling experiments (Waugh, Song et al. 1992). The difference in the energy of the liposome from its aspirated state to its probed state is accounted for by the change in the bending energy of the liposome as it is probed by the injection pipette.

The local bending energy of a liposome is determined from,

$$E_b = \int [\frac{1}{2}\kappa_B (c_1 + c_2 + c_0)^2 + \kappa_G (c_1 c_2)] dA \,, \tag{16}$$

where E_b is the local bending energy of the membrane, κ_B is the mean bending modulus of the membrane, c_1 and c_2 are the principal curvatures of the membrane, c_0 is the spontaneous (intrinsic) curvature of the membrane, κ_G is the Gaussian bending modulus of the membrane, and A is the surface area of the neutral plane of the membrane bilayer

(Bozic, Svetina et al. 1992; Gompper and Kroll 1995; Morikawa, Saito et al. 1999; Boal 2002; Jung, Lee et al. 2002).

The non-local bending energy is determined from,

$$E_r = \frac{1}{2}\frac{K_r}{A}(\Delta A_{io} - \Delta A_{0io})^2, \tag{17}$$

where E_r is the non-local bending energy of the membrane, K_r is a measure of the relative expansivity of the two layers of the bilayer, ΔA_{io} is the difference in the surface areas of the inner and outer membranes, and ΔA_{0io} is the difference in surface areas between the lowest energy state of the two layers of the bilayer (Lasic 1996).

The mean bending modulus of the membrane, κ_B, has been predicted to be proportional to the area expansion modulus of the membrane and scale as the square of the membrane thickness (Helfrich, 1974; Bloom *et al.*, 1991; Boal, 2002; Marsh, 2006). This has been estimated as,

$$\kappa_B = \frac{K_A t^2}{24}, \tag{18}$$

where K_A is the area expansion modulus of the membrane, and t is the thickness of the bilayer (Rawicz, Olbrich et al. 2000). The area expansion modulus is the tension that is required for a unit increase in strain. The area expansion modulus of the DOPC:DOPS liposomes has previously been determined to be 0.067 N/m, Chapter III. This was done using a micropipette aspiration technique similar to that developed by Evans et al. (1990) (Evans and Rawicz 1990).

The spontaneous curvature is the curvature of a membrane that may arise due to compositional inhomogeneities in the two layers of the bilayer, or to differences in the solution inside and outside of the liposomes (Boal 2002; Jung, Lee et al. 2002; Majhenc,

Bozic et al. 2004). The two layers of the DOPC:DOPS liposomes are considered to be composed of the same chemical composition, and the solution inside and outside the liposomes is the same, 0.9% saline solution. The spontaneous curvature of the membranes of the DOPC:DOPS liposomes was therefore taken to be zero.

The Gaussian bending modulus, which affects the local bending energy of the liposome, is the modulus for the shear deformation of the membrane (Templer 2003). For a phospholipid bilayer, a fluid membrane, shear stress is not supported, and κ_G has been estimated to be approximately zero (Marsh 2006). K_r has been estimated as $K_A/4$ (Lasic 1996). Assuming the two layers of the bilayer are composed of the same type and number of phospholipid molecules, ΔA_{0io} is also zero. The total bending energy of an aspirated liposome, E, is then reduced to,

$$E = \int \frac{K_A t^2}{48}(c_1 + c_2)^2 dA + \frac{K_A}{8A}(\Delta A_{io})^2 \quad . \tag{19}$$

An aspirated liposome can be created by a combination of two to three shapes. The shapes that create the aspirated liposome are determined by the relationship between L and R_P. These shapes include: a sphere, a spherical or spheroidal cap, and if $L > R_P$, a cylinder, Figure 27.

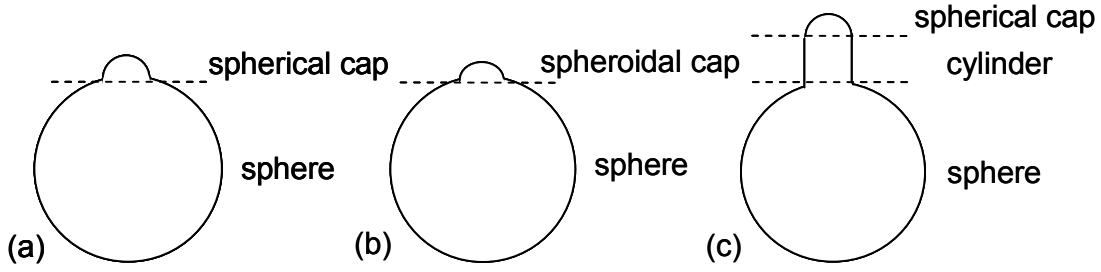

Figure 27: *The shapes composing an aspirated liposome are dependent on the relationship between L and R_P: (a) $L = R_P$, (b) $L < R_P$, (c) $L > R_P$.*

Similarly, an aspirated liposome that is being probed with an injection pipette is also composed of a combination of shapes, Figure 28. When the injection pipette is inserted into the spherical portion of an aspirated liposome, the spherical portion of the liposome outside the holding pipette becomes spheroidal in shape, and a conical frustum indentation representing the injection pipette is created inside this spheroidal shape. Additionally, L decreases.

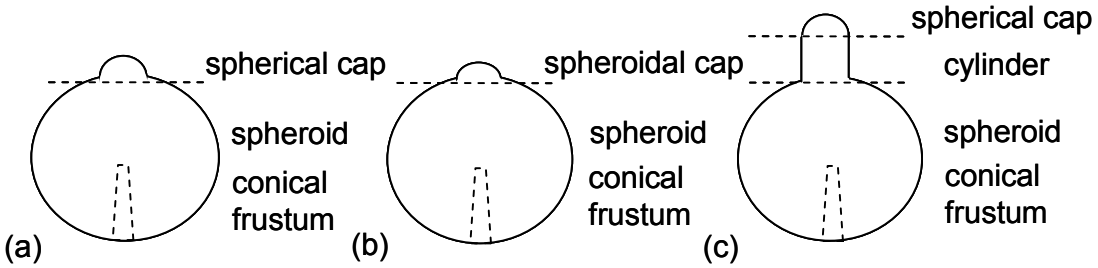

Figure 28: *The shapes composing an aspirated liposome that is being probed with an injection pipette are dependent on the relationship between L and R_P: (a) $L = R_P$, (b) $L < R_P$, (c) $L > R_P$.*

The energy of an aspirated liposome is equal to the sum of the bending energies of the individual shapes that create the liposome. The energy exerted onto the liposome by the injection pipette is equal to the difference in the energy of the liposome from its pre-probed to its probed state. The force in which the injection pipette exerts onto the liposome is then,

$$\overline{F} = \frac{\Delta E}{\Delta x}, \tag{20}$$

where $\overline{F}$ is the force of the injection pipe, ΔE is the change in the bending energy of the liposome from its pre-probed to probed state, and Δx is the change in the distance in which the injection pipette is inserted into the liposome.

Liposome Creation

Hollow, spherical liposome vesicles were created from a phospholipid membrane based on the method of Fygenson et al. (1997) (Fygenson, Elbaum et al. 1997). Liposomes were composed of DOPC:DOPS (7:3) phospholipids. A full explanation of liposome creation is described in Chapter III. The liposomes created were ~10-50 μm in diameter with a thickness of ~4.5 nm (Boal 2002; Kucerka, Pencer et al. 2007).

Experimental Setup

The liposome aspiration and probing experiments were performed on an inverted light microscope (Olympus IX-81) with a 400× total magnification, Figure 29. To reduce background vibrations, the microscope was floated on a TMC 63-500 vibration table. Liposomes were aspirated with a CellTram air pressure transmitter (Eppendorf), and pressure measurements were recorded using a Traceable® pressure meter (Control Company) with a resolution of 2 mmHg (~ 266 Pa). The holding pipettes had an inner diameter of ~15 μm (Eppendorf Vacutips), and their tips were bent at 35˚ angles. The holding pipette was installed in the left micromanipulator so that its tip was parallel to the microscope stage. Liposomes were probed with injection pipettes having outer diameters that ranged from 25 nm (in-house pulled quartz pipettes) to 2000 nm (World Precision Instruments, Sarasota, FL). The tips of the injection pipettes were not bent. An adapter for the right micromanipulator was created in order for the injection pipettes to be nearly parallel (< 5˚) to the tip of the holding pipette and microscope stage. The movements of both the holding pipette and the injection pipette were controlled using two Eppendorf NK-2 micromanipulators (B&B Microscopes, Ardmore, PA). The manipulators were controlled manually, using the manipulator joystick, and through a serial port that

connected the manipulators to a compute. The "Hyper Terminal" program supplied with Windows® was used to control the manipulators remotely. Images of the liposomes during the experiments were taken using SPOT Advanced software (Sterling Heights, MI).

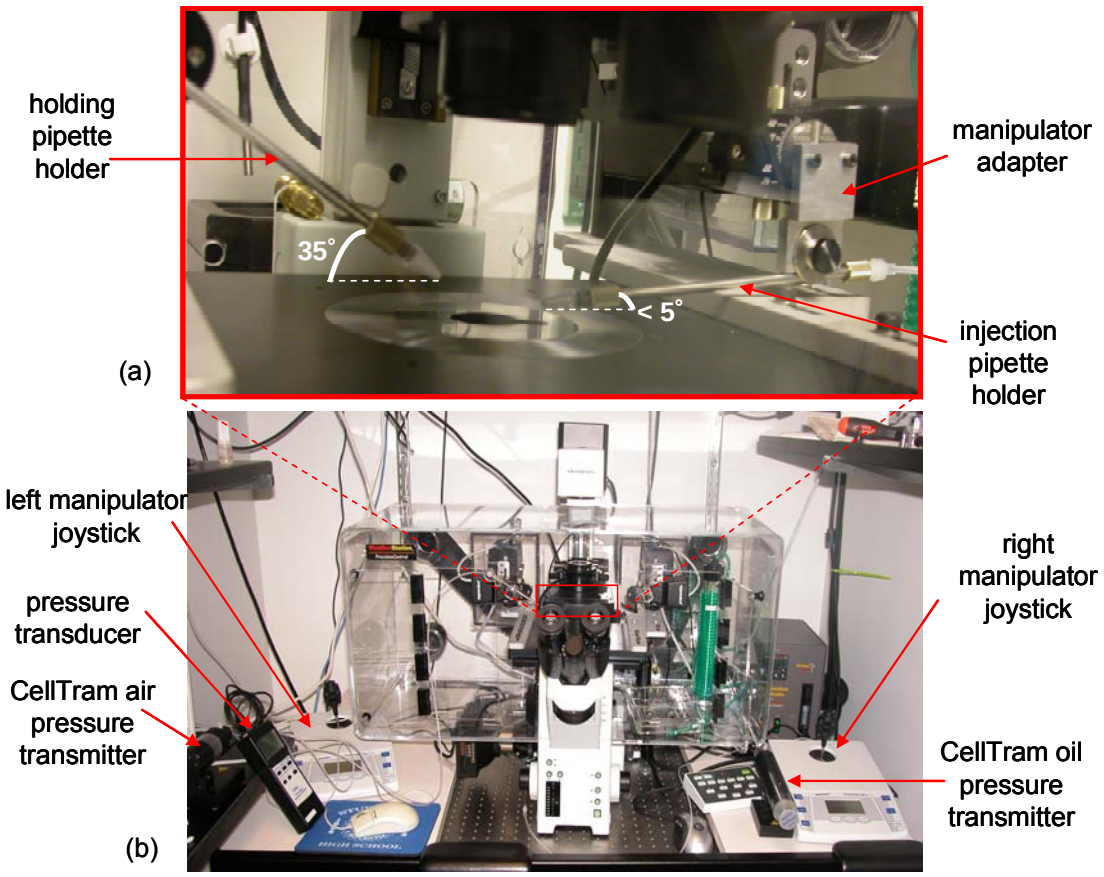

Figure 29: *Photo of the experimental setup (b) with a close up of the pipette holders (a). The pipette holders are aligned so that the pipettes are parallel to the stage. An adapter was built for the right micromanipulator in order to probe the liposomes at a small angle (< 5°).*

A coverslip was placed on the microscope stage and 100 µL of 0.9% (w/v) saline solution was deposited onto the coverslip. Next, 10 µL of liposome solution was added to the center of the saline droplet. After the liposomes were added to the saline solution,

the holding pipette was inserted into the grip head of the pipette holder that was connected to the CellTram air pressure transmitter. The pipette holder was then attached to the left micromanipulator so that the tip of the pipette was directly above the solution on the coverslip. Next, the injection pipette was inserted into the grip head of the CellTram oil pressure transmitter, and the injection pipette was connected to adapter on the right micromanipulator.

Once the setup was complete, the joystick was used to position the tip of the holding pipette into the microscope field of view. To do this, the *x* and *y* positions of the manipulator were adjusted using the course control of the manipulator (manipulator speed 4000 μm/sec). The height of the pipette above the coverslip (*z* position) was not adjusted at this time. When the light from the microscope could be seen on the tip of the pipette, the pipette was considered to be within the microscope field of view. Next, the 10× objective was used to focus on the liposomes that were floating within the saline solution. While looking through the eyepiece of the microscope, the joystick was used to move the manipulator fore and aft (*y* direction). A shadow from the pipette could be observed through the eyepiece, and when the pipette shadow was in the center of the field of view, the manipulator was locked in the *y* direction. Next, the joystick was used to lower the pipette tip into the saline solution (*z* direction). When the pipette tip had entered the solution, the manipulator was switched to fine control (manipulator speed 450 μm/sec), and the tip of the pipette was slowly brought into focus.

After the tip of the holding pipette and the liposomes were in focus, the *y* direction of the left manipulator was unlocked, and the holding pipette tip was manipulated in the *x* and *y* directions until it was next to a liposome that appeared to be ~45 μm in diameter.

Both unilamellar (composed of a single bilayer) and multilamellar (composed of multiple bilayers) liposomes were used in the experiments. Next, suction was created by increasing the piston volume of the CellTram pressure transmitter until the chosen liposome was "caught" by the holding pipette. The aspiration pressure was then decreased slowly until the smallest pressure necessary to hold the liposome inside the pipette was applied to the liposome. At this time, the aspiration pressure inside the pipette was smaller than the resolution of the pressure transducer, but the membrane of the liposome that was inside the pipette had conformed to the walls of the pipette, and the membrane of the liposome that was outside of the pipette was spherical.

Next, the injection pipette was manipulated above the saline solution in the *x* and *y* directions until the shadow of the injection pipette was observed in the microscope field of view. The injection pipette was then slowly lowered into the liposome solution (manipulator speed 100 μm/sec) until the injection pipette was aligned opposite the holding pipette on the other side of the liposome. Once the pipettes were aligned, the 40× objective (resolution of 177 nm/pixel) was used for the remainder of the experiment.

A test was conducted to ensure that the injection pipette was inserted into the liposome at the mid-plane of its *z* axis. This was considered to be the equator of the liposome. To find the equator, the injection pipette was manipulated so that it was in contact with the aspirated liposome. The injection pipette was then slowly moved up and down in the z-direction, and the deformation of the liposome was observed. The presumed equator of the liposome corresponded with the *z*-location of the injection pipette in which maximum liposome deformation occurred, Figure 30.

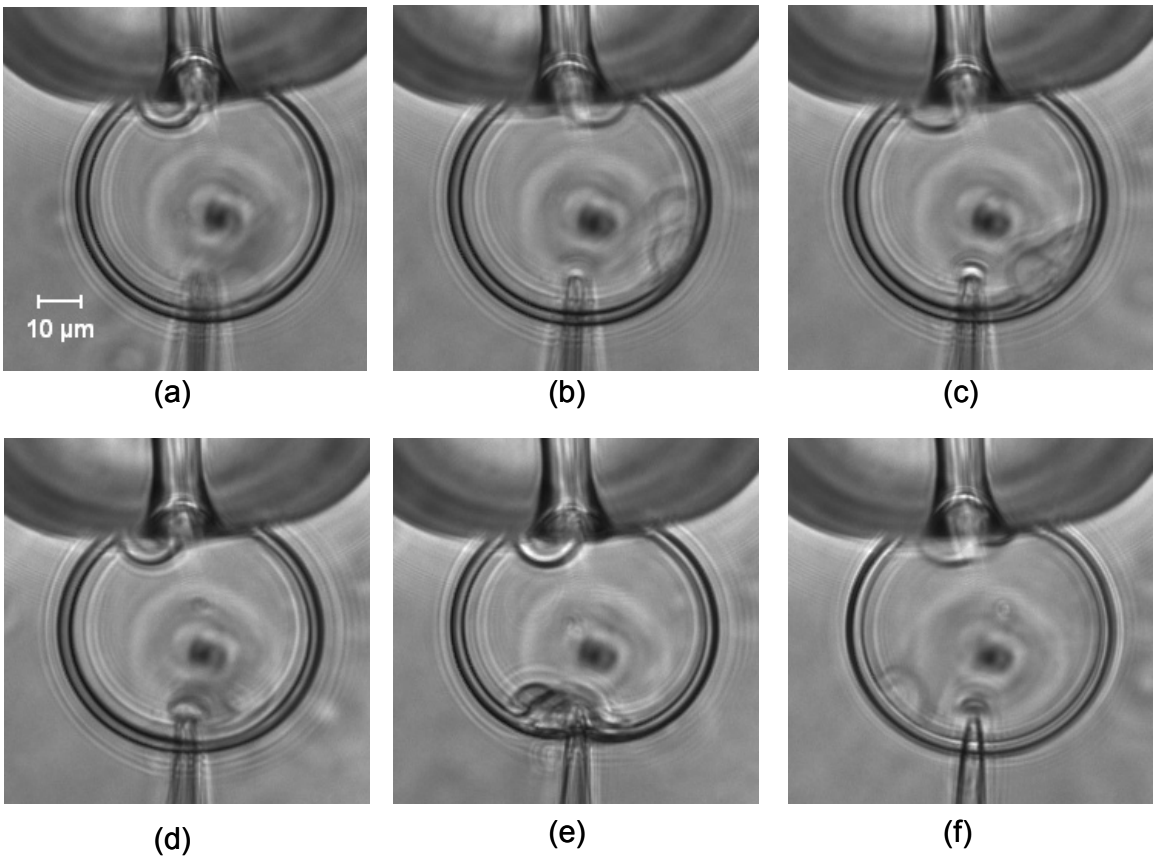

Figure 30: *Injection pipette positioned below the equator of the liposome (a). The pipette is slowly raised in the z direction, and the deformation of the liposome is observed (b-f). The injection pipette is assumed to be at the equator of the liposome when the maximum deformation of the liposome is observed (e).*

Once the equator of the liposomes was located, the injection pipette was manually manipulated until it was as close to the liposome as possible without touching the membrane. The injection pipette was aligned at the center of the liposome along the *x*-direction. The manipulator speed was 100 µm/sec during the manual manipulation of the injection pipette. After aligning the injection pipette, the manipulator was set to remote control. The rest of the liposome manipulations were conducted through the computer using the Hyper Terminal program.

The injection pipette probed the liposome in a controlled manual. First, the position of the manipulator, in microsteps, was retrieved. A manipulator microstep is ~40 nm. Once the position of the injection pipette was known, an image was captured of the aspirated liposome. Next, the injection pipette insertion distance, Δx, and the injection pipette speed were entered into Hyper Terminal. All position and velocity inputs were entered into Hyper Terminal in microsteps and microsteps/sec, respectively. Injection pipette insertion distances were set to either 10 μm (250 microsteps) or 20 μm (500 microsteps), and the injection pipette insertion speed was set to 4 μm/sec (100 microsteps/sec). The injection pipette was then inserted into the liposome. An image of the liposome with the injection pipette probing the liposome was collected, and then the injection pipette was moved back to its original location at the same velocity.

Three different injection pipettes were used in the experiments. Injection pipettes were purchased with outer diameters of ~ 200 nm and ~ 2000 nm (inner diameters 100 nm and 1000 nm, respectively from World Precision Instruments) and the in-house pulled quartz pipette had an outer diameter of ~ 25 nm. For the 200 nm and 25 nm outer diameter pipette sizes, three different liposomes were probed three times each at the two pipette insertion distances. The 2000 nm outer diameter pipette probed three different liposomes three times each at an insertion distance of 10 μm. This resulted in a total of nine different liposomes being used in the experiments, three for each pipette size. The repeated probing of the liposome was done to determine if any permanent deformation resulted when the injection pipette was inserted into the liposome. Images were collected both before and during the probing of the liposome.

Liposome Bending Energy Determination

Once all of the 256, grayscale images were collected, they were imported into MATLAB in JPG format (size 201 x 277 pixels). A MATLAB algorithm was written that would perform the following manipulations to each image: crop the image to isolate the liposome from the background, perform histogram equalization to the image to enhance its contrast, and convert the grayscale image to a binary image based on a user-specified threshold, Appendix B. The threshold value chosen ranged from 0.2 - 0.3, and the same threshold value was used for the pre-probed and probed images of each liposome used in the experiments. Changes in the focus and brightness of the different liposomes required that the threshold value be slightly adjusted for each set of experiments. The processed, binary image was saved as a bitmap, and then Paint Shop Pro was used to manually remove pixels from the image. This involved removing pixels from the image that did not represent the edges of the liposome or the outer edge of the holding pipette with the Magic Wand tool. The Magic Wand tool selects all neighboring pixels that have the same threshold value as the selected pixel, threshold value 1. The "cleaned" images were then imported into another MATLAB algorithm where the diameter of the liposome outside the pipette, D, and the total length of the liposome, L_T, were determined for all of the images of the aspirated liposome before manipulation, Appendix C. The distance between the leftmost and rightmost pixels with a threshold value of 1 was taken as D, and the distance between the uppermost and lowermost pixels with a threshold value of 1 was computed as L_T. Once D and L_T were known for each of the aspirated liposomes, the radius of the liposome outside the pipette, R, was determined

from $R = D/2$, and the length of the liposome inside the pipette, L, was determined from $L = L_T - D$ for each image.

For the aspirated, probed liposomes, the distances between the uppermost and lowermost pixels were also taken as L_T, but the distances between the leftmost and rightmost pixels were taken as the width of the spheroidal portions of the liposomes outside the holding pipette, W. Once L_T and W were found for an image, the area of the liposome inside the holding pipette was removed from the cleaned, binary image using Paint Shop Pro. The MATLAB code was then run again, and the distance between the uppermost and lowermost pixels with a threshold value of 1 was determined. This was taken as the height of the spheroidal portion on the liposome, H. For the aspirated, probed liposome, $L = L_T - H$, Figure 31.

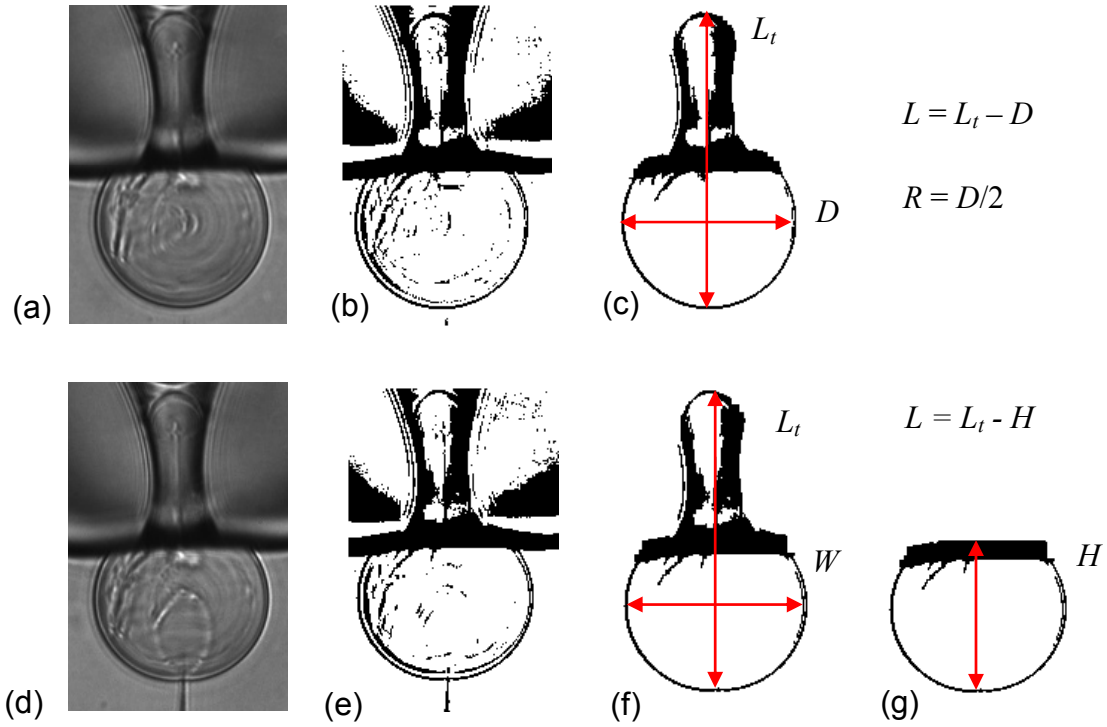

Figure 31: *Image of an aspirated liposome, 019-112-02, (a). The binary image was created in MATLAB (b), "cleaned" in Paint Shop Pro (c), and then MATLAB was used to determine L and R. Image of this same liposome with the 25 nm outer diameter injection pipette inserted 10 μm into the liposome (d). This image was also converted to a binary image (e), "cleaned" in Paint Shop Pro (f), and the total length of the aspirated-probed liposome, L_t, and W were determined. Next, the area inside the pipette was removed using Paint Shop Pro (g), and the MATLAB image processing code was run again on this image to compute H.*

The outer membranes of the bilayers of the liposomes that were outside the holding pipette had dimensions *R, W,* and *H*. The inner layers of the bilayers had dimensions of *R - t, W - t,* and *H - t*. The outer layer of the cylindrical section of the liposome inside the pipette was taken as R_P. The inner layer of this section had a radius of $R_P - t$. Similarly, the outer layer of the spherical or spheroidal cap inside the pipette had a height of R_P or *L* and a width of R_P, and the inner membrane of this cap had a height of $R_P - t$ or $L - t$ and a width of $R_P - t$. The outer radius of the injection pipette tip, R_i, corresponded to the radius of the inner layer of the membrane at the conical indentation in the spheroidal portion of

the probed liposome. The outer layer of the membrane at the tip of the conical indention had a radius of $R_i + t$. Similarly, the outer radius of the injection pipette at Δx, R_{ie}, corresponded to the inner layer of the membrane at the base of the conical indentation, and the therefore the outer layer of the membrane of the liposome at this location was $R_{ie} + t$. The neutral plane of the membrane was measured as midway between the outer and inner layers of the membrane. The calculations for the surface areas and bending energies of the pre-probed and probed liposomes were based on the geometries of the neutral plane of these liposomes, and they were computed using MATLAB, Appendix D.

The surface areas and curvatures of the liposomes before and during probing were calculated in order to determine the bending energies of the individual shapes that created the aspirated liposome (19). For the aspirated, pre-probed liposome, the surface area of the spherical portion of the liposome was determined from,

$$A_{sphere} = 4\pi(R - \frac{t}{2})^2 - \pi R_P{}^2, \tag{21}$$

where A_{sphere} is the surface area of the neutral plane of the spherical portion of the aspirated liposome outside the holding pipette. The term $\pi R_P{}^2$ represents the surface area at the opening of the holding pipette. This is not included in the surface area of the spherical section of the liposome.

The surface area of the cylindrical section of the liposome inside the holding pipette is,

$$A_{cylinder} = 2\pi(R_p - \frac{t}{2})(L - R_p), \tag{22}$$

where $A_{cylinder}$ is the surface area of the neutral plane of the cylinder inside the holding pipette. The surface area of the spherical cap inside the holding pipette is similar to (21),

but R_P is substituted for R, and the area is divided by two. For the spheroidal cap, the surface area can be approximated with a maximum error of 1.2% as,

$$A_{spheroidcap} = \pi(n^2 + mop(1 - \frac{m^2 - n^2}{6m^2} p^2 (1 - \frac{3m^2 + 10n^2}{56m^2} p))), \quad (23)$$

where $A_{spheroidcap}$ is the surface area of the neutral plane of the spheroidal cap, m is the half the width of the spheroidal cap, R_P - $t/2$, n is half the depth of the spheroidal cap, n = m, o is half the height of the spheroidal cap, L - $t/2$, and $p = m\cos(\frac{n}{o}) / \sqrt{1 - (\frac{n}{o})^2}$ (Wolfram 1999). The bending energy of an aspirated liposome before the injection pipette was inserted into the liposome membrane was taken as the sum of the bending energies of the individual shapes that made up the aspirated liposome.

The curvatures, c_1 and c_2, of the spherical portion of the liposome outside the pipette were taken as $1/(R - t/2)$. For the cylindrical section of the liposome inside the pipette, c_1 = $1/(R_P - t/2)$ and $c_2 = 0$. For the spherical cap of the liposome inside the holding pipette $c_1 = c_2 = 1/(R_P - t/2)$. When $L < R_P$ and an spheroidal cap filled the inside of the holding pipette, $c_1 = 1/(R_P - t/2)$ and $c_2 = 1/(L - t/2)$.

For the aspirated, probed liposome, the surface area of the conical indentation in the spheroidal portion of the liposome outside the holding pipette was calculated using,

$$A_{conical\ frustum} = \pi(R_i + R_{ie})\sqrt{(R_i - R_{ie})^2 + x^2}\ , \quad (24)$$

where $A_{conical\ frustum}$ is the surface area of the walls of the injection pipette, R_{ie} is the radius of the injection pipette at a distance x from the tip (the base of the conical indentation inside the liposome). R_{ie} is determined as x multiplied by the tangent of the taper angle of the injection pipette, 2.5˚. The taper angle of the injection pipette was assumed to be constant throughout x. The taper angle was determined from scanning electron

microscope (SEM) images of the 25 nm and 2000 nm outer diameter injection pipettes, and this angle was assumed for the three different pipettes used in the experiments, Figure 32. The circular area at the tip of the injection pipette, πR_i^2, was added to this calculation as well. The surface area of the spheroidal portion of the liposome outside the holding pipette, $A_{spheroid}$, was calculated using (23). However, in this case, $m = W/2 - t/2$, $n = W/2 - t/2$, and $o = H/2 - t/2$, and the area calculated was doubled to represent a full spheroid. The surface areas at the opening of the holding pipette, πR_P^2, and at the location of the injection pipette, πR_{ie}^2, were removed from the calculated surface area of the spheroid.

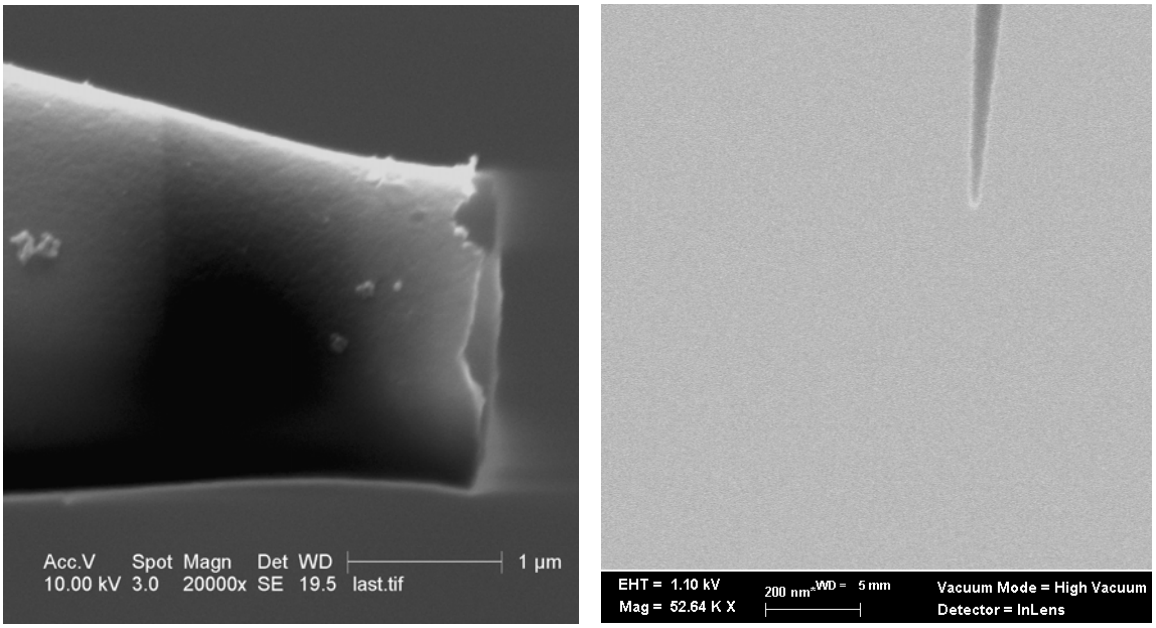

Figure 32: *SEM images of the 2000 nm outer diameter pipette (a) and the 25 nm outer diameter pipette (b). The taper angle of the injection pipettes was determined from these images.*

The portion of the liposome outside of the holding pipette is not a perfect oblate spheroid, but rather an intermediate shape between an oblate spheroid and a cylinder, Figure 33. In order to determine a better approximation of the surface area of this section, $W/2$ was plotted against $H/2$. A fourth order quadratic equation was fitted to this curve, and then the integral of this curve was taken from 0 to $H/2$. This value was then multiplied by 4π to determine the surface area of this portion of the liposome. The surface area for liposome 5, 019-111-02 was computed using this method, and this area was compared to the area determined using the approximation for an oblate spheroid.

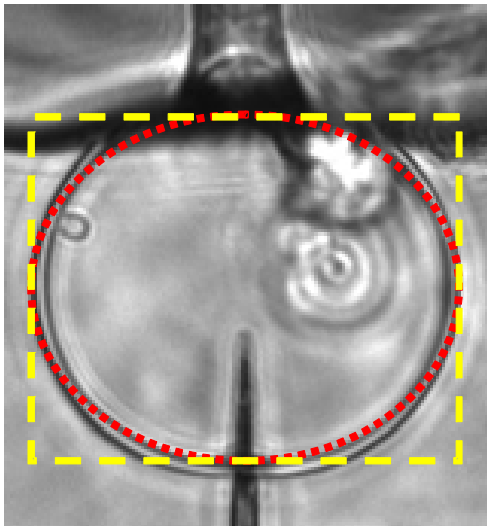

Figure 33: *Image of liposome 5, 019-111-02, being probed with a 100 nm inner diameter, 200 nm outer diameter injection pipette. The red dotted line outlines an ellipse, and the yellow line outlines a cylinder. The surface area of the portion of the probed liposome outside of the holding pipette is a hybrid of these two shapes.*

The curvatures, c_1 and c_2, of the spheroidal portion of the liposome outside the pipette were taken as $1/(W/2 - t/2)$ and $1/(H/2 - t/2)$. For the cylindrical section of the

liposome inside the holding pipette, $c_1 = 1/(R_P - t/2)$ and $c_2 = 0$. For the spherical cap of a liposome inside the holding pipette $c_1 = c_2 = 1/(R_P - t/2)$. When $L < R_P$ and an spheroidal cap filled the inside of the holding pipette, $c_1 = 1/(R_P - t/2)$ and $c_2 = 1/(L - t/2)$.

The conical indentation in the spheroidal portion of the liposome outside the holding pipette had a varying c_1 along the surface of the conical frustum and $c_2 = 0$. The integral for the bending energy of this surface was determined by writing c_1, in terms of the radius of the surface, $c_1 = 1/r$, and then computing this radius in terms of R_i, R_{ie}, and x,

$$r = 2\pi(R_{ie} - R_i)\frac{y}{x} + 2\pi R_i , \tag{25}$$

where r is the radius of the conical frustum at a given point and y is the distance along x.

The local bending energy of the conical frustum is then

$$E_{conical\ frustum} = \pi\kappa_B \int_0^x \frac{1}{r} dy , \tag{26}$$

where $E_{conical\ frustum}$ is the local bending energy of the conical frustum indentation. Mathematica was used to determine $E_{conical\ frustum}$ for the various pipette sizes and insertion distances. The bending energy of an aspirated liposome during the insertion of the injection pipette was taken as the sum of the bending energies of the individual shapes that made up the aspirated, probed liposome.

After the forces on the liposomes were determined, the stresses on the inner walls of the injection pipettes were also computed. This was done to ensure that the injection pipette tips would not break when they acted against a liposome. The stresses on the inner walls of the pipettes were determined from,

$$S_{pipette} = \frac{F}{A_{conical\ frustum}}\ , \tag{27}$$

where $S_{pipette}$ is the stress on the inner walls of an injection pipette.

Table 6: *List of Parameters*

parameter	description
independent	
D_i	diameter of injection pipette
R_i	radius of injection pipette
R_P	radius of holding pipette
t	liposome membrane thickness
x	length in which the injection pipette is inserted into the liposome
Δx	change in length in which the injection pipette is inserted into liposome
measured	
$A_{cylinder}$	surface area of the cylindrical section of an aspirated liposome
$A_{conical\,frustum}$	surface area of the conical indentation due to the injection pipette
$A_{spheroidcap}$	surface area of the spheroidal cap aspirated liposome
$A_{spheroid}$	surface area of the spheroidal section of an aspirated liposome
A_i	surface area of the walls of the injection pipette
A_{scap}	surface area of the spherical cap of an aspirated liposome
A_{sphere}	surface area of the spherical section of an aspirated liposome
ΔA_{io}	difference in the surface areas of the inner and outer membrane layers
ΔA_{0io}	difference in surface areas between the lowest energy state of the two layers
c_0	spontaneous curvature of liposome
c_1 *and* c_2	principal curvatures of the liposome
D	diameter of the liposome outside the holding pipette
E	total bending energy of the liposome
$E_{conical\,frustum}$	local bending energy of the liposome around the injection pipette
E_b	local bending energy of the liposome
E_r	non-local bending energy of the liposome
ΔE	change in the bending energy of the liposome
$\overline{F}$	pipette force acting on the liposome
H	height of the spheroidal portion of the liposome outside holding pipette
κ_B	mean bending modulus of liposome membrane
κ_G	Gaussian bending modulus of liposome membrane
K_A	area expansion modulus of liposome membrane
K_r	relative expansivity of the layers of the membrane
L	length of liposome inside the holding pipette
L_T	total length of aspirated liposome
ΔL	change in length of the liposome inside the holding pipette
m	constant representing the width of an ellipse
n	constant representing the depth of an ellipse
o	constant representing the height of an ellipse
p	constant used to determine the surface area of a nearly spherical ellipse
r	radius of curvature
R	radius of the liposome outside the holding pipette
R_{ie}	radius of the injection pipette at length x from its tip
$S_{pipette}$	stress inside the injection pipette during probing
W	width of the spheroidal portion of the liposome outside the holding pipette
y	distance along x

Results

Nine different liposomes with an average diameter during aspiration of 45.6 μm were used in the experiments. Injection pipettes with outer diameters of 25 nm and 200 nm were inserted into the liposomes distances of 10 μm and 20 μm (~25% and 50% of the length of the aspirated liposome), and the injection pipette with an outer diameter of 2000 nm was inserted into the liposomes a distance of 10 μm. When the 2000 nm pipette was inserted 20 μm into an aspirated liposome, the liposome was pushed out of the plane of the injection pipette, Figure 34.

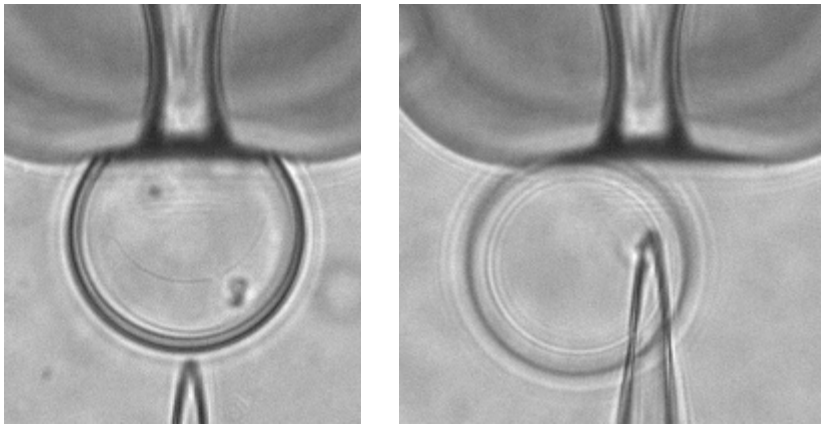

Figure 34: *Aspirated liposome being approached by 2000 nm outer diameter injection pipette (a). Liposome is pushed out of the plane of the injection pipette when the pipette insertion distance exceeds ~10 μm.*

Images were collected both before and during the probing of the liposomes with the injection pipette. A total of 36 images (18 undeformed, 9 deformed 10 μm, and 9 deformed 20 μm) for the 25 nm and 200 nm outer diameter injection pipettes and 18

images (9 undeformed and 9 deformed 10 μm) for the 2000 nm outer diameter pipette were collected, Figure 35-Figure 49.

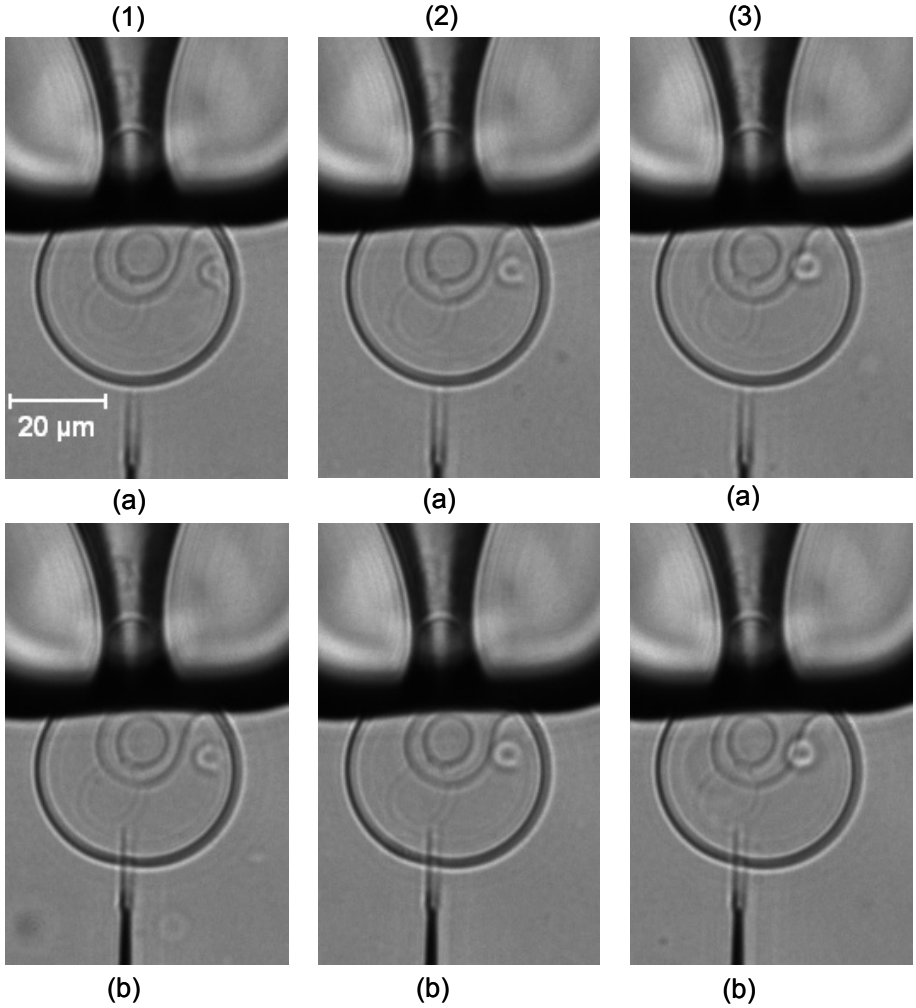

Figure 35: *Liposome 1, 019-112-01, before (a) and during (b) probing with a 25 nm outer diameter injection pipette. The injection pipette was inserted into the liposome a distance of 10 μm. The pipette was inserted and removed a total of three times (1-3).*

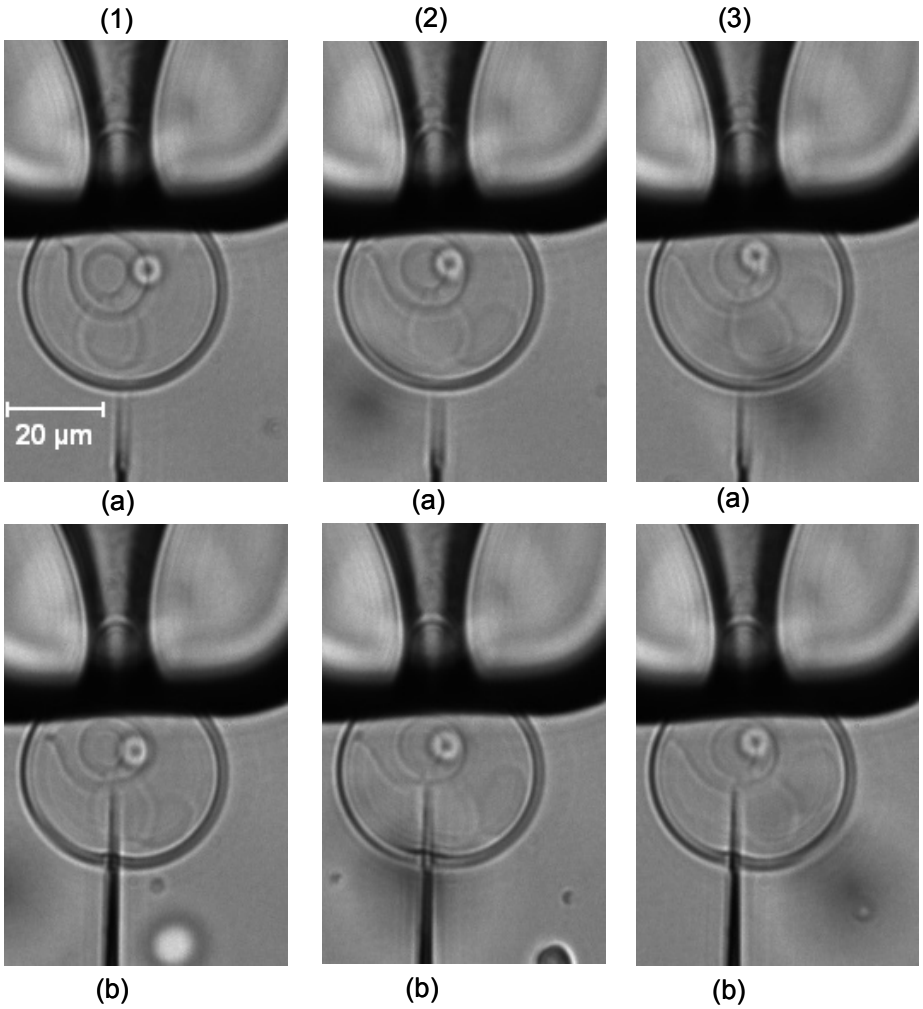

Figure 36: *Liposome 1, 019-112-01, before (a) and during (b) probing with a 25 nm outer diameter injection pipette. The injection pipette was inserted into the liposome a distance of 20 µm. The pipette was inserted and removed a total of three times (1-3).*

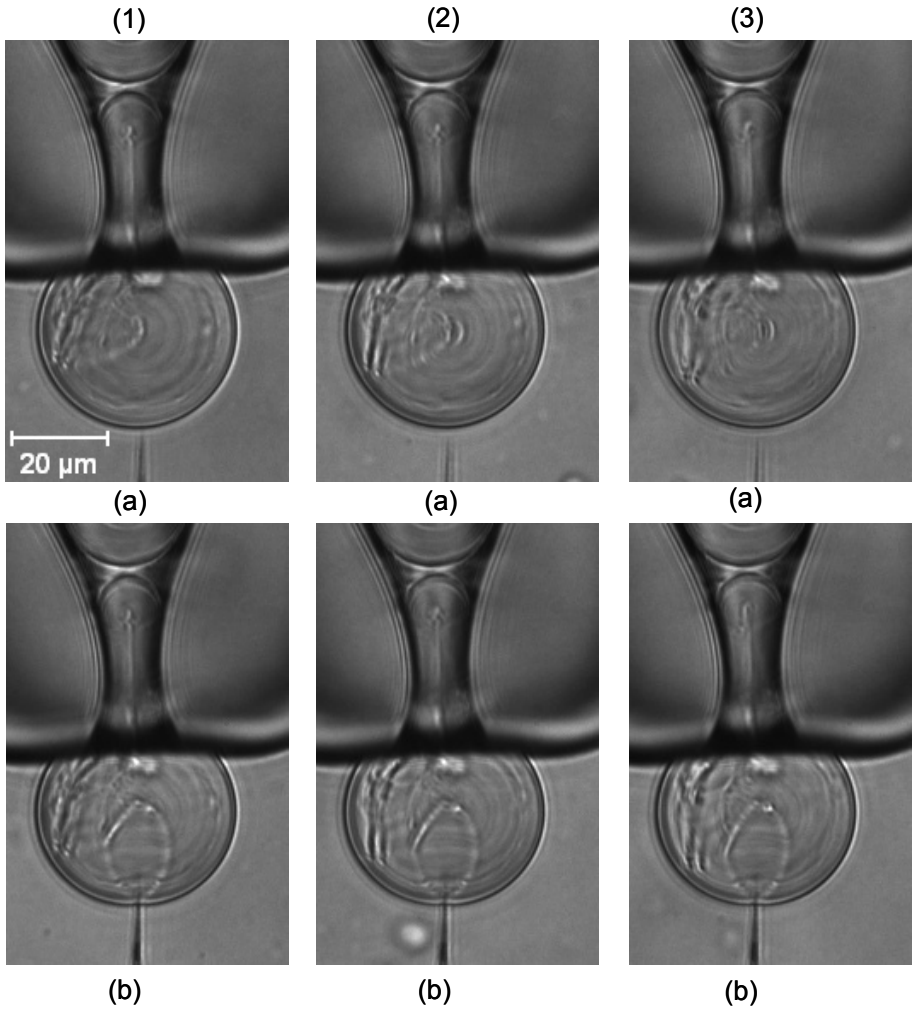

Figure 37: *Liposome 2, 019-112-02, before (a) and during (b) probing with a 25 nm outer diameter injection pipette. The injection pipette was inserted into the liposome a distance of 10 µm. The pipette was inserted and removed a total of three times (1-3).*

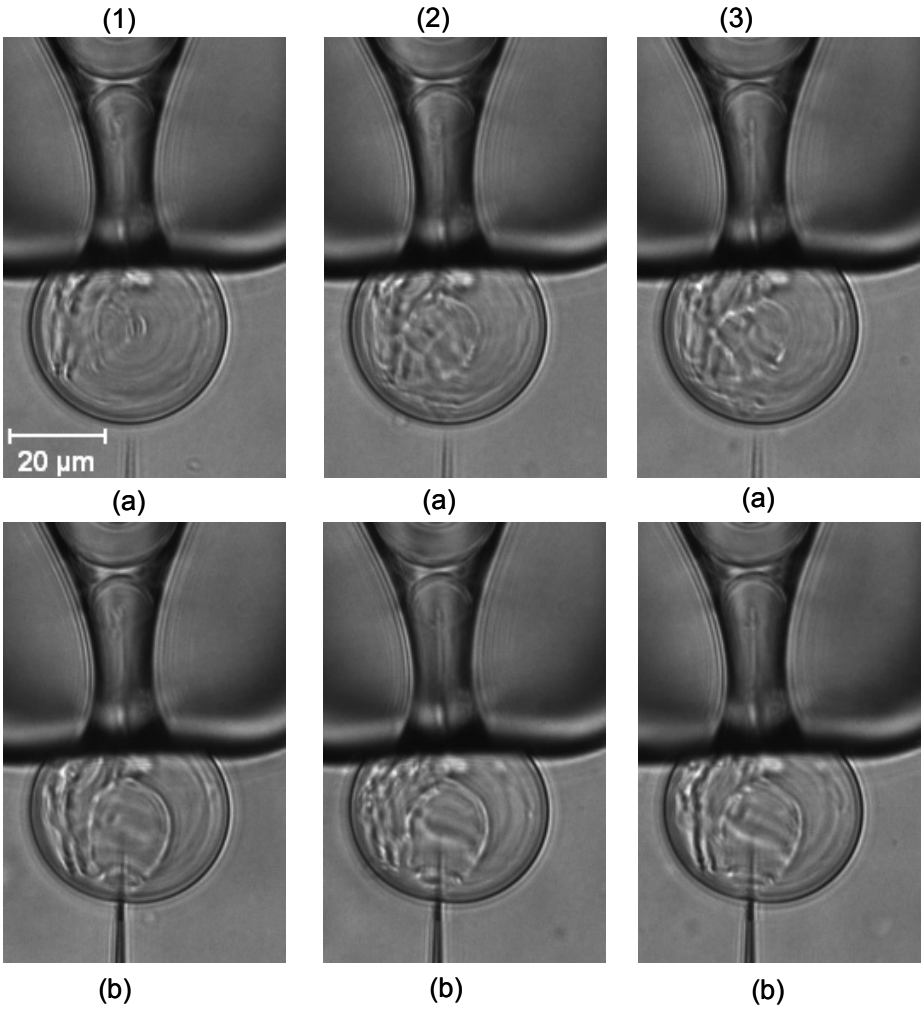

Figure 38: *Liposome 2, 019-112-02, before (a) and during (b) probing with a 25 nm outer diameter injection pipette. The injection pipette was inserted into the liposome a distance of 20 µm. The pipette was inserted and removed a total of three times (1-3).*

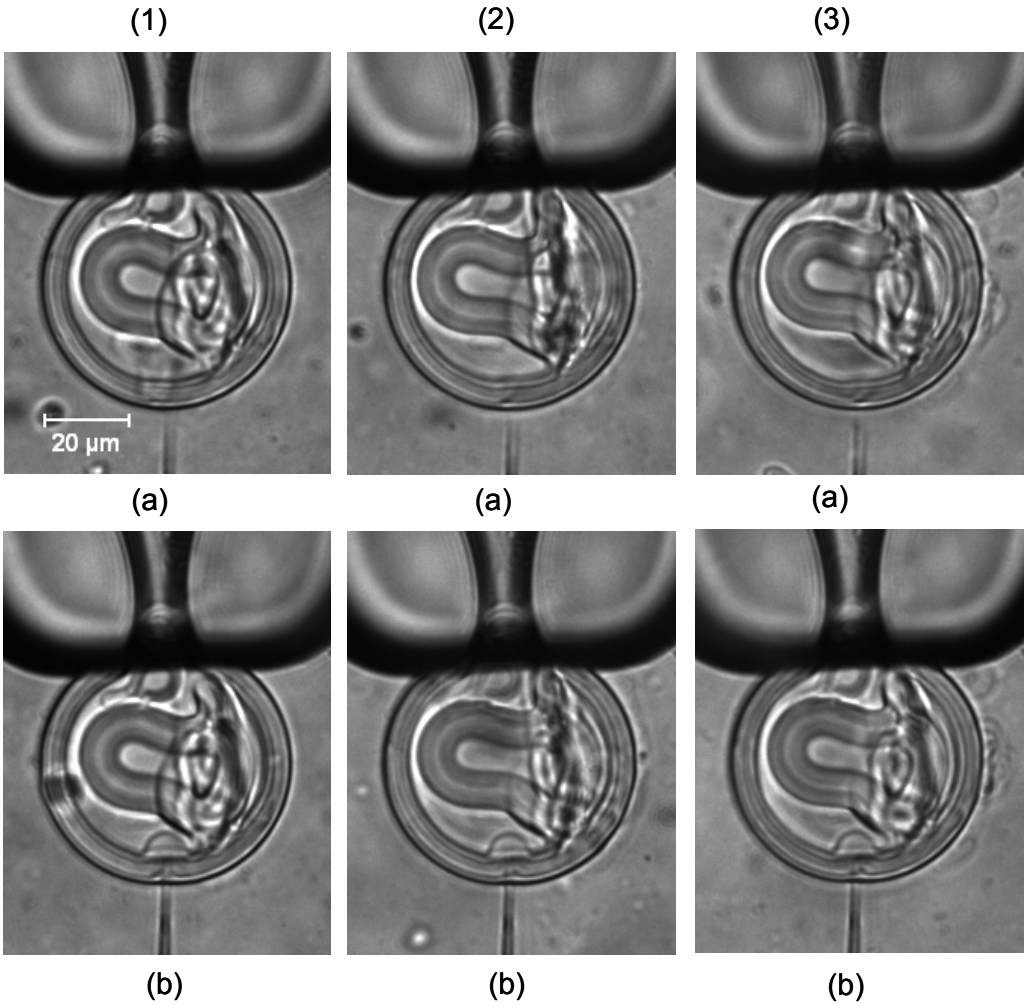

Figure 39: *Liposome 3, 019-112-03, before (a) and during (b) probing with a 25 nm outer diameter injection pipette. The injection pipette was inserted into the liposome a distance of 10 µm. The pipette was inserted and removed a total of three times (1-3).*

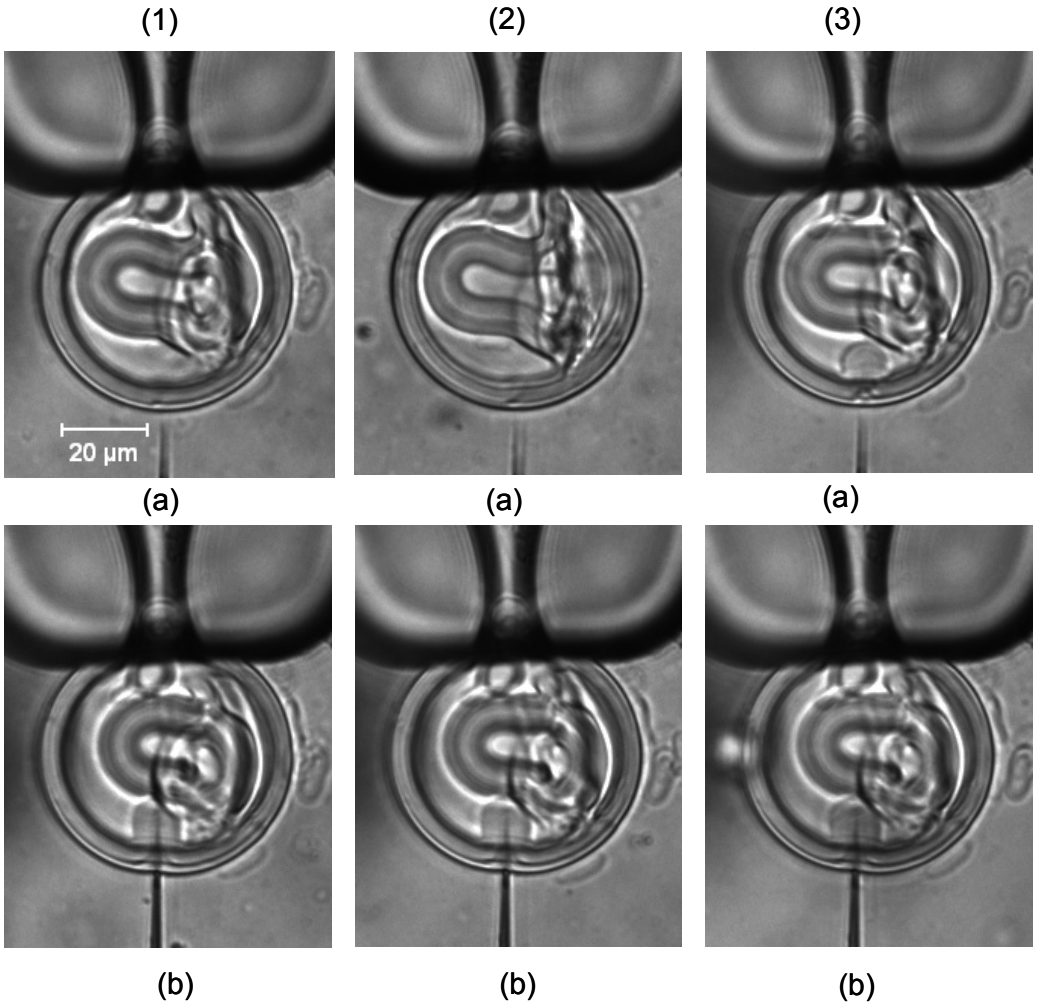

Figure 40: *Liposome 3, 019-112-03, before (a) and during (b) probing with a 25 nm outer diameter injection pipette. The injection pipette was inserted into the liposome a distance of 20 µm. The pipette was inserted and removed a total of three times (1-3).*

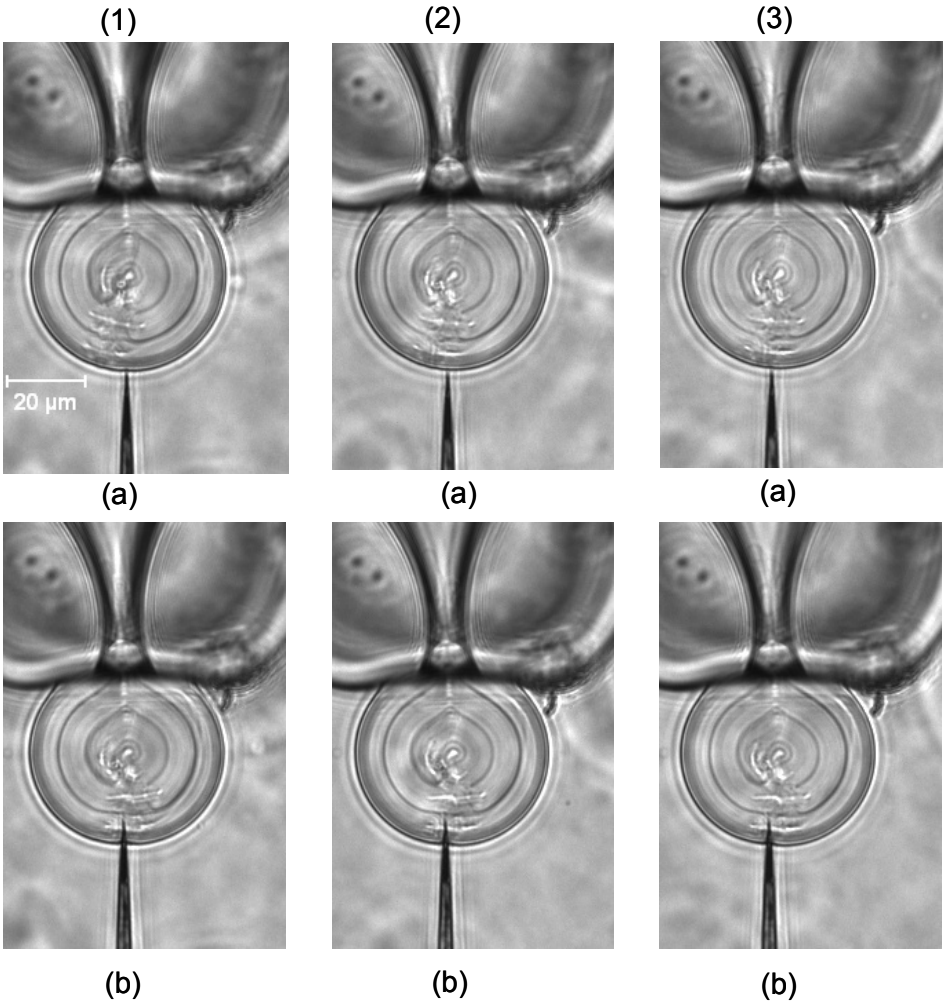

Figure 41: *Liposome 4, 019-111-01, before (a) and during (b) probing with a 200 nm outer diameter injection pipette. The injection pipette was inserted into the liposome a distance of 10 µm. The pipette was inserted and removed a total of three times (1-3).*

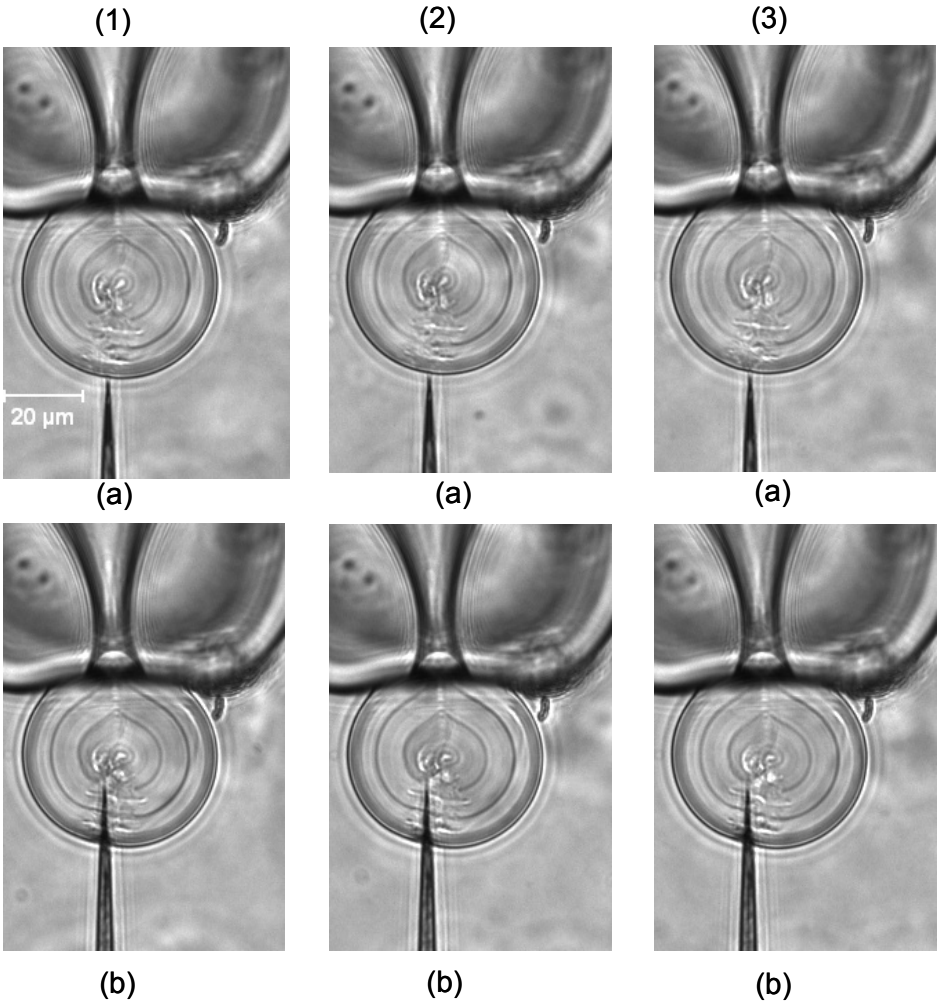

Figure 42: *Liposome 4, 019-111-01, before (a) and during (b) probing with a 200 nm outer diameter injection pipette. The injection pipette was inserted into the liposome a distance of 20 µm. The pipette was inserted and removed a total of three times (1-3).*

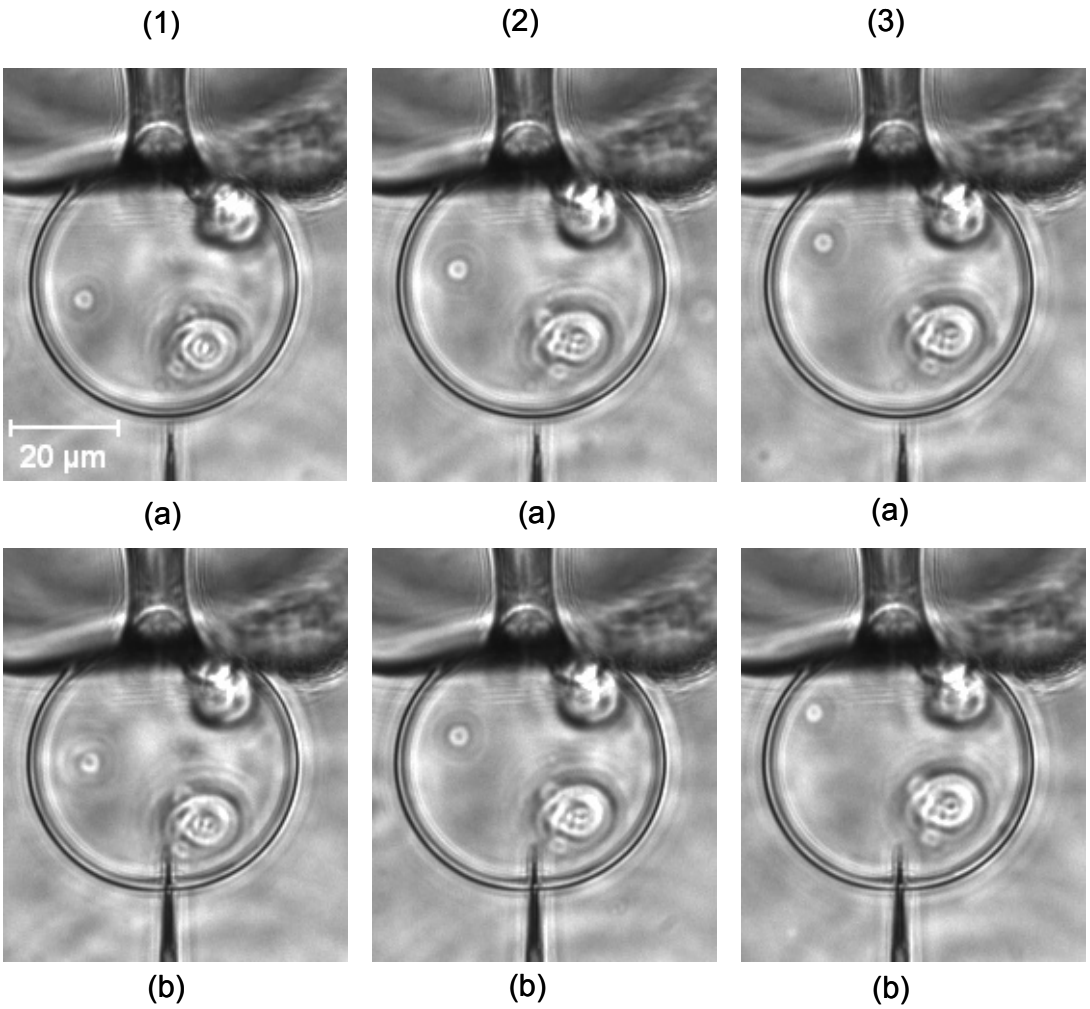

Figure 43: *Liposome 5, 019-111-02, before (a) and during (b) probing with a 200 nm outer diameter injection pipette. The injection pipette was inserted into the liposome a distance of 10 µm. The pipette was inserted and removed a total of three times (1-3).*

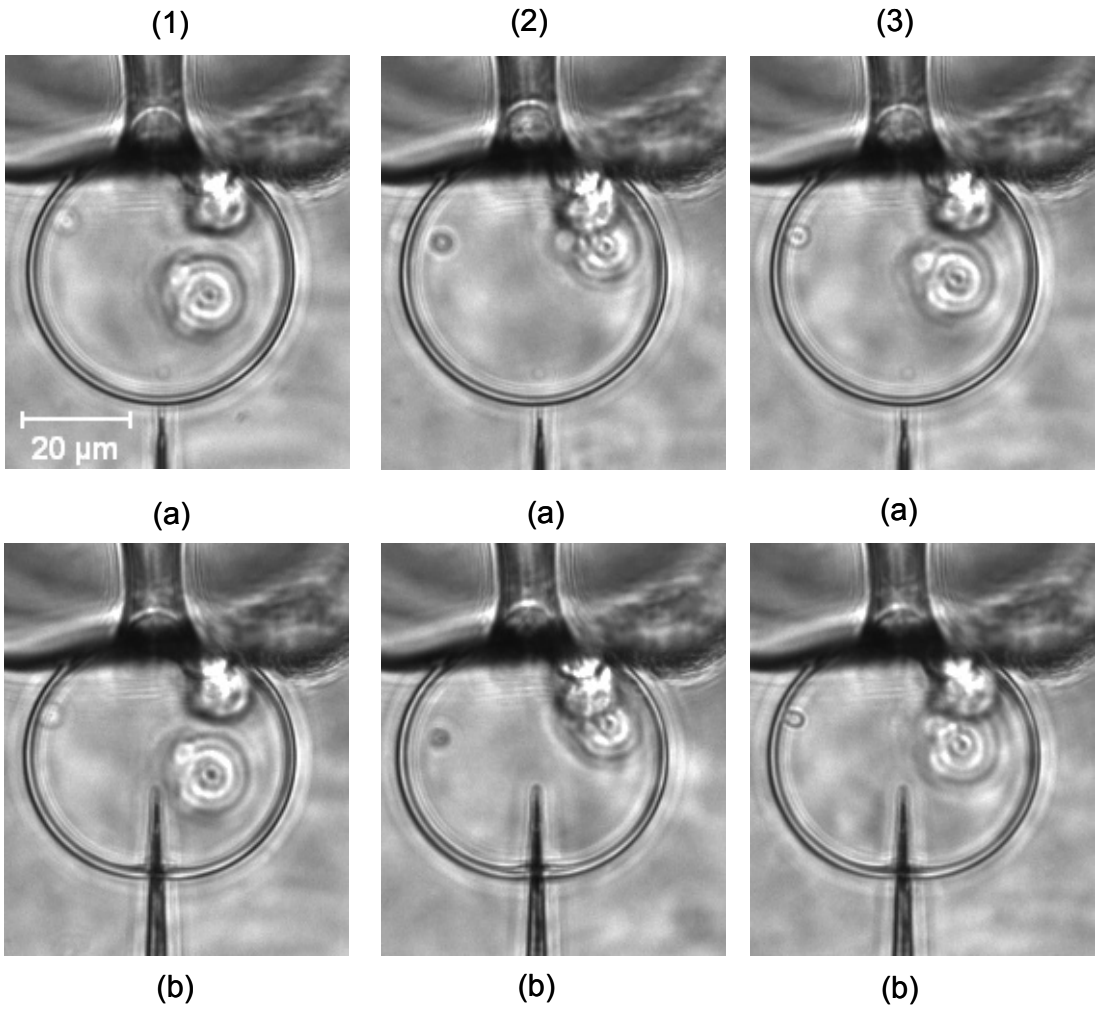

Figure 44: *Liposome 5, 019-111-02, before (a) and during (b) probing with a 200 nm outer diameter injection pipette. The injection pipette was inserted into the liposome a distance of 20 µm. The pipette was inserted and removed a total of three times (1-3).*

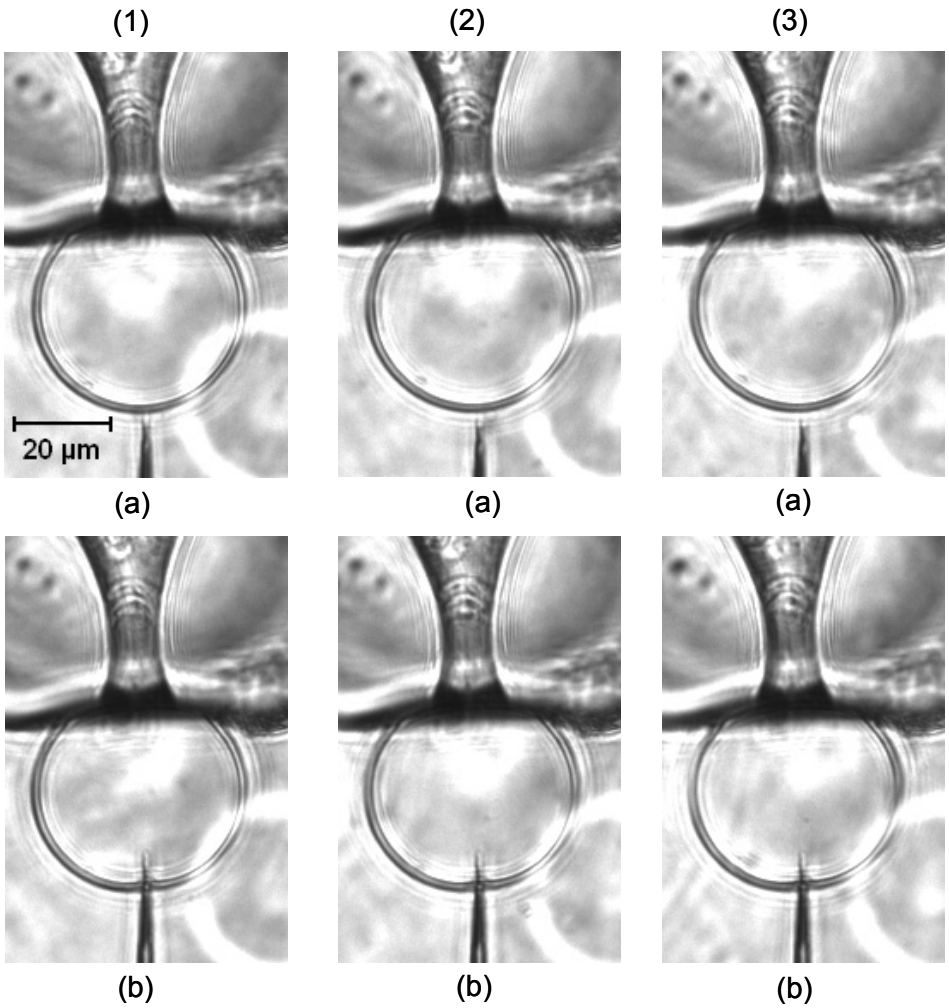

Figure 45: *Liposome 6, 019-111-03, before (a) and during (b) probing with a 200 nm outer diameter injection pipette. The injection pipette was inserted into the liposome a distance of 10 µm. The pipette was inserted and removed a total of three times (1-3).*

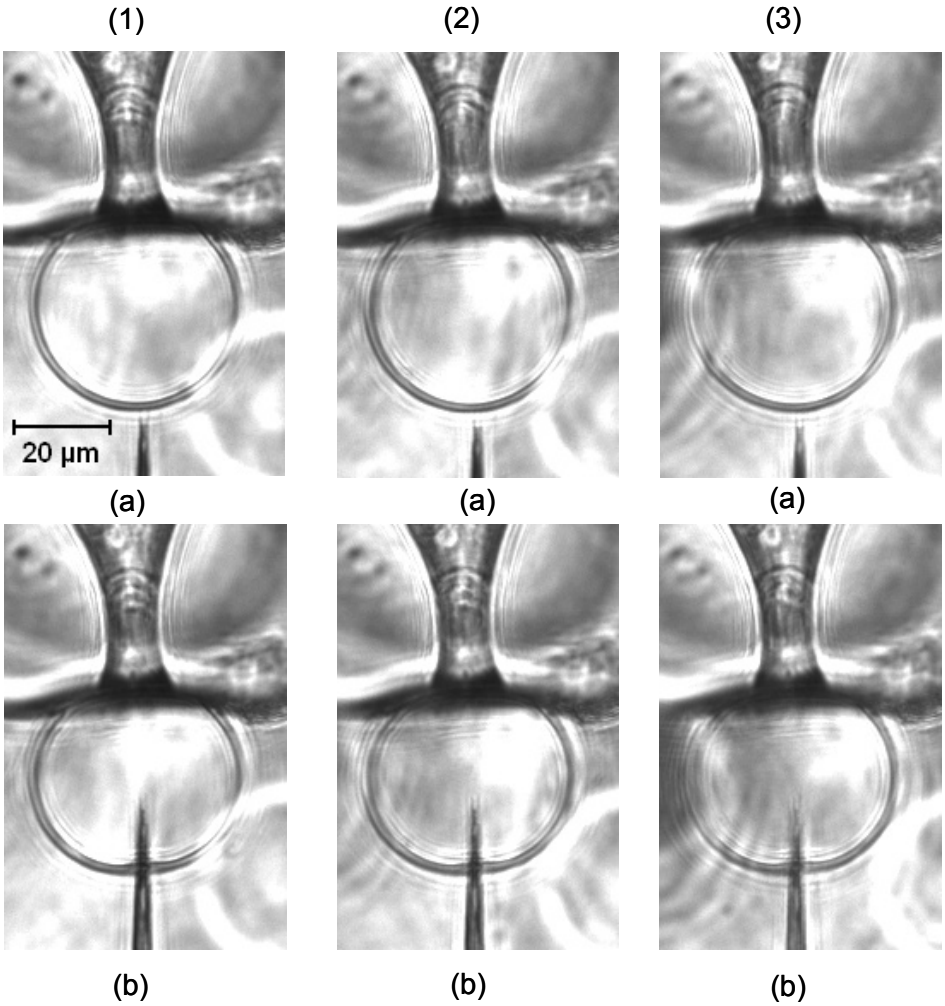

Figure 46: *Liposome 6, 019-111-03, before (a) and during (b) probing with a 200 nm outer diameter injection pipette. The injection pipette was inserted into the liposome a distance of 20 µm. The pipette was inserted and removed a total of three times (1-3).*

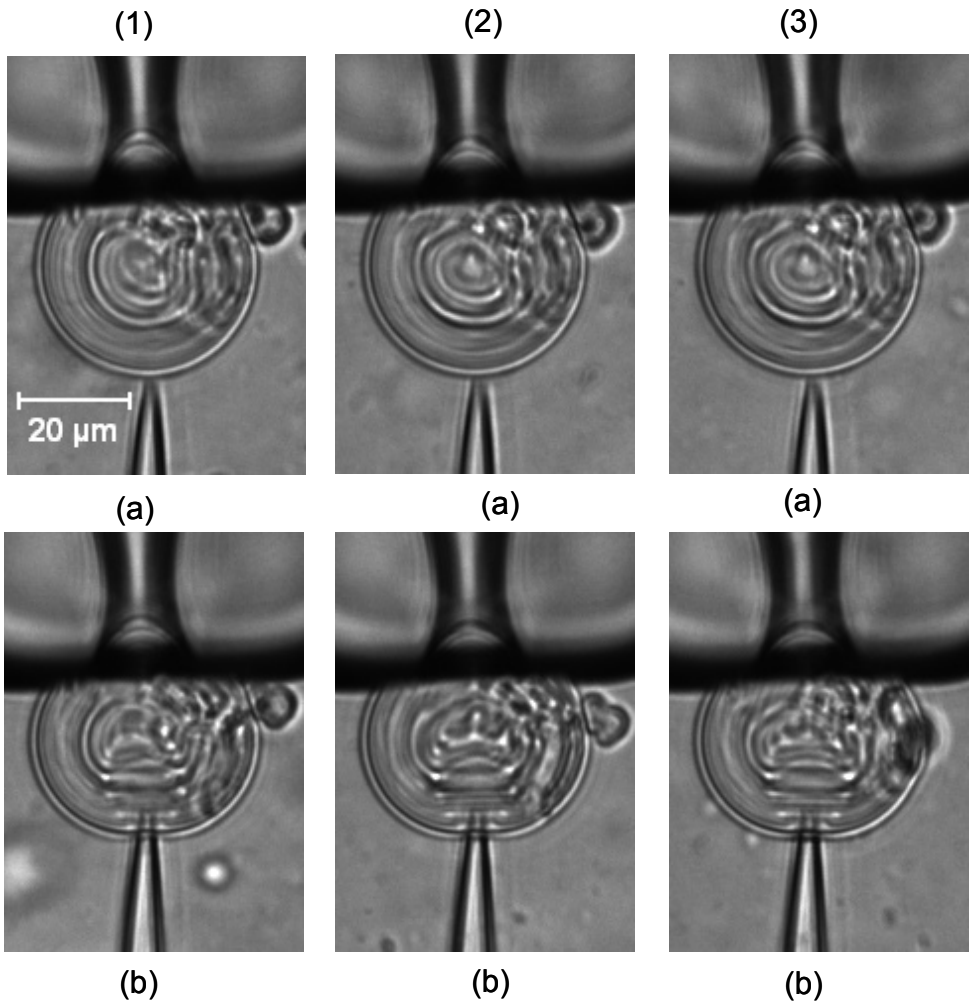

Figure 47: *Liposome 7, 019-113-01, before (a) and during (b) probing with a 2000 nm outer diameter injection pipette. The injection pipette was inserted into the liposome a distance of 10 µm. The pipette was inserted and removed a total of three times (1-3).*

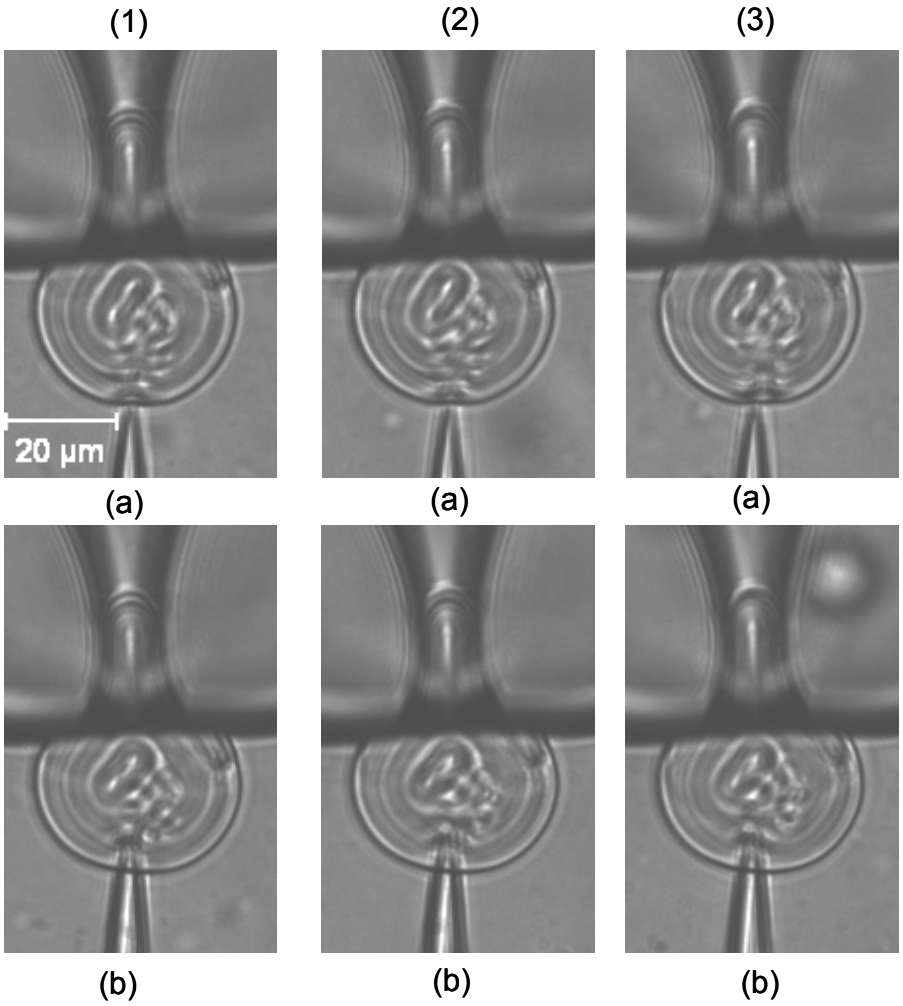

Figure 48: *Liposome 8, 019-113-02, before (a) and during (b) probing with a 2000 nm outer diameter injection pipette. The injection pipette was inserted into the liposome a distance of 10 µm. The pipette was inserted and removed a total of three times (1-3).*

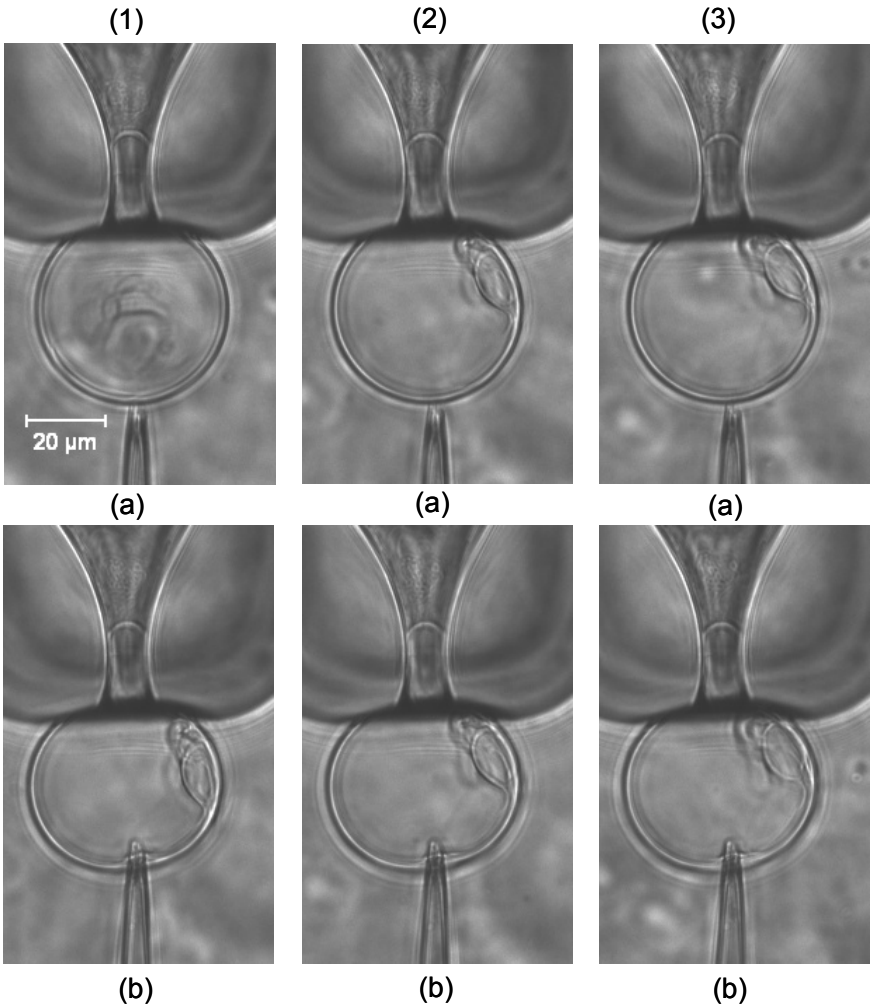

Figure 49: *Liposome 9, 019-109-02, before (a) and during (b) probing with a 2000 nm outer diameter injection pipette. The injection pipette was inserted into the liposome a distance of 10 µm. The pipette was inserted and removed a total of three times (1-3).*

After all of the images were collected, they were converted to binary images, and the geometries of the liposomes at each stage of the experiment were determined. During probing, the spherical section of the liposome outside the pipette became spheroidal in shape. The width of the spheroidal section of the liposome outside the holding pipette, *W*, the height of the liposome outside the holding pipette, *H*, and *L* were determined for the probed images, Figure 31. It appears as though liposome 8, 019-113-02, was being

impinged by the injection pipette in its pre-probed state, Figure 48. The portion of the liposome outside the pipette for this liposome is spheroidal in shape, and the membrane appears to be indented. The change in bending energies for the pre-probed to probed state for this liposome were inconsistent with the other two liposomes, ~ 2 - 3 orders of magnitude lower. The data collected from this liposome was therefore omitted from our bending energy and force calculations.

The average geometries and surface areas of the liposomes for each of the injection pipette sizes and insertion distances were used to calculate the change in the bending energies of the liposomes from the aspirated to the aspirated, probed state (19). From the changes in the bending energies, the forces in which the different injection pipettes exerted against the liposomes were determined (20), Table 5.

Table 7: *The average change in energy, ΔE, from the pre-probed and probed liposome state and the corresponding pipette force, F, for each of the pipette insertion lengths, x, and outer diameters, D_i, used in the experiments.*

x (μm)	D_i (nm)	ΔE (10^{-17} J)	F (pN)
10	25	5.68 ± 0.25	5.68 ± 0.060
	200	4.28 ± 0.11	4.28 ± 0.019
	2000	1.44 ± 0.06	1.44 ± 0.013
20	25	5.86 ± 0.24	5.86 ± 0.060
	200	5.00 ± 0.11	5.00 ± 0.016

The bending energies of the aspirated liposomes before manipulation with the injection pipette (x = 0) were on the order of 10^{-17} J, Figure 50. As the injection pipette was pressed into the liposome, i.e. x was increased, the bending energies of the liposomes increased. Also, as the outer diameter of the injection pipettes decreased, the bending energies of the probed liposomes increased.

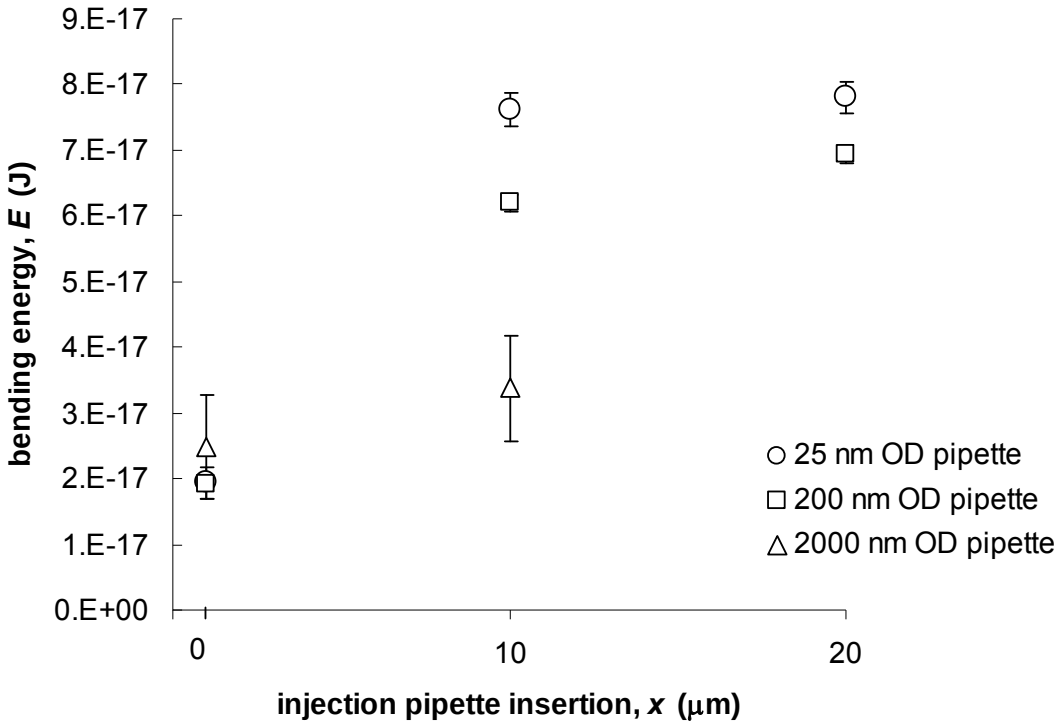

Figure 50: *Liposome bending energy, E, vs. injection pipette insertion length, x. Bending energies increased with increased injection pipette insertion lengths and decreased outer diameters of the injection pipettes.*

The bending energy calculations using the 25 nm outer diameter injection pipette before probing had a standard deviation of 2.2 x 10^{-18} J, when the injection pipette was inserted into the liposome x = 10 μm, the standard deviation was 2.5 x 10^{-18} J, and when x = 20 μm, the standard deviation was 2.4 x 10^{-18} J. For the 200 nm outer diameter pipette, the calculated bending energies had standard deviations before probing of 1.1 x 10^{-18} J, 1.1 x 10^{-18} J when x = 10 μm, and 1.1 x 10^{-18} J when x = 20 μm. The 2000 nm outer diameter pipette had standard deviations in bending energy of 8.1 x 10^{-18} J for the pre-probed state and 6.1x10^{-19} J when x = 10 μm.

The force of the injection pipette on the liposomes increased as the size of the injection pipette decreased, Figure 51. This increase in force was greater for the 200 nm

outer diameter pipette, ~17% increase in force, then for the 25 nm outer diameter pipette, ~3% increase in force.

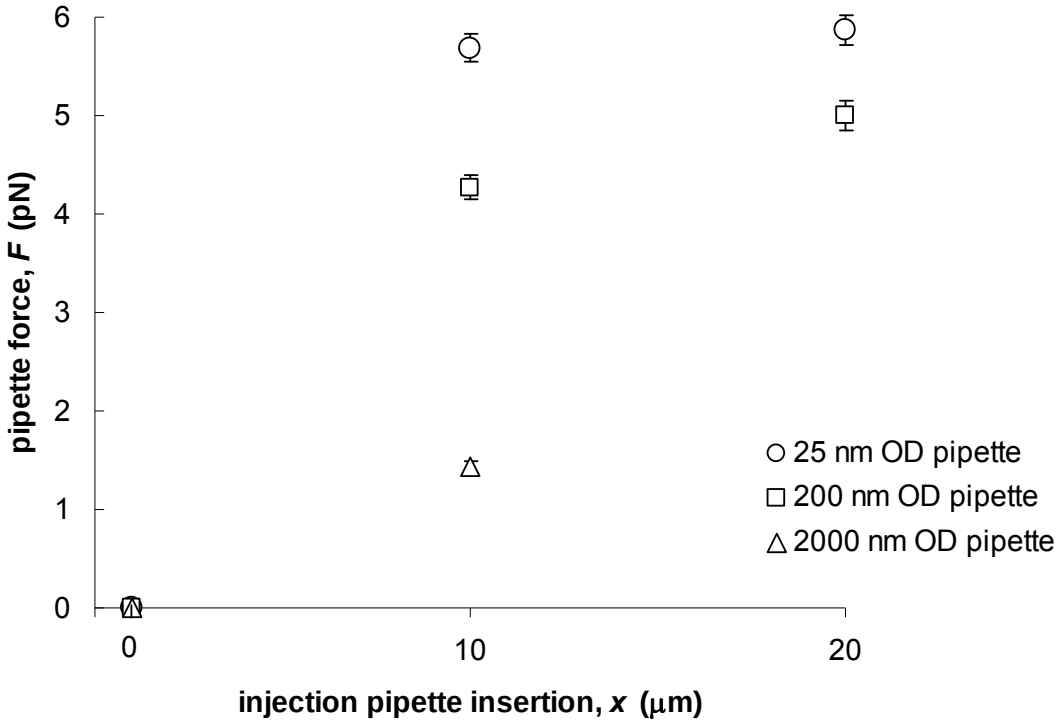

Figure 51: *Pipette injection force, F, vs. injection pipette insertion length, x. The force on the liposome increased as the size of the outer diameter of the pipette decreased. Once the pipette was in contact with the liposome, pipette force was not greatly affected by the pipette insertion length.*

The force calculations using the 25 nm outer diameter injection pipette had a standard deviation of 0.060 pN when x = 10 μm and 0.063 when x = 20 μm. For the 200 nm outer diameter pipette, the calculated forces had standard deviations of 0.019 pN when x = 10 μm, and 0.016 pN when x = 20 μm. The 2000 nm outer diameter pipette had a standard of 0.013 pN when x = 10 μm.

The surface area of the neutral plane of the liposome was calculated for the aspirated liposome, and the aspirated, probed liposome. The portion of the probed liposome outside of the holding pipette was approximated as an oblate spheroid. Using this approximation, the surface of the liposome decreased from the pre-probed to probed state, ~1 – 3%. However, using the curve fitting method, the surface area of the probed liposome increased from the pre-probed to probed state. A curve was fitted using to the geometry of liposome 5, 019-111-02, during probing with a 200 nm outer diameter injection pipette and a pipette insertion distance of 20 μm, Figure 52. The results of the total surface area of the liposome using the curve fitting method was compared to the surface area of the pre-probed liposome and the surface area when the probed liposome was assumed to be an oblate spheroid, Table 8.

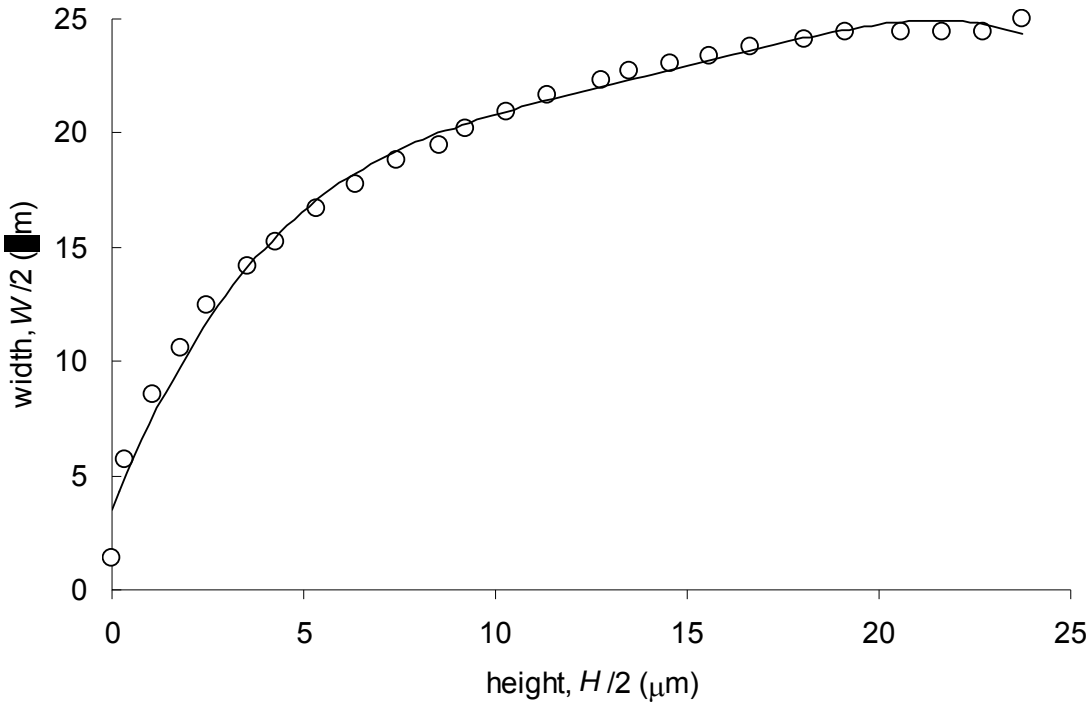

Figure 52: *Plot of W/2 of the probed liposome vs. H/2 of the probed liposome. A fourth order polynomial was fitted to the data, and this equation was used to determine the surface area of the probed liposome.*

Table 8: *Surface areas of the pre-probed and probed liposome using the approximation of surface area for an oblate spheroid and for the curve fitting method.*

shape approximation	**surface area, *A* (μm^2)**
sphere (pre-probed)	7797
oblate spheroid (probed)	7738
curve fitting method (probed)	7824

To ensure that the forces calculated would not cause the pipette tip to break, the stresses on the inner walls of the injection pipette during loading were determined (27), Table 9. Both the 2000 nm and 200 nm outer diameter pipettes were made from glass, Young's modulus ~48-83 GPa (Gere 2001), and the 25 nm outer diameter pipette was made of quartz, Young's modulus ~52-71 GPa (Drane 1929).

Table 9: *The stresses on the walls of the injection pipette, $S_{pipette}$, for the various pipette sizes and insertion distances.*

x (μm)	D_i (nm)	$S_{pipette}$ (Pa)
10	25	0.39
	200	0.21
	2000	0.02
20	25	0.10
	200	0.07

Discussion

The bending energies and forces calculated are dependent on the bending modulus of the DOPC:DOPS liposomes. The bending modulus was calculated from the experimentally derived area expansion modulus of the liposomes, Chapter III. It is important to mention that this modulus is dependent on the temperature of the liposomes. Thermally induced membrane fluctuations could lead to a determined bending modulus that is artificially small. Both the area expansion modulus determination experiments and the experiments described in this chapter took place in the same room, using the same equipment. It is assumed that the temperature of the

liposomes was similar for both of the experiments, and therefore the bending modulus of the liposomes during both sets of experiments should also be similar.

Given the determined injection pipette forces and insertion distances, the stresses on the pipette tips during the experiment were eleven to twelve orders of magnitude smaller than the Young's modulus of glass or quartz, Table 9. The tips of the injection pipettes should therefore not break during the described manipulations, and they did not.

The bending energies of the liposomes and the forces exerted onto the liposomes increased as the outer diameters of the injection pipettes decreased. This was to be expected. The lipids in the phospholipid membranes conformed to the walls of the injection pipettes as the injection pipettes probed the liposomes. As the diameter of the injection pipettes decreased, the curvature of the membranes around the pipette increased, and the molecules in the membrane became more bent. This caused the bending energy of the liposome and the force acting on the liposome to increase (19) and (20).

In addition to the energy involved in the shape changes of the liposomes during probing, the energy due to the interactions of the phospholipid molecules and the glass and quartz pipettes needed to be considered as well. The attractive forces between the phospholipids and the glass pipettes will decrease the energy required to change the shape of the liposome. The adhesion energy density of a DOPC:DOPG (9:1) liposome to a pure glass substrate is 1-10 x 10^{-9} J/m^2 (Gruhn, Franke et al. 2007). Although the liposomes used in these experiments are not the same as those used in the experiments described here (DOPC:DOPS, 7:3), DOPC is the major component of both of these

liposomes. Therefore it is assumed that the adhesion energy density of DOPC:DOPS liposomes is within an order of magnitude to the results obtained by Gruhn et al. (2007).

The adhesion energy between the liposome and the glass pipettes was determined by multiplying the adhesion energy density, 1-10 x 10^{-9} J/m^2, by the contact areas of the glass injection pipettes (200 nm and 2000 nm outer diameter pipettes) and liposome membrane for the two insertion distances, 10 μm and 20 μm. The adhesion energies calculated were all on the order of 1-10 x 10^{-20} J, 2 - 3 orders of magnitude smaller then the energy that is required to change the shapes of the liposomes during probing. The adhesion energy between the molecules and the glass is therefore considered to be negligible. Furthermore, an adhesion energy density of 1-10 x 10^{-9} J/m^2 is considered to be ultra-weak. For ultra-weak adhesion energy densities, the influence of gravity on the liposome-glass adhesion is important (Gruhn, Franke et al. 2007). When a glass, injection pipette is inserted into the liposome membrane, the adhesion of the liposomes to the sides and top of the injection pipettes will be less then 1-10 x 10^{-19} J because gravity will not be pulling the liposome onto these surfaces. The influence of the adhesion energy on our calculations is therefore even smaller then calculated, further justifying our reasoning for neglecting adhesion energies.

The calculated surface area for the aspirated, probed liposome assuming the shape of this liposome was an oblate spheroid was ~1 - 3% smaller than the surface area calculated for the aspirated liposome before insertion of the injection pipette. The shape of the liposome during probing is not perfectly spheroidal, but instead a hybrid cylinder-oblate spheroid. To obtain a more accurate estimate of the surface area, it is necessary to fit the geometric data obtained during probing of the liposome to an equation using a

curve fitting method. When a fourth order polynomial representing the shape of our "spheroidal" portion was used to determine the surface area of this portion of the liposome outside the holding pipette, an increase in surface area of 0.3% was determined from the liposome's pre-probed to the probed state. This result is expected as the liposome should experience some areal strain during probing. However, the curve fitting method was time consuming and because most of the bending energy of the liposome was due to the bending of the membrane around the injection pipette, and not from the change of the liposome from a sphere to an oblate spheroid, the spheroidal approximation for determining the surface area of the liposome was appropriate for our calculations. Furthermore, the spheroidal approximation was used for all of the probed liposomes, regardless of the size of the injection pipette. Therefore differences in the pipette forces for the various sized injection pipettes should not be influenced by this approximation.

It was assumed that the outer diameters of the injection pipettes had a constant taper angle along x, taper = 2.5˚. A more accurate depiction of the injection pipettes would involve determining their exact shapes, and then using these shapes in the energy equation. However, this chapter was written to serve as a protocol for determining pipette forces during spherical cell or liposome manipulations. The exact pipette forces and liposome bending energies calculated for the DOPC:DOPS liposomes is therefore not as important as the implementation of this technique. Assuming a constant pipette taper over x is thereby valid for our purposes.

Understanding the relationship between pipette size, force, and cell or liposome deformation can assist in quantifying the forces that cells experience during manipulation by an injection pipette. If the minimum force required to perform a

specific manipulation of a cell is known, measures can be taken to ensure that this force is not exceeded during these manipulation. This would serve to decrease the magnitude of the damage done to a liposome or cell during single-liposome, single-cell, and single-organelle injections and surgeries.

Chapter V: Liposome and Cell Behavior during Membrane Puncture and Injection with Micro and Nanopipettes

Abstract

Using micropipette aspiration and injection methods, the behaviors of aspirated DOPC:DOPS liposomes and porcine aortic endothelial cells were observed during the probing and puncturing of the liposomes and cells with micro and nanopipettes. Determining the responses of liposomes and cells during and after probing with various sized injection devices can assist in determining how these membranes will respond to single-liposome, single-cell, and single-organelle injection. We found that endothelial cells are penetrable by pipettes having outer diameters as large as 2000 nm and at speeds as slow as ~ 4 μm/sec. However, liposomes, which do not have a cytoskeleton to resist deformation, are impenetrable by pipettes having outer diameters as small as 200 nm and speeds as great as ~ 4000 μm/sec. Understanding how liposomes and cells respond to probing by various sized injection pipettes can assist in determining the amount of damage done to a cell or liposome during manipulation.

Introduction

The injection of drugs, genetic information, and macromolecules into single-cells or single-organelles is currently being used to modulate and monitor individual cell activity (Han, Nakamura et al. 2005; Obataya, Nakamura et al. 2005; Leary, Liu et al. 2006). However, damage to the cells often results from these procedures, and this damage is often fatal (Laffafian and Hallett 1998; Han, Nakamura et al. 2005; Freedman, Mattia et al. 2007). In addition to cell injection, the injection of single-liposomes has potential in creating drug encapsulated vesicles for targeted drug delivery applications.

In the previous chapter, the amount of force that injection pipettes of various sizes exerted against liposomes was determined, Chapter IV. This force was dependent on the bending modulus of the liposomes, and the geometries of the injection pipettes. However, it was unclear during the probing of the liposomes if the membranes of the liposomes were ruptured, and if they had ruptured, at what forces and pipette insertion lengths membrane puncture actually occurred. By determining the amount of force and deformation that is required to just puncture the membranes of liposomes and cells during injection, measures can be taken to ensure that these forces and deformations aren't exceeded during these procedures, minimizing the damage done to the cell or liposome.

Injection pipette size and rates were varied to determine the necessary size and speeds required to penetrate the membranes of aspirated liposomes and aspirated endothelial cells. The amount of deformation, and therefore possible damage, during the injection of the liposomes and cells using the various pipette sizes and injection rates were compared.

Methods

Liposome Creation

Hollow, spherical liposome vesicles were created from a phospholipid membrane based on the method of Fygenson et al. (1997) (Fygenson, Elbaum et al. 1997). Liposomes were composed of DOPC:DOPS (7:3) phospholipids. A full explanation of liposome creation is described in Chapter III. The liposomes created were ~ 10 - 50 μm in diameter with a thickness of ~ 4.5 nm (Boal 2002; Kucerka, Pencer et al. 2007).

Endothelial Cell Culture

Porcine aortic endothelial cells (PAEC), isolated by the collagenase dispersion method, were maintained in low glucose Dulbecco's modified Eagle's medium (DMEM) supplemented with 5% fetal bovine serum, 1% penicillin-streptomycin, and 2% glutamine (Invitrogen). Culture media was changed every 48 hours and cells between passages four and nine were used. The cells were then trypsinized in order to detach the endothelial cells from their extracellular matrix. Suspending the cells in the medium was necessary in order to aspirate them into the holding pipette for injection. Suspended cells were spherical in shape, diameters ~ 10 μm.

Experimental Setup

Liposome and cell puncture attempts were performed on an inverted light microscope (Olympus IX-81) with a 400× total magnification. Liposomes and cells were aspirated with a CellTram air pressure transmitter (Eppendorf). The holding pipette used to aspirate the liposomes had an inner diameter of ~ 15 μm (Eppendorf Vacutips). The holding pipettes used to aspirate the endothelial cells had an inner diameter of ~ 5 μm (World Precision Instruments (WPI), Sarasota, FL). The holding pipettes were installed in the left micromanipulator. Liposome and cell puncture were attempted with injection pipettes having outer diameters that ranged from 25 nm (in-house pulled quartz pipettes) to 2000 nm (WPI glass pipettes). The movements of both the holding pipette and the injection pipette were controlled using two Eppendorf NK-2 micromanipulators (B&B Microscopes, Ardmore, PA). The manipulators were controlled manually, using the manipulator joystick, and through a serial port that connected the manipulators to a computer. The "Hyper Terminal" program supplied with Windows® was used to control

the manipulators remotely. Images of the liposomes during the experiments were taken using SPOT Advanced software (Sterling Heights, MI). More detailed descriptions of the experimental setup and the aspiration and probing of liposomes are described in Chapter IV. This same technique is also used to aspirate and probe endothelial cells.

Injection Pipette Injection Capabilities

Four different pipettes were used to ensure that injection is possible with the store-bought micropipettes (WPI) and the in-house pulled nanopipettes. Two different WPI micropipettes with outer diameters at their tips of 2000 nm and 200 nm (inner diameters 1000 nm and 100 nm, respectively) and two different in-house pulled nanopipettes with outer diameters ~ 35 nm (inner diameters < 35 nm) were used. To begin the experiment, the capillaries of the pipettes were filled from the breach-end with Trypan blue using a MicroFil™ (WPI), and then inserted into the grip head of the CellTram oil pressure transmitter. The grip head was fully tightened. Next, the tip of the pipette was inserted into a Petri dish that had been filled with distilled water. A pressure ranging from approximately 0.02-2 MPa was applied to the pipette by slowly decreasing the volume of the piston. The water near the tip of the injection pipette was monitored to determine if Trypan blue was ejected from the tip of the micro or nanopipettes.

Liposome and Cell Injection

Membrane puncture attempts were performed using liposomes having diameters of ~45 μm and endothelial cells having diameters of ~ 10 μm. Only the injection pipettes capable of injection were used for these experiments, and the equator test was performed before each experiment to ensure that the injection pipettes were acting at the mid-planes of the liposomes or cells, Chapter IV.

To ensure liposome or cell membrane puncture had or had not occurred, Trypan blue was ejected from the pipette tip after insertion of the injection pipette into the membrane. If the Trypan blue was confined within the membrane, it was assumed the membrane had been penetrated by the injection pipette. If, however, the Trypan blue was observed to diffuse outside the confines of the membrane, it was assumed that the membrane was not punctured by the injection pipette.

Injection pipettes were inserted into the aspirated liposomes distances of 20 μm, and the pipette velocities ranged from ~ 0.4 - 4000 μm/sec. Injection pipette manipulations for the given velocities and insertion distances were controlled using Hyper Terminal. Additionally, liposome injection was attempted using manual control of the manipulator and a joystick speed of 4500 μm/sec.

Endothelial cell injection was also performed. Endothelial cells had an average diameter of ~10 μm when they were suspended in the medium. Injection pipettes were controlled using Hyper Terminal, and the pipettes were inserted a distance of 5 μm into the aspirated cells at rates of ~ 4 μm/sec and ~ 40 μm/sec. A new cell was used for each pipette size and injection speed.

The deformation of an endothelial cell was observed before, during, and after insertion of the injection pipettes. This was done to determine if any permanent deformation, or possibly damage, to the cell resulted from the cellular injection process. Deformation was observed using pipettes with outer diameters of 2000 nm, 200 nm, and 25 nm.

The deformations of an endothelial cell when the pipette penetrated the cell at rates of ~ 4 μm/sec, ~ 40 μm/sec, and ~ 400 μm/sec were also compared. The same cell was

used for the different pipette sizes and injection velocities. The smallest pipette, outer diameter 25 nm, was inserted into the cell first, followed by the second smallest pipette, 200 nm outer diameter, and then finally the largest pipette. The slower injection rate was performed first for each of the pipette sizes.

Applying Constraints to the Liposome during Probing

Poly-L-lysine was used in an attempt to adhere the aspirated liposome to the inner walls of the holding pipette. Constraining the movement of the liposome inside the holding pipette would prevent the liposome from sliding out of the holding pipette during injection pipette probing, as was observed in Chapter IV. This would prevent the phospholipid molecules from relieving any local strain caused by the injection pipette, and it was thought that this might allow for membrane puncture of the liposomes during probing. Polylysine has been used to coat glass slides in order to increase the adhesion energy between liposomes and glass from ~ 10 x 10^{-9} J/m^2 to ~ 1200 - 1400 x 10^{-9} J/m^2 (Gruhn, Franke et al. 2007; Limozin and Sengupta 2007).

A variety of polylysine concentrations and incubation times were considered in an attempt to optimize the adhesion of liposomes to the insides of the holding pipettes. Polylysine was diluted using phosphate buffered saline (PBS) to concentrations of 0.01 mg/ml (Limozin and Sengupta 2007), 1 mg/ml, and 10 mg/ml. Glass slides were then coated with 500 μl of the various concentrations of polylysine, and the slides were incubated (temperature 4˚ C) for periods of time ranging from 30 minutes to 24 hours. After incubation, the slides were removed from the refrigerator, and washed three times with 1 ml of PBS per washing. Washing of the cover slides was performed by tilting the

cover slide, applying 1 ml of PBS to the top of slide, and then allowing gravity to pull the PBS off of the slide. The slides were then dried using nitrogen gas.

After washing, the slides were placed on the microscope stage, and 150 µl of 0.9% saline solution was deposited onto the slide. Next, 10 µl of liposome solution was added to the saline solution, and the liposomes were allowed to settle onto the bottom of the protein-coated slide. The liposomes then remained undisturbed for ~10 minutes. It had been observed that liposomes will adhere to polylysine-coated glass cover slides on the order of 100 milliseconds (Limozin and Sengupta 2007). It was therefore assumed that 10 minutes was a sufficient amount of time to allow the liposomes to adhere to the slide. The liposomes at the bottom of the glass slide were brought into focus using the 10x objective. The 10x objective allowed for ~ 20 liposomes to be observed simultaneously.

After 10 minutes, 100 µl of saline solution was slowly deposited onto the slide, rinsing away any unattached liposomes. The adhesion of the liposomes to a slide was quantified by determining the percentage of the liposomes that remained attached to the slide after rinsing. This percentage was computed by merging the images of the liposomes before and after rinsing and then dividing the number of liposomes that remained attached to the slide by the number of liposomes that were on the slide before rinsing. This number was then multiplied by one hundred.

The quantification of liposome adhesion to a glass slide that had been incubated for 30 minutes with pure PBS was also performed. This was done to determine if the polylysine was in fact responsible for liposome adhesion to the glass slide, or if the rinsing of the slide with saline was not a suitable means of disrupting liposomes.

After the optimal values for polylysine protein concentration and incubation time had been determined, the tips of two different holding pipettes were coated using this polylysine concentration and incubation time. The CellTram air pressure transmitter was used to aspirate the polylysine into the tip of each holding pipette, and then the tip of each holding pipette was placed into 500 μl of the protein solution. The pipettes were then incubated for the designated period of time. After incubation, the pipettes were washed with PBS by aspirating and expelling PBS from the tips of the holding pipettes three times. The outsides of the holding pipettes were also washed with PBS three times with 1 ml of PBS. The pipettes were then dried with nitrogen. The polylysine coated holding pipettes were used to slightly aspirate liposomes, and the behaviors of the liposomes inside the holding pipettes both before and during probing were observed.

The adhesion energy of the liposome inside the polylysine coated holding pipette was determined by multiplying the surface area of the liposome that was in contact with the walls of the holding pipette, $2\pi R_P L$, where R_P is the radius of the holding pipette and L is the length of the liposome inside the holding pipette, by the adhesion energy density of liposomes to polylysine-coated glass, ~1300 x 10^{-9} J/m^2 (Gruhn, Franke et al. 2007; Limozin and Sengupta 2007). The adhesion energy between the liposome and the walls of the holding pipette was then compared to the amount of energy that injection pipettes had been observed to exert onto liposomes, Chapter IV.

Results

Pipette Injection Capabilities

When using the WPI micropipettes, outer diameters 2000 nm and 200 nm, Trypan blue was ejected from the tip of these pipettes at a flow rate of approximately 1 μL/sec

and 100 μL/sec, respectively. However, the in-house pulled nanopipettes (038-09 and 038-10), outer diameters ~35 nm, were not able to eject Trypan blue from their tips when pressure was applied. When the maximum pressure was applied to these pipettes, the nanopipettes were expelled from the grip head. This indicated that pressure was in fact building up inside the pressure transmitter, but that it had no means to be released.

Liposome and Cell Injection

Liposome injection was attempted using the two pipettes capable of injection, WPI, glass pipettes having outer diameters of 2000 nm and 200 nm. When the injection pipettes were inserted into the liposomes at a slow rate, ~ 0.4 μm/sec to ~ 4 μm/sec, the liposomes would conform to the walls of the injection pipette while slightly pulling out of the holding pipette, Chapter IV. It did not appear as though the membrane was penetrated by the injection pipettes. This was confirmed by ejecting Trypan blue from these pipettes and then observing the Trypan blue diffuse away into the solution.

It was thought that the faster injection times (~ 40 μm/sec to ~ 4000 μm/sec) would allow for the membrane to be penetrated at the injection site before the phospholipid molecules would have sufficient time to rearrange themselves and relieve any local strain. However, instead of membrane penetration occurring, the liposomes were pushed out of the plane of the injection pipettes. Often times this resulted in the liposomes tearing, and the portion of the liposome outside the holding pipette would form a new, spherical liposome, and the portion of the liposome inside the holding pipette would be aspirated into the holding pipette, Figure 53.

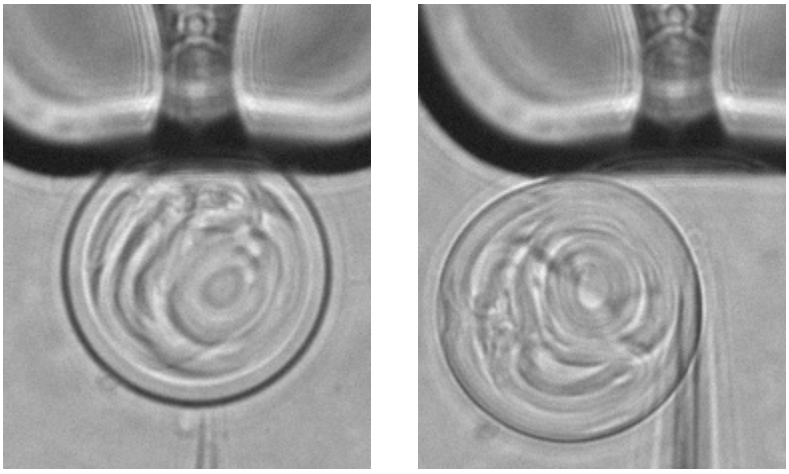

(a) (b)

Figure 53: *Liposome being approached by 200 nm outer diameter injection pipette (a). The injection pipette is inserted into the liposome at a rate of ~ 400 μm/sec (b). The portion of the liposome outside the holding pipette is torn away from the portion of the liposome inside the holding pipette, and a new liposome results.*

Endothelial cell injection was performed using the WPI micropipettes, outer diameters 2000 nm and 200 nm. The injection pipettes were brought into close proximity of the aspirated cells, and then inserted into the cells at rates of ~ 4 μm/sec and ~ 40 μm/sec. Trypan blue was then ejected from the tips of the pipettes. The Trypan blue appeared to stay within the confines of the membrane during injection, turning the cells blue, Figure 54. This indicated that the membrane of the cells had been penetrated by the injection pipettes. Injection was confirmed at pipettes rates of ~ 4 μm/sec and ~40 μm/sec.

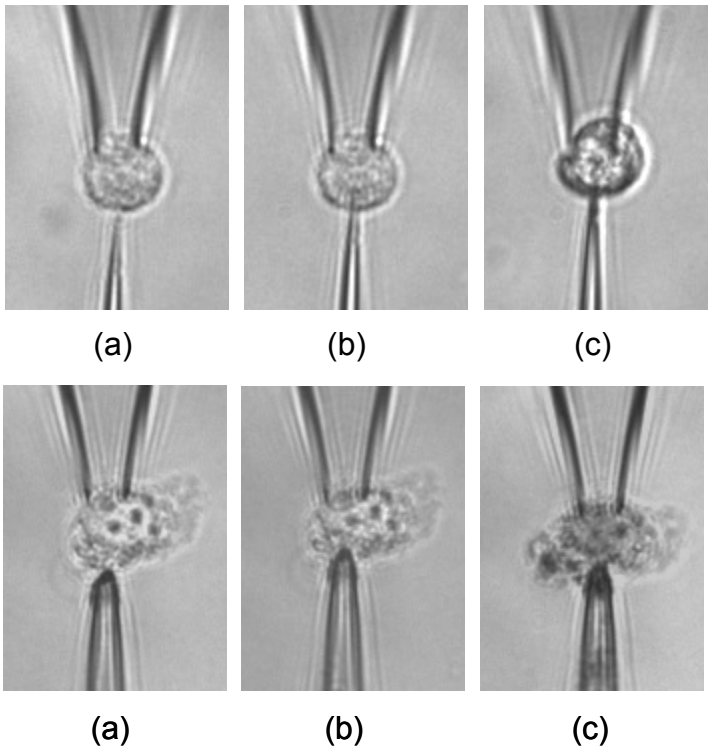

Figure 54: *Endothelial cell injection using the micropipettes with outer diameter 200 nm (above) and outer diameter 2000 nm (below). The injection pipettes approach the cells (a), are inserted into the cells a distance of 5 μm at a rate of ~ 4 μm/sec (b), and the Trypan blue is injected into the cells, turning them blue (c).*

After endothelial cell injection was confirmed, the deformation of the cell during injection was observed using the micropipettes and nanopipette 038-08, outer diameter 25 nm. Pipette insertion rates were at ~ 4 μm/sec, ~ 40 μm/sec, and ~ 400 μm/sec. The 200 nm and 25 nm outer diameter pipettes did not appear to deform the cell during pipette insertion, but a marking on the cell corresponding to the tip of the 200 nm injection pipette remained on the cell after injection pipette removal. The 2000 nm pipette caused the endothelial cell to change from a spherical shape to a spheroidal shape when the pipette was inserted into the cell. Removing the 2000 nm pipette from the cell resulted in

the cell becoming more spherical than when the pipette was probing the cell, but it did not return to its pre-probed shape, Figure 55. A marking on the cell corresponding with the tip of the 2000 nm injection pipette was observed after the injection pipette was removed. The deformation of the cells during injection pipette insertion did not appear to be dependent on pipette insertion rate, results not shown.

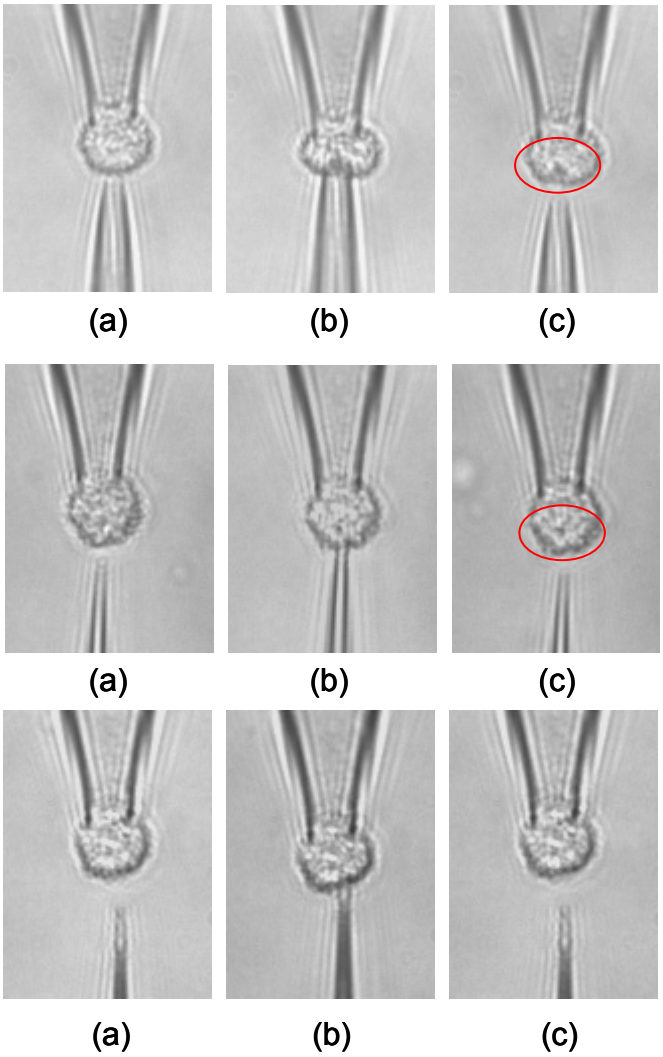

Figure 55: *Insertion of the 2000 nm outer diameter pipette (top), 200 nm outer diameter pipette (middle), and 25 nm outer diameter pipette (bottom) into an endothelial cell. Pipette insertion velocity was ~ 4 μm/sec. The deformation of the cell before pipette insertion (a) was compared to the deformation of the cell during probing (b) and after the injection pipette was removed from the cell (c). Markings on the cell after removal of the injection pipette, possibly indicating cell damage, are circled.*

Applying Constraints to the Liposome during Probing

The attachment of liposomes to a glass slide that was incubated for 30 minutes with pure PBS was compared to the attachment of liposomes to a glass slide that was incubated for 30 minutes with 1 mg/ml polylysine solution. The liposomes on the slide

that was coated with PBS demonstrated no adhesion to the slide, and they were washed away completely when the slide was rinsed with the saline solution. However, ~ 30% of the liposomes that were deposited onto the 1 mg/ml protein coated slide remained attached to the slide after rinsing.

During attachment, only a section of a liposome appeared to interact with the slide. This indicated that the polylysine did not coat the entire slide evenly and some areas of the slide did not contain polylysine. As the liposomes adhered to the slide they tended to flatten out. On occasion, they were observed to change from a spherical to a non-spherical shape during attachment. Additionally, the liposomes appeared to form blisters at their attachment site. Indeed Limozin and Sengupta (2007) also reported the formation of blisters during liposome attachment (Limozin and Sengupta 2007). It is thought the blisters formed as the phospholipids attached to the slide in one section and unattached phosopholipids in this section formed a bubble inside the liposome. A close up of an attached liposome onto a cover slide with a protein concentration of 1 mg/ml and an incubation time of 2 hours is shown, Figure 56. In the pre-rinsed image (Figure 56a), a blister in the lower right portion of the liposome was observed. Movement of this section of the liposome before rinsing indicated that the liposome was adhering to the polylysine-coated glass at this location. After rinsing with the saline solution, the body of the liposome was not in the same location, but the blistered area of the liposome remained attached.

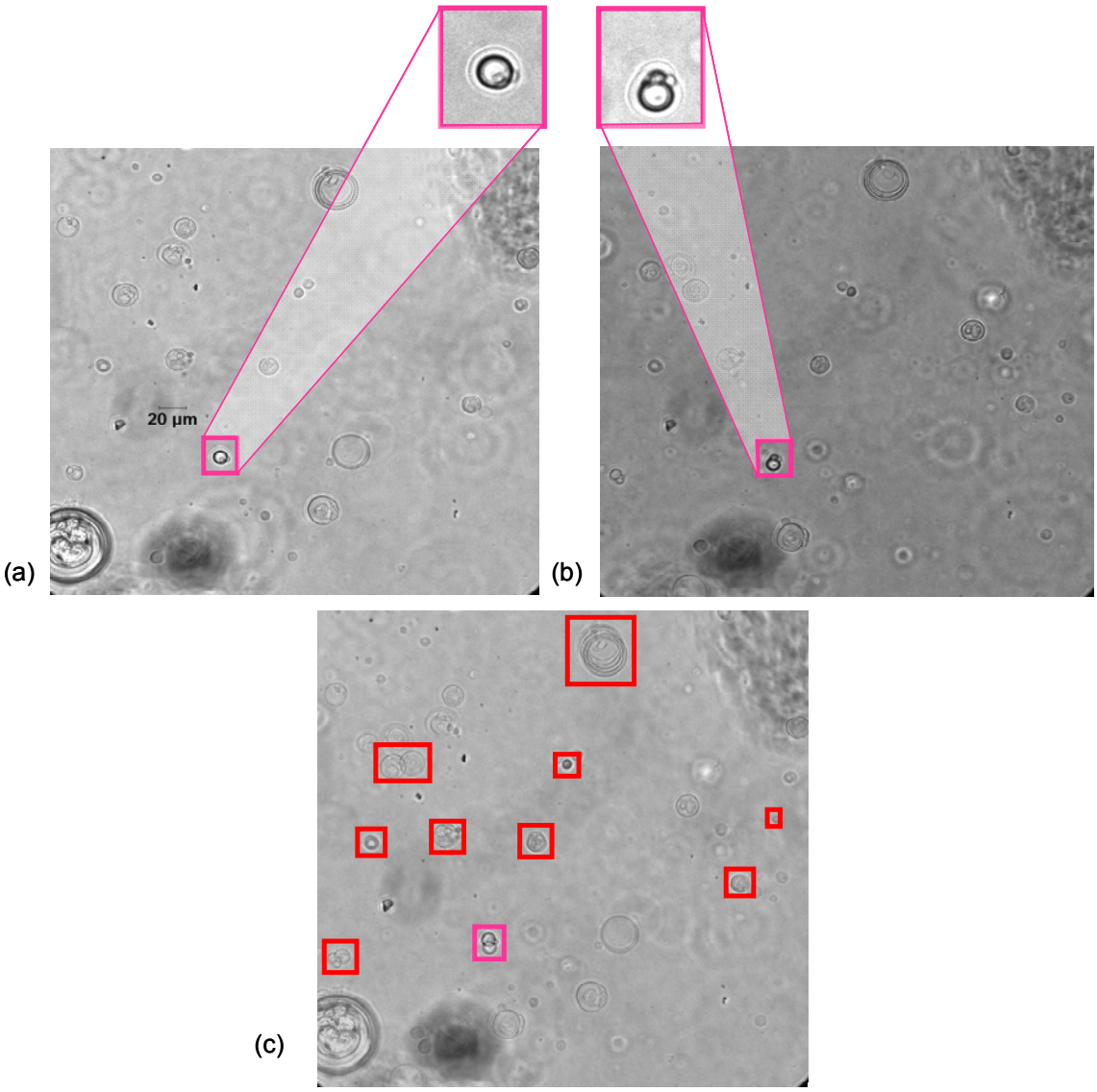

Figure 56: *Liposomes at the bottom of a glass slide that had been incubated with 500 µl of 1 mg/ml polylysine solution for 2 hours (a). The same section of the slide after the slide was slowly rinsed with 100 µl of saline solution (b). Close-ups of an attached liposome before and after rinsing are outlined in pink. The images (a) and (b) were combined to determine if any of the liposomes had adhered to the glass slide (c). Liposomes that were attached to the slide are outlined in red.*

The percentage of liposome adhesion to the polylysine coated glass cover slides using different protein concentrations and incubation times were compared, Table 10. The adhesion of the liposomes tended to increase as the protein concentration and incubation time increased. Increasing the protein concentration above 1 mg/ml did not

seem to affect the percentage of liposome adhesion. Additionally, incubating the protein for 24 hours resulted in no liposome adhesion. Liposomes on slides that had been incubated for 24 hours appeared to be interacting with the protein-coated slides, but they were all rinsed away when the saline solution was added to the slide. The optimal adhesion of the DOPC:DOPS liposomes to the polylysine-coated glass was taken when a protein concentration of 1 mg/ml and an incubation time of ~ 6 hours was used.

Table 10: *Percentage of liposomes attached to the polylysine coated slide after rinsing the slide with 100 µl of saline solution.*

	incubation time (hours)			
protein concentration (mg/ml)	**0.5**	**2**	**6**	**24**
0	0	-	-	-
0.01	0	0	-	-
1	30	40	45	0
10	-	-	40	0

A protein concentration of 1 mg/ml with an incubation time of 6 hours was then used to coat the inside and outside of a holding pipette with polylysine. A liposome was caught by the holding pipette by slowly aspirating the liposome. The aspiration pressure was then held constant, and the liposome was left undisturbed for 10 minutes, Figure 57. During this time, the liposome was slowly pulled into the holding pipette. This indicated that the membrane of the liposome had not attached to the walls of the protein-coated pipette.

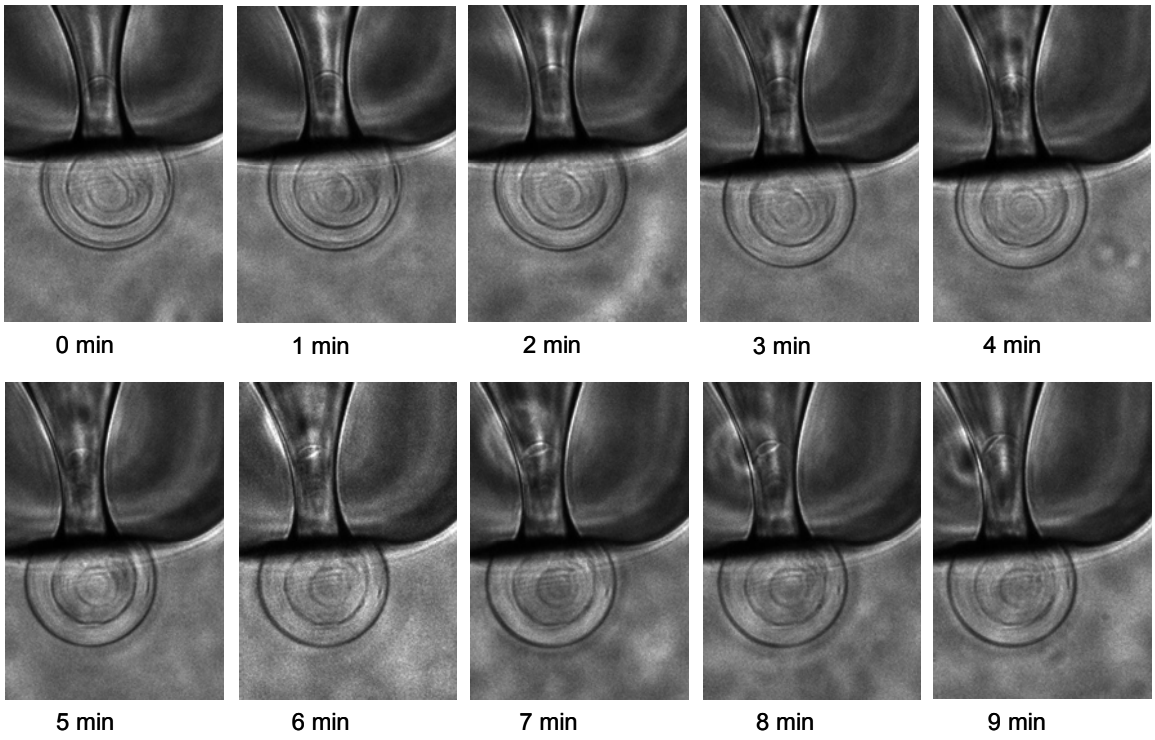

Figure 57: *Images of an aspirated liposome inside a polylysine-coated pipette. The liposome was slowly pulled into the holding pipette over a ten minute period. This indicates that the membrane of the liposome was not attached to the walls of the holding pipette.*

The pipette experiment was performed again with the same protein concentration and incubation period. This time, liposomes attached to the outside of the holding pipette, Figure 58a. Again, a liposome was aspirated with the smallest pressure necessary to keep the liposome inside the holding pipette, and the behavior of the liposome was observed both before and during probing with a 2000 nm outer diameter injection pipette, Figure 58. The caught liposome was allowed to remain undisturbed in the holding pipette for 10 minutes. During this time, the liposome did not appear to move within the holding pipette. However, when the injection pipette was inserted into the liposome, the length of the liposome inside the holding pipette decreased, indicating that once again the liposome was not constrained along the walls of the pipette.

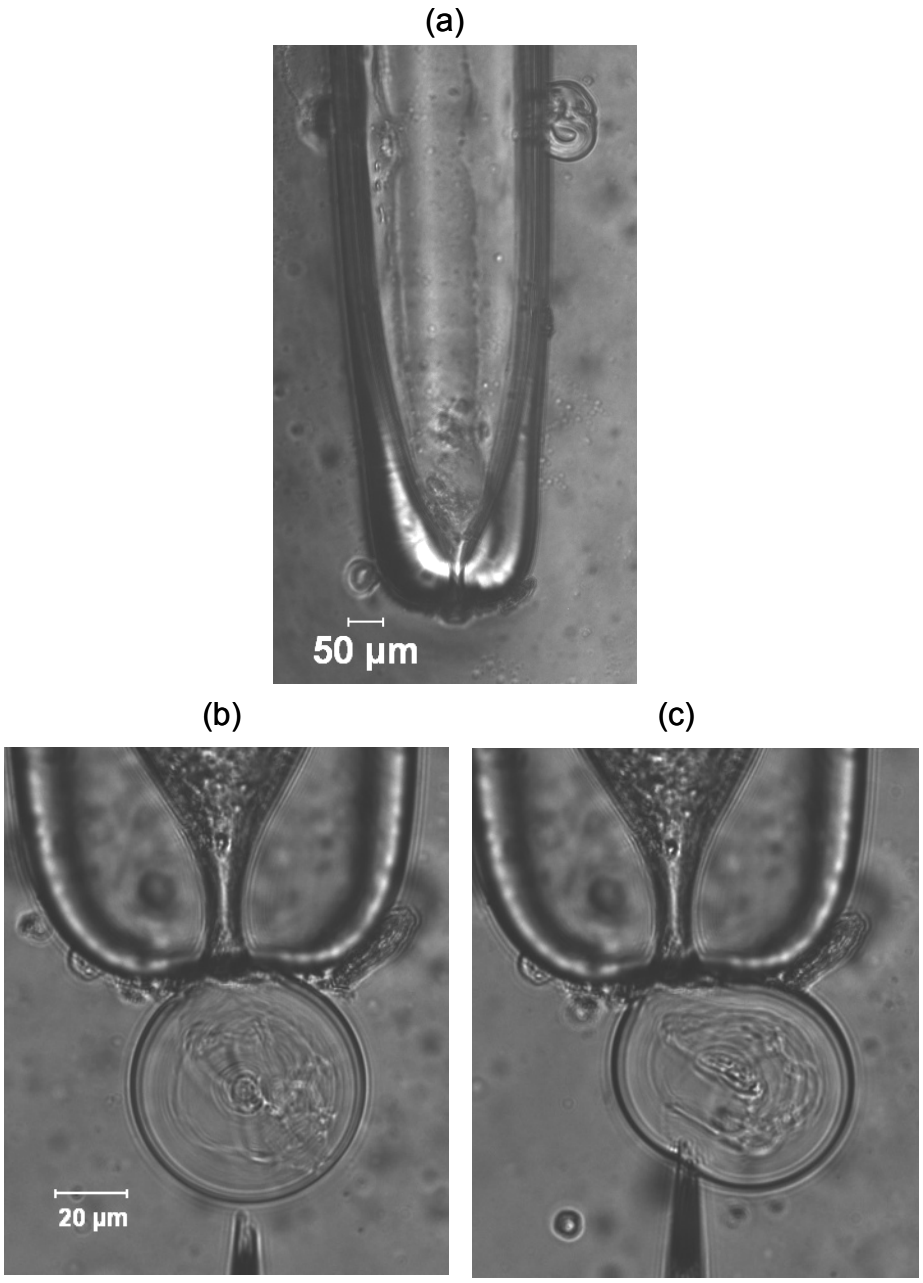

Figure 58: *A holding pipette that had been coated with polylysine (concentration 1 mg/ml) for 6 hours. Liposomes are attached to the outside of the holding pipette (a). Phospholipid fragments are observed on the outside and inside of the tip of the holding pipette before (b) and during (c) probing of the liposome with a 2000 nm outer diameter injection pipette. The membrane of the liposome inside the holding pipette moved during injection pipette manipulation.*

The energy in which a 2000 nm outer diameter injection pipette can exert onto a ~ 45 μm liposome during probing has been found to be ~6 x 10^{-17} J, Chapter IV. The adhesion energy calculated between the liposome, Figure 58, and the walls of the polylysine-coated holding pipette was ~6 x 10^{-16} J. If the holding pipette was not coated with polylysine, the adhesion energy between the liposome membrane and the glass would have been on the order of 10^{-18} J.

Discussion

There are several mechanisms that may have prevented the flow of Trypan blue through the nanopipettes. First, the pipettes may have been closed. This may have occurred during the manufacturing process of the nanopipettes on the Sutter Instruments P-97 Flaming/Brown Micropipette Puller. Additionally, the viscosity of Trypan blue may be too great to flow through the < 35 nm opening of the pipette. Also, the surface tension generated by the meniscus of the Trypan blue at the end of the tip of the nanopipette may have been too great for the fluid pressure to overcome. Finally, hydrophobic interactions between the quartz pipette tip and the Trypan blue may have inhibited the flow.

The endothelial cells were able to be penetrated and injected by injection pipettes having outer diameters as large as 2000 nm and injection speeds as slow as ~ 4 μm/sec. The membrane of a cell contains cholesterols, proteins, and channels. These membrane components increase the stiffness of the cell membrane and restrict the movement of the phospholipid molecules of the membrane. Additionally, interactions between the cytoskeleton of the cell and these membrane components further inhibit the flow of the membrane, and they also decrease the amount of deformation that the cell can undergo. Therefore, when a local strain is produced in the cell membrane, such as in the case in

which an injection pipette acts on the cell, the cell is not able to reconfigure itself and reduce the strain in this area. This results in membrane rupture.

Liposomes, however, have been shown to be impenetrable using injection pipettes with outer diameters as small as 200 nm and injection speeds as high as ~ 4000 μm/sec. The liposomes do not contain cholesterols, proteins, channels, or a cytoskeleton. When a local strain is induced in the membrane of a liposome, the molecules of the membrane quickly reorganize themselves to reduce this strain, and membrane rupture is avoided.

The adhesion of the liposomes to the polylysine coated slides increased as the protein concentration and incubation time increased. The percentage of liposomes adhered to the slides seemed to stabilize at a protein concentration of 1 mg/ml and 6 hours. After 24 hours, there wasn't any attachment of the liposomes to the 1 mg/ml or 10 mg/ml protein-coated slides. However, liposomes did appear to be interacting with these slides before the slides were rinsed with the saline solution. It is uncertain if the liposomes were rinsed away by the saline solution because attachment of the liposomes to the protein after 24 hours was weaker (e.g. if the conformation of the protein changed), or if the rinsing of the liposomes with the saline solution was done more forcefully in this experiment then in the 30 minute, 2 hour, and 6 hour incubation period experiments. The volumetric flow rate in which the saline was added to slides would influence the forces that acted on the liposomes at the bottom of the slides. It is possible that the saline was added more quickly in the 24 hour experiment, and therefore the liposomes attached to these slides were subjected to a greater force, resulting in no liposome attachment.

The adhesion energy density of a DMPC:Cholesterol (1:1) liposome to a polylysine-coated glass substrate is 1200×10^{-9} J/m^2 (Limozin and Sengupta 2007). Although the

liposomes used in these experiments are not the same as those used in the experiments described here (DOPC:DOPS, 7:3), DMPC has the same phosphor head group as the DOPC phospholipids. It is therefore assumed that the adhesion energy density of DOPC:DOPS liposomes is within an order of magnitude to the results obtained by Limozin and Sengupta (2007). Given the geometry of the aspirated liposome, Figure 58, the adhesion strength of the liposome should be an order of magnitude greater than the force in which an injection pipette having an outer diameter of 2000 nm would exert against the liposome, Chapter IV. It was therefore expected that the liposome would be constrained along the walls of the holding pipette. However, this was not the case. There are several reasons for why this liposome was not constrained.

It is possible that the polylysine did not coat the walls of the holding pipette over its entire surface. If the protein uniformly coated the surface of the holding pipette, the membrane of the liposome inside the holding pipette should not have moved during probing with the injection pipette. However, if none of the protein coated the inside of the holding pipette, then the adhesion energy between the holding pipette and the liposome would have been an order of magnitude less than the energy exerted onto the liposome by the injection pipette. Since the liposome was observed to move out of the holding pipette during probing, it is likely that the polylysine did not create a uniform coating inside the walls of the holding pipette. The adhesion energy would then be somewhere in between the adhesion energy if the pipette were fully coated and if it were not coated at all, making it possible that the adhesion energy of the liposome to the polylysine coated pipette was less than the energy of the injection pipette. Indeed, during the adhesion of the liposomes to the protein-coated glass slides, only small sections of the

liposomes were observed to interact and adhere to the slides, indicating the protein did not coat the entire area.

The protein concentration and incubation time for optimal liposome attachment was determined from experiments done on the adhesion of the liposomes to protein-coated glass slides. The holding pipette has a different geometry than the flat slide, and the curvature of the holding pipette may have affected the adhesion of the liposomes. Additionally, gravity has been shown to be a factor in liposome adhesion (Gruhn, Franke et al. 2007). Due to the geometry of the pipette, gravity would not influence the adhesion of the liposome to the left, right, and upper walls of the holding pipette, and therefore the adhesion energy between the holding pipette and the liposome may have been less than the energy that was calculated.

Additionally, the glass slides were washed with 1 ml of PBS before depositing liposomes onto the slide. The washing of the slides was done in a very controlled manner. When rinsing the inside of the holding pipette to remove excess polylysine, PBS was aspirated and expelled from the tip of the pipette at some rate. The shear stresses that the protein-coated pipettes experienced during this time are unknown. It is possible that the force of the PBS over the protein-coated surface was powerful enough to remove the polylysine from the walls of the holding pipette.

Finally, phospholipid fragments were observed in and around the entrance of the polylysine-coated, holding pipette. It is possible that small phospholipid fragments had lined the walls of the holding pipette and prevented the aspirated liposome from attaching.

The injection of single-liposomes and single-cells with pharmaceuticals or other macromolecules shows potential in improving the diagnosis, detection, and treatment of disease (Kao and Sterling 2003; Han, Nakamura et al. 2005; Obataya, Nakamura et al. 2005; Storrie 2005; Leary, Liu et al. 2006; Zucchi, Sanzone et al. 2007). Establishing a relationship between the size of the injection device, injection rate, and the deformation or damage done to a liposome or cell during injection can assist in optimizing the success rate of these procedures.

Chapter VI: Forces Required by Micro and Nanopipettes for Liposome Injection: A Finite Analysis Study

Abstract

Determining the minimum amount of force required to puncture biological membranes is important in minimizing the damage done to these membranes during single-liposome, single-cell, and single-organelle injections and surgeries. Using finite element analysis, the normal contact stresses produced by injection pipettes of varying sizes acting against the deformable membrane of an aspirated liposome were modeled, and the deformations and strains of the membrane were computed. Parameters to represent the geometries of the holding and injection pipettes, as well as the mechanical properties of liposome membranes were used in the simulations. The model predicts that injection pipette with outer diameters of 100 nm, 1000 nm, and 2000 nm and inner diameters of 50 nm, 500 nm, and 1000 nm, respectively, are able to produce a normal contact stress on the liposome membrane that is sufficient to cause membrane rupture. Increasing the radius of the membrane upon which the normal force of the pipette was acting, i.e. increasing the size of the injection pipette, allowed for an increase in the amount of pipette force that the membrane could withstand before rupture. The model predicts that an aspirated liposome can withstand 50 pN of force with the 2000 nm outer diameter pipette, 20 pN of force with the 1000 nm outer diameter pipette, and 5 pN of force with the 100 nm outer diameter pipette before rupturing. Understanding how the mechanical properties of cells or liposomes affect the amount of force that is required to penetrate biological membranes can assist in minimizing membrane damage during single-cell and single-liposome injections.

Introduction

Computer models are often used to predict the behaviors of biological systems during normal physiological conditions or when an external stress is applied to the system. Examples of simulations in biology include the use of a finite element model to determine the deformation of the cytoskeleton of an endothelial cell during cell rounding (Jean, Chen et al. 2005), the creation of Monte Carlo simulations to determine the diffusion of an ultra-flexible vesicle through a pore (Gompper and Kroll 1995) or to determine the deformation of a red blood cell as it is being aspirated by a micropipette (Discher, Boal et al. 1998), and the use of a micromechanical model to determine the elastic properties of the structural support network of a cell (Roy and Qi 2008).

A computer model had been created to determine the forces and deformations of a neuronal membrane when a protein filament inside the cell acts against the membrane, Chapter II (Allen 2008). It was determined from this model that although a filament can cause membrane deformation, membrane rupture is unlikely to occur during the probing of the membrane by the protein filament. This was unlike the response of an aspirated endothelial cell that experiences membrane rupture when micro and nanopipettes probes its membrane, Chapter V.

The amount of force required to puncture human epidermal melanocytes has been determined using atomic force microscopy (AFM) (Obataya, Nakamura et al. 2005). This force was dependent on the size and geometry of the AFM tip, but all of the forces were on the order of ~ 1 nN. However, the AFM tips used were not hollow, and therefore they cannot be used for injection purposes. Additionally, the cells used in this

study were attached to a substrate. It remains uncertain how a aspirated cell will respond to forces created by various injection devices.

We have created a numerical model to determine the indentations and forces required to puncture constrained, aspirated liposomes using both micro and nanopipettes. This information can be used to ensure that these forces and deformations are not exceeded during single-liposome and single-cell injections and surgeries, thereby minimizing damage during these procedures.

Methods

Model Parameters

In the present model it was assumed that the membrane is homogeneous. It was also assumed that under quasi-static loading conditions, the membrane may be modeled as a transversely isotropic material, with the membrane normal serving as the axis of symmetry. A transversely isotropic material requires that five elastic constants be specified. Since phospholipid membranes have been observed to behave as a two-dimensional fluid with the two layers of the membrane flowing smoothly past each other and with individual phospholipid molecules diffusing freely and exchanging locations (Dai and Sheetz 1995; Fygenson, Elbaum et al. 1997), both the in-plane and out-of-plane Poisson's ratios have been modeled as 0.49. Indeed, Charras et al., (2004) previously assumed a Poisson's ratio of 0.49 for the cell membrane (Charras, Williams et al. 2004). This ratio was based on a paper by Hamill and Martinac (2001) in which the cell membrane is assumed to be incompressible (Hamill and Martinac 2001). To our knowledge, this is yet to be experimentally verified or theoretically predicted. The in-plane Young's moduli, $Y_{r\theta}$, was computed by dividing the area expansion modulus, K_A,

of the DOPC:DOPS lipid vesicle, 0.067 Nm^{-1}, by the thickness of the membrane, 4.5 nm (Boal 2002; Kucerka, Pencer et al. 2007). This resulted in an $Y_{r\theta}$ of 15 MPa. The micropipette aspiration technique similar to the one developed by Evans et al. (1990) was used to measure K_A (Evans and Rawicz 1990). The details of this experiment are found in Chapter III.

For an isotropic material with a Poisson's ratio of 0.5, the shear modulus is equal to $Y/3$, and therefore 5 MPa. This value was chosen for the through-plane shear moduli, G_{rz} and $G_{\theta z}$. However, because the layers of the membrane flow freely over one another, the in-plane shear modulus, $G_{r\theta}$, must be lower. This was taken to be 0.15 MPa, two orders of magnitude smaller than the out-of-plane shear modulus.

The forces used in the simulations were estimated. In order to puncture a phospholipid membrane, a force that results in a ~ 3 - 4% areal strain needs to be applied to the membrane (Nichol and Hutter 1996; Boal 2002; Heidemann and Wirtz 2004). A force that resulted in an areal strain greater than 3% was taken as the puncture force of the membrane. The simulated puncture forces were on the order of 1-10s of pN.

The estimated force was used to determine the normal contact stress acting on the membrane. The normal contact stress was, $s = F / A_i$, where s is the normal contact stress acting on the membrane due to the injection pipette pressing against the liposome and A_i is the area of the injection pipette. The injection pipette was treated as a hollow cylinder, and therefore the area of the membrane in which the pipette acts is, $A_i = \pi R_{io}^{\ 2} - \pi R_{ii}^{\ 2}$, where R_{io} is the outer radius of the injection pipette, and R_{ii} is the inner radius of the injection pipette. The injection pipettes simulated had outer radii of 1000 nm, 500 nm,

and 50 nm, with corresponding inner radii of 500 nm, 250 nm, and 25 nm. The contact areas were then 2.4 μm^2, 0.59 μm^2, and 0.0059 μm^2, respectively.

Given the estimated range of forces, the normal contact stresses exerted on the membrane by the injection pipettes was ~ 0.42 - 1700 Pa. These contact stresses were modeled such that the center of the injection pipette was in the center of the spherical portion of the liposome outside the holding pipette, Figure 59. The deformations and strains of the membrane when these stresses were applied to the membrane were determined.

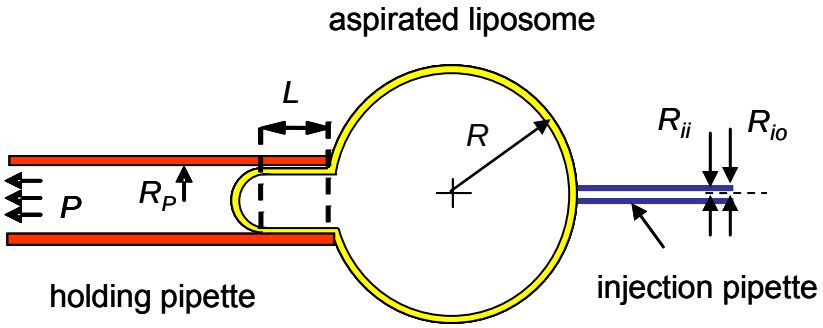

Figure 59: *Schematic of an aspirated liposome before probing with an injection pipette. The injection pipette acts against the membrane at the center of the spherical portion of the liposome outside the holding pipette, and parallel and opposite the entrance to the holding pipette.*

The geometry of the aspirated liposome was determined based on experimental results, such as in Chapter III. The liposome was created by defining the radius of the spherical portion of the liposome outside the holding pipette, R, the length of the liposome inside the pipette, L, and the radius of the holding pipette, R_P, Table 1. A holding pipette with an inner radius of 7.5 μm was used in the experiments described in Chapter IV, and this size holding pipette was model here as well. The aspiration

pressure on the liposome, P, was set to 0 Pa, representing a situation where the aspiration pressure was too small to be measured by the pressure transducer, such as in the experiment described in Chapter IV.

For modeling purposes, the aspirated liposome was assumed to be taut, and therefore any stress on the membrane due to the injection pipette caused an areal strain in the membrane. From previous experiments, it was determined that liposomes are not taut at low aspiration pressures, Chapter III. Instead, there are membrane undulations due to thermal fluctuations of the membrane. Thermal fluctuations are not included within the scope of this work.

Given the chosen geometry of the aspirated liposome, the length-to-thickness ratio of the membrane was ~27000, and therefore a large deflection analysis was required to analyze the deformations and strains in the membrane as the liposome was deformed by the injection pipettes.

Table 11: *Model parameters*

parameter	description	value	reference
A_i	area in which injection pipette can exert force	2.4 μm^2, 0.59 μm^2, and 0.0059 μm^2	-
F	filament force acting on membrane	1 - 50 pN	-
$G_{r\theta}$	in-plane shear modulus of membrane	0.15 MPa	(Allen 2008)
G_{zr} and $G_{\theta z}$	out of plane shear moduli of the membrane	5 MPa	(Allen 2008)
L	length of liposome inside the holding pipette	45 μm	-
P	aspiration pressure of the holding pipette	0 Pa	-
R	radius of the liposome outside the holding pipette	25 μm	-
R_{ii}	inner radius of the injection pipette	25 nm, 50 nm, and 500 nm	-
R_{io}	outer radius of the injection pipette	50 nm, 100 nm, and 1000 nm	-
R_P	inner radius of the holding pipette	7.5 μm	-
s	normal contact stress acting on liposome	0.42 - 1700 Pa	-
t	thickness of neuronal membrane	4.5 nm	(Boal 2002)
$Y_{r\theta}$, Y_{zr}, $Y_{\theta z}$	Young's modulus of membrane	15 MPa	Chapter III
$\upsilon_{r\theta}$, υ_{zr}, $\upsilon_{\theta z}$	Poisson's ratio membrane	0.49	(Elbaum, Fygenson et al. 1996; Dimova, Dietrich et al. 1999; Helfer, Harlepp et al. 2001)

Boundary Conditions

Boundary conditions were applied along the liposome where the liposome was in contact with the holding pipette. This included the inner walls of the holding pipette and the entrance to the tip of the holding pipette. Along L, the liposome was fully

constrained. This boundary condition represents a bounding case that is similar to what a cell or liposome might encounter if it were loaded very quickly, and the membrane did not have sufficient time to "flow into the boundary". This is the case during cellular injection when integral proteins interact with both the cytoskeleton and the extracellular matrix, restricting membrane flow. This appears to also be the case during the injection of aspirated, endothelial cells, when the injection pipette penetrates the cell membrane without any visible movement of the membrane, Chapter V. In fact, some modern cell injectors utilize a very fast jabbing or hammering motion to inject neuronal growth cones after the pipette tip has been brought into close proximity to the cell (Dent, Callaway et al. 1999) (personal observation). It should be noted that this fully constrained boundary condition is not appropriate for pure phospholipid membranes, i.e. fluid membranes. In fluid membranes, molecules can quickly rearrange themselves in order to reduce the local strain caused by the injection pipette, making them impenetrable, Chapter V.

At the entrance of the holding pipette, where the outside of the holding pipette was in contact with the spherical portion of the liposome, the membrane was constrained in the y direction (the liposome was not able to move through the walls of the holding pipette).

Element Type

The aspirated liposome was modeled as axisymmetric along the *y* axis, and therefore an axisymmetric element type was used, Figure 60. The use of an axisymmetric element type allows for only one section of the membrane to be modeled, but the entire membrane was represented. This permitted the use of fewer elements in the simulation, resulting in faster computation times.

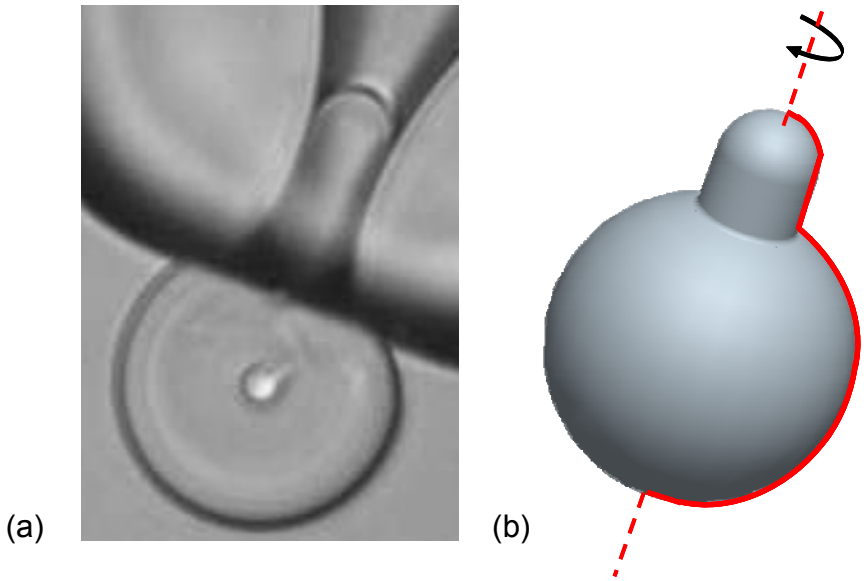

Figure 60: *Image of an aspirated liposome (a). ProEngineer model of an aspirated liposome (b). The axis of symmetry is represented by the dotted line. A line, highlighted in red, is used to represent the liposome. This line can be rotated around the axis of symmetry in order to create the aspirated liposome.*

Due to the geometry of the liposome, i.e. the large length-to-thickness ratio, the aspirated liposome was treated as a shell. The axisymmetric, shell element type SHELL208 was used to model the membrane. SHELL208 is typically used to model thin to moderately thick shell structures (Allen 2008). SHELL208 elements are composed of

two nodes, and each node contains three degrees of freedom: two translational and one rotational.

The model of the aspirated liposome was created by defining the parameters to represent the geometry of the liposome, holding pipette, and injection pipette, as well as the number of nodes to use in the simulation. The code was written so that the geometries of the liposome, holding pipette, and injection pipette, as well as the number of nodes, aspiration pressure, and contact forces could be easily changed to represent a variety of different injection conditions. Once the nodes were created, elements were created between the nodes, and the boundary conditions were applied to model. Next, a normal contact stress was applied to the elements that would be affected by the injection pipette. The number and location of these elements were determined based on the inner and outer radius of the tip of the injection pipette, Figure 61.

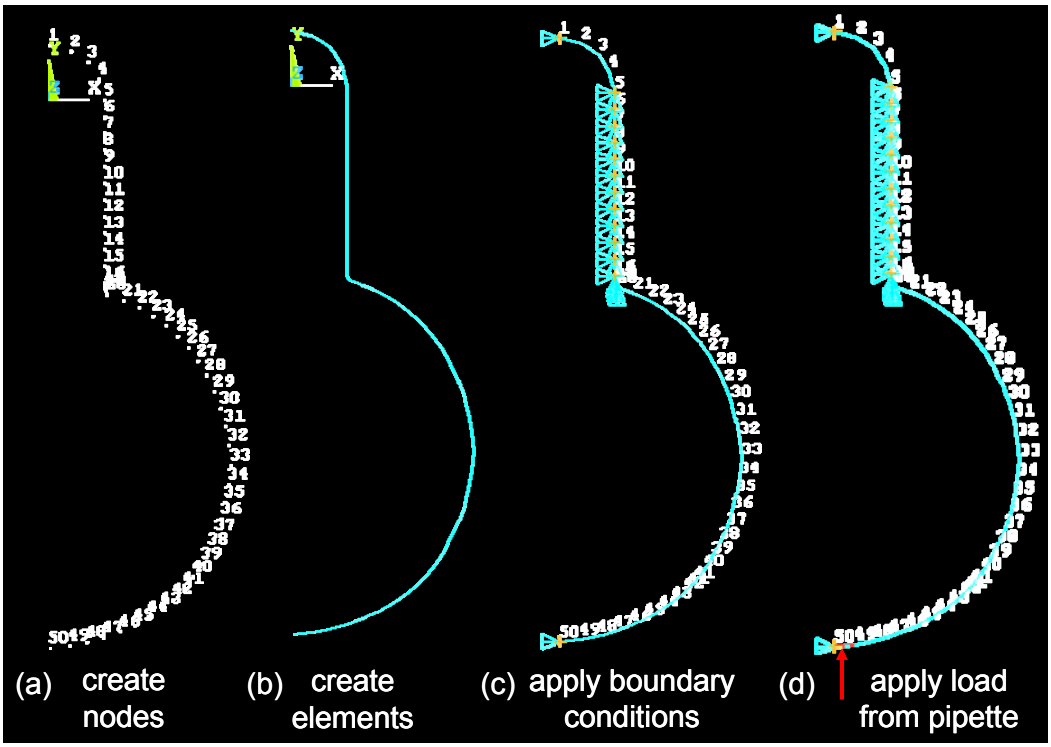

Figure 61: *Nodes were created to represent the aspirated liposome (a), and then elements were created connecting the nodes. Boundary conditions were applied along the walls of the holding pipette and at the entrance to the holding pipette (c). A normal contact stress representing the pressure on the liposome due to the injection pipette was applied to the appropriate elements (d).*

An attempt was made to model the entire liposome using 3D element types in order to compare the axisymmetric element results with a 3D model. ProEngineer wa used to model the membrane, but the geometry of liposome prevented the model from being created: the liposome membrane was too thin. The creation of the liposome in ANSYS was also attempted, but even when the liposome was treated as a hollow sphere, due to the aspect ratio of the liposome, the number of elements necessary to model the liposome exceeded our ANSYS license limit of 32000 elements.

Convergence Study

A strain convergence study was performed to determine the number of elements needed to model the liposome when the largest area, 2.4 μm^2, of the membrane was acted

on by the injection pipette (inner diameter 500 nm, outer diameter 1000 nm). The maximum strain in the radial direction on the inner and outer surface of the membrane was determined numerically, and the forces that caused an areal strain greater than 3% in either surface of the membrane were compared for membranes comprised of 8000, 10000, 15000, 20000, 25000, and 30000 elements. The solution was considered to be converged when the force required to create an areal strain larger than 3% (puncture force) was within 5% of the puncture force determined when the number of elements was increased. The convergence study indicated that a 20000-element mesh was sufficient to model an aspirated liposome with $R = 25$ μm and $L = 45$ μm, Figure 62.

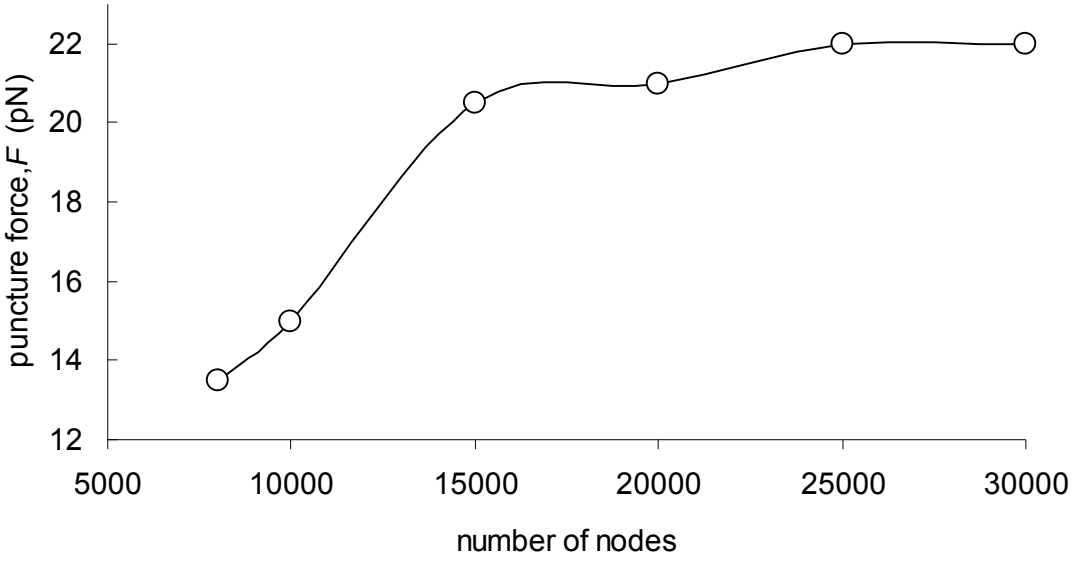

Figure 62: *Puncture force, F, vs. number of nodes used to create the simulation. The force required to puncture the aspirated liposome with an injection pipette, inner diameter 500 nm and outer diameter 1000 nm, converged on a solution when 20000-30000 elements were used to model the membrane.*

Liposome Puncture Force Determination

After verifying that ANSYS is capable of solving the simulation given the geometries and boundary conditions, the deflections and stains of aspirated liposomes was computed. Liposomes were modeled as transversely isotropic with the values listed, Table 1.

If the areal strain in a single element of the membrane exceeded ~3 %, the membrane was considered to have ruptured. The areal strain of an element is the sum of its in-plane strains such that,

$$\varepsilon_{areal} = \varepsilon_r + \varepsilon_\theta , \tag{28}$$

where ε_{areal} is the areal strain, ε_r is the radial in-plane membrane strain, and ε_θ is the circumferential in-plane strain.

Results

Liposome Puncture Force Determination

Since ANSYS does not have a transversely isotropic material type, an orthotropic material type was chosen. Of the nine constants necessary to define an orthotropic material, five unique values were entered as summarized, Table 1. The low in-plane shear modulus was selected to simulate a fluid incapable of supporting shear load. Although the static in-plane shear modulus of the membrane is unknown, the ability of the layers of the membrane to flow freely across one another indicates that the membrane has a low in-plane shear modulus.

The forces necessary to puncture the membrane increased as the size of the injection device increased. For the 100 nm outer diameter pipette, the force required to puncture the membrane was 5 pN. The 1000 nm outer diameter pipette required 22 pN of force to puncture the membrane, and the 2000 nm inner diameter pipette required 49 pN of force be applied to the membrane in order for the membrane to rupture, Figure 63. Similarly, the deformation of the membrane increased as the force of the injection pipette increased. When probing the taut, liposome with a 100 nm outer diameter pipette, the membrane deformed 26 nm before rupture. The 1000 nm outer diameter pipette deformed 71 nm before rupture, and the 2000 nm outer diameter pipette deformed 140 nm before membrane penetration.

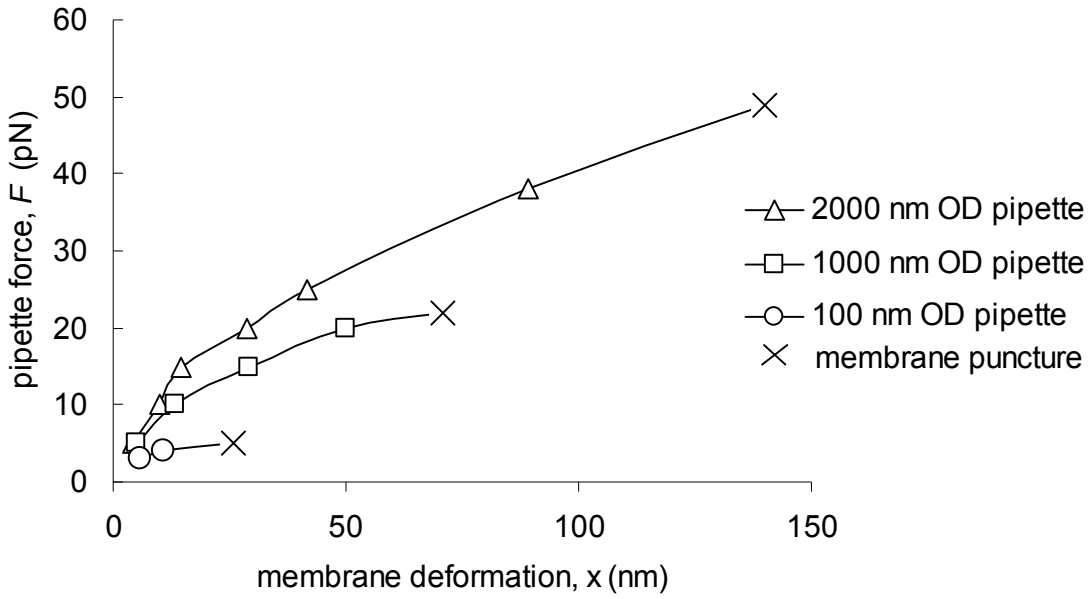

Figure 63: *membrane puncture force, F, vs. membrane deformation, x. The amount of force required to puncture the membrane increased as the contact area of the pipette increased.*

Discussion

As expected, the amount of force that was required to penetrate an aspirated membrane increased as the size of the injection device increased. Also, the deformation of a liposome when probed by three different sized pipettes at the same force increased as the size of the pipette decreased. This was due to the stress on the membrane increasing as the size of the injection device decreased.

The forces calculated for membrane injection using computer simulation were within an order of magnitude of the forces that were applied during the probing of aspirated liposomes, Chapter IV. The experimentally determined forces in which the injection pipettes acted on the liposome were ~ 1 pN for the 2000 nm outer diameter, 1000 nm inner diameter pipette, a force numerically determined to be too small for membrane rupture, and increased to ~ 6 pN for the 25 nm outer diameter pipette. We modeled a

pipette with an outer diameter of 50 nm and an inner diameter of 25 nm, and it was determined that when a force of ~ 5 pN was applied to the membrane, the membrane would rupture. According to our model, a 25 nm outer diameter pipette acting on the membrane should have ruptured the membrane at a force less than 5 pN, but this did not appear to be the case, Chapter V. However when probing the liposomes with this pipette, membrane puncture could not be confirmed because the nanopipette was not capable of injection, Chapter V. Regardless, there are several differences between the model and the experimental setup that may result in the model inaccurately predicting membrane puncture.

When the aspirated liposomes were probed with the injection pipettes, the liposomes would slide out of the holding pipette and conform to the walls of the injection pipette. This demonstrated that the aspirated liposomes were not fixed within the holding pipette, and therefore the fully constrained boundary conditions of the model do not apply for liposomes. If, however, the movement of the liposome inside the holding pipette was restricted, a situation that could possibly be created by using polylysine to attach the liposome to the holding pipette, the fixed boundary conditions of the model would apply, and the model would more accurately represent liposome injection.

A lightly aspirated liposome is not taut, Chapter III. As an injection pipette probed a liposome, the unfolding of the membrane undulations would allow for the membrane to be deformed without causing any areal strain in the membrane. The model however assumed that the liposome membrane was taut. The strain computed using the numerical model of the aspirated, probed liposome would therefore be greater than the actual areal strain of an aspirated, probed liposome. As a result, the actual forces and deformations

required for membrane puncture would be greater than the puncture forces and deformations that were computed numerically.

The numerical model performed a static analysis. The cell however is viscoelastic (Canetta, Duperray et al. 2005; Coldren, Foteinopoulou et al. 2008; Yang, Effler et al. 2008), and therefore the speed in which the injection pipette acts upon the cell will affect the force and deformation required for membrane penetration. A dynamic simulation would more accurately represent cellular injection.

Although the model does not accurately portray the boundary conditions of an aspirated liposome, nor does it take into account the membrane undulations of the liposome, the forces that were numerically determined to puncture the liposome are within an order of magnitude of the forces that the various sized injection pipettes were found to exert against the liposome membranes, Chapter IV. The model therefore has potential to be used as a tool for determining the forces and deformations required for single-liposome and single-cell injection.

Cell membranes contain membrane proteins, ion channels, and sterols. Depending on the cell type, the concentration and type of each of these membrane components will change, and the mechanical properties of the membranes will change as well. Different cell types will therefore require different forces to be applied to them in order for their membranes to be penetrated. The use of a computer model allows for the properties of the cell to be easily adjusted, and then the forces and deformations required for membrane penetration using a variety of injection devices can be easily predicted.

Future work could include creating a more accurate model of the injection of aspirated liposomes and cells by including thermal undulations of the membrane and

redefining the boundary conditions in the model. Additionally, the mechanical properties of spherical cells can be determined using the micropipette aspiration technique described in Chapter III, and then the forces and deformations of living cells can be determined using the methods described in Chapter IV. Examples of cells that are spherical during micropipette aspiration, and are therefore good candidates for the force and deformation determination methods used in Chapters III and IV, include chondrocytes, neutrophils, red blood cells, and endothelial cells (Hochmuth, Shao et al. 1996).

List of References

Allen, K. B., Sasoglu, F.M., Layton, B.E. (2008). "A Mechanical Model for Cytoskeleton and Membrane Interactions in Neuronal Growth Cones." ASME Journal of Biomechanics.

Atilgan, E., D. Wirtz, et al. (2006). "Mechanics and dynamics of actin-driven thin membrane protrusions." Biophys J **90**(1): 65-76.

Baas, P. W. (2000). "Strategies for studying microtubule transport in the neuron." Microsc Res Tech **48**(2): 75-84.

Boal, D. H. (2002). Mechanics of the cell. Cambridge, UK ; New York, Cambridge University Press.

Brangwynne, C. P., F. C. MacKintosh, et al. (2006). "Microtubules can bear enhanced compressive loads in living cells because of lateral reinforcement." J Cell Biol **173**(5): 733-41.

Charras, G. T., B. A. Williams, et al. (2004). "Estimating the sensitivity of mechanosensitive ion channels to membrane strain and tension." Biophysical Journal **87**(4): 2870-2884.

Dai, J. and M. P. Sheetz (1995). "Axon membrane flows from the growth cone to the cell body." Cell **83**(5): 693-701.

Dai, J. and M. P. Sheetz (1995). "Mechanical properties of neuronal growth cone membranes studied by tether formation with laser optical tweezers." Biophys J **68**(3): 988-96.

Dennerll, T. J., H. C. Joshi, et al. (1988). "Tension and compression in the cytoskeleton of PC-12 neurites. II: Quantitative measurements." J Cell Biol **107**(2): 665-74.

Dent, E. W., J. L. Callaway, et al. (1999). "Reorganization and movement of microtubules in axonal growth cones and developing interstitial branches." J Neurosci **19**(20): 8894-908.

Dent, E. W. and K. Kalil (2001). "Axon branching requires interactions between dynamic microtubules and actin filaments." J Neurosci **21**(24): 9757-69.

Dimova, R., C. Dietrich, et al. (1999). "Falling ball viscosimetry of giant vesicle membranes: Finite-size effects." European Physical Journal B **12**(4): 589-598.

Dong, L. X., F. Arai, et al. (2004). "Destructive constructions of nanostructures with carbon nanotubes through nanorobotic manipulation." Ieee-Asme Transactions on Mechatronics **9**(2): 350-357.

Dupuis, D. E., W. H. Guilford, et al. (1997). "Actin filament mechanics in the laser trap." J Muscle Res Cell Motil **18**(1): 17-30.

Elbaum, M., D. K. Fygenson, et al. (1996). "Buckling microtubules in vesicles." Physical Review Letters **76**(21): 4078-4081.

Ergenc, A. F. and N. Olgac (2007). "New technology for cellular piercing: rotationally oscillating mu-injector, description and validation tests." Biomed Microdevices.

Ermilov, S. A., D. R. Murdock, et al. (2007). "Studies of plasma membrane mechanics and plasma membrane-cytoskeleton interactions using optical tweezers and fluorescence imaging." J Biomech **40**(2): 476-80.

Evans, E. and W. Rawicz (1990). "Entropy-driven tension and bending elasticity in condensed-fluid membranes." Physical Review Letters **64**(17): 2094-2097.

Felgner, H., R. Frank, et al. (1996). "Flexural rigidity of microtubules measured with the use of optical tweezers." J Cell Sci **109 (Pt 2)**: 509-16.

Freedman, J. R., D. Mattia, et al. (2007). "Magnetically assembled carbon nanotube tipped pipettes." Applied Physics Letters **90**(10): -.

Fygenson, D. K., M. Elbaum, et al. (1997). "Microtubules and vesicles under controlled tension." Physical Review E **55**(1): 850-859.

Gittes, F., B. Mickey, et al. (1993). "Flexural rigidity of microtubules and actin filaments measured from thermal fluctuations in shape." J Cell Biol **120**(4): 923-34.

Gordon-Weeks, P. R. (2004). "Microtubules and growth cone function." J Neurobiol **58**(1): 70-83.

Hamill, O. P. and B. Martinac (2001). "Molecular basis of mechanotransduction in living cells." Physiol Rev **81**(2): 685-740.

Heidemann, S. R. and D. Wirtz (2004). "Towards a regional approach to cell mechanics." Trends Cell Biol **14**(4): 160-6.

Helfer, E., S. Harlepp, et al. (2001). "Viscoelastic properties of actin-coated membranes." Phys Rev E Stat Nonlin Soft Matter Phys **63**(2 Pt 1): 021904.

Hill, T. L. (1987). Linear Aggregation Theory in Cell Biology. New York, Springer-Verlag.

Ingber, D. E. (1993). "Cellular tensegrity: defining new rules of biological design that govern the cytoskeleton." J Cell Sci **104 (Pt 3)**: 613-27.

Jean, R. P., C. S. Chen, et al. (2005). "Finite-element analysis of the adhesion-cytoskeleton-nucleus mechanotransduction pathway during endothelial cell rounding: axisymmetric model." J Biomech Eng **127**(4): 594-600.

Karafyllidis, I. G. and D. C. Lagoudas (2007). "Microtubules as mechanical force sensors." Biosystems **88**(1-2): 137-46.

Kas, J., H. Strey, et al. (1993). "Direct Measurement of the Wave-Vector-Dependent Bending Stiffness of Freely Flickering Actin-Filaments." Europhysics Letters **21**(8): 865-870.

Kerssemakers, J. W., E. L. Munteanu, et al. (2006). "Assembly dynamics of microtubules at molecular resolution." Nature **442**(7103): 709-12.

Kikumoto, M., M. Kurachi, et al. (2006). "Flexural rigidity of individual microtubules measured by a buckling force with optical traps." Biophys J **90**(5): 1687-96.

Kojima, H., A. Ishijima, et al. (1994). "Direct measurement of stiffness of single actin filaments with and without tropomyosin by in vitro nanomanipulation." Proc Natl Acad Sci U S A **91**(26): 12962-6.

Kurz, J. C. and R. C. Williams, Jr. (1995). "Microtubule-associated proteins and the flexibility of microtubules." Biochemistry **34**(41): 13374-80.

Lewis, A. K. and P. C. Bridgman (1992). "Nerve growth cone lamellipodia contain two populations of actin filaments that differ in organization and polarity." J Cell Biol **119**(5): 1219-43.

Mogilner, A. and G. Oster (2003). "Force generation by actin polymerization II: the elastic ratchet and tethered filaments." Biophys J **84**(3): 1591-605.

Nichol, J. A. and O. F. Hutter (1996). "Tensile strength and dilatational elasticity of giant sarcolemmal vesicles shed from rabbit muscle." J Physiol **493 (Pt 1)**: 187-98.

Odde, D. J., L. Ma, et al. (1999). "Microtubule bending and breaking in living fibroblast cells." J Cell Sci **112 (Pt 19)**: 3283-8.

Odde, D. J. and M. J. Renn (2000). "Laser-guided direct writing of living cells." Biotechnol Bioeng **67**(3): 312-8.

Pollard, T. D. and G. G. Borisy (2003). "Cellular motility driven by assembly and disassembly of actin filaments." Cell **112**(4): 453-65.

Pollard, T. D. and W. C. Earnshaw (2002). Cell biology. Philadelphia, Saunders.

Roth, T. L., J. Howard, et al. (1994). "Zona pellucida piercing enhances zona penetration by spermatozoa from normospermic and teratospermic domestic cats." J Androl **15**(2): 165-73.

Schaefer, A. W., N. Kabir, et al. (2002). "Filopodia and actin arcs guide the assembly and transport of two populations of microtubules with unique dynamic parameters in neuronal growth cones." J Cell Biol **158**(1): 139-52.

Schrlau, M., Erica Falls, Barry Ziober, and Haim Bar (2007). "Carbon nanopipettes for cell probes and intracellular injection." Nanotechnology **19**: 1-4.

Sheetz, M. P. and J. Dai (1996). "Modulation of membrane dynamics and cell motility by membrane tension." Trends Cell Biol **6**(3): 85-9.

Smith, A. E., K. E. Moxham, et al. (2000). "Wall material properties of yeast cells. Part II. Analysis." Chemical Engineering Science **55**(11): 2043-2053.

Stamenovic, D., S. M. Mijailovich, et al. (2002). "Cell prestress. II. Contribution of microtubules." Am J Physiol Cell Physiol **282**(3): C617-24.

Takamatsu, H. and N. Kumagae (2002). "Survival of biological cells deformed in a narrow gap." J Biomech Eng **124**(6): 780-3.

Timoshenko, S., S. Woinowsky-Krieger, et al. (1959). Theory of plates and shells. New York, McGraw-Hill**:** 580 p.

Tuszynski, J. A., T. Luchko, et al. (2005). "Anisotropic elastic properties of microtubules." Eur Phys J E Soft Matter **17**(1): 29-35.

Venier, P., A. C. Maggs, et al. (1994). "Analysis of microtubule rigidity using hydrodynamic flow and thermal fluctuations." J Biol Chem **269**(18): 13353-60.

Volokh, K. Y. (2007). "Prediction of arterial failure based on a microstructural bi-layer fiber-matrix model with softening." J Biomech.

Xing, M., N. Pan, et al. (2007). "Skin friction blistering: computer model." Skin Res Technol **13**(3): 310-6.

Yu, S., F. Son, et al. (2006). "Acrylamide alters cytoskeletal protein level in rat sciatic nerves." Neurochem Res **31**(10): 1197-204.

Appendix A: ANSYS code to determine the areal strain in a neuronal membrane when a protein filament acts against the membrane

```
! This code calculates the maximum deformation and strain of a
! transversely isotropic, circular membrane that is clamped at its edge
! and subjected to a stress at its center. The elements chosen in which
! to apply the load are determined by the number of elements in the
! model, and the contact area of the protein filament that is acting on
! the membrane.  The contact stress on the membrane is equal to the
! force the protein filament can exert onto the membrane divided by the
! cross sectional area of the protein filament


/CLEAR,NOSTART

! Define parameters for simulation
a = 250E-6              ! Radius of membrane (mm)
f = 8.01E-12            ! Force to exert on membrane (N)
r = 4E-6                ! Radius of filament acting on membrane (mm)
s = f/(3.1416*r*r)      ! Normal contact stress on membrane due to
                          protein force (MPa)
t = 4.5E-6              ! Thickness of the membrane (mm)
n = 1001                ! Number of nodes
yx = 128                ! Young's modulus of membrane (in-plane) (MPa)
yz = 128                ! Young's modulus of membrane (in-plane) (MPa)
yy = 128                ! Young's modulus of membrane (through-plane)
                          (MPa)
gxz = yx/100            ! Shear Modulus (in-plane) (MPa)
gxy = yy/3              ! Shear Modulus (through-plane) (MPa)
gyz = yz/3              ! Shear Modulus (through-plane) (MPa)
vxz = 0.49              ! Poisson's ratio (in-plane)
vxy = 0.49              ! Poisson's ratio (in-plane with through-plane)
vyz = 0.49              ! Poisson's ratio (in-plane with through-plane)


! Define element type
/PREP7
ET,1,SHELL208           ! Set element type, SHELL208
SECT,1,SHELL            ! Set element type, shell
SECD,t                  ! Set membrane thickness
CSYS,1                  ! Define coordinate system, cylindrical
KEYOPT,1,8,2            ! Store information for top, middle, and bottom
                          surfaces of membrane

! Set Young's modulus of membrane, in and out of plane
MP,EX,1,yx
MP,EZ,1,yz
MP,EY,1,yy

! Set Poisson's ratio of membrane, in and out of plane
MP,NUXZ,1,vxz
MP,NUXY,1,vxy
```

```
MP,NUYZ,1,vyz

! Set shear modulus of membrane, in and out of plane
MP,GXZ,1,gxz
MP,GXY,1,gxy
MP,GYZ,1,gyz

! Create nodes
N,1
N,n,a
FILL

! Create elements between nodes
E,1,2
EGEN,n-1,1,1
FINISH

! Set parameters for analysis
/SOLU
ANTYPE,STATIC           ! Static analysis
NLGEOM,ON               ! Include large-deflection effects
SSTIF,ON                ! Include stress stiffening option
NSEL,S,LOC,X,0          ! Activate node at x=0
DSYM,SYMM,X             ! Symmetric boundary conditions at active node
                        (x=0)
NSEL,ALL                ! Activate all nodes

! Set boundary conditions (one must always be commented out)
!D,n,ALL,0              ! Clamped-Immoveable (BC1)
D,n,UY,0,,,,ROTZ        ! Clamped-Moveable (BC2)

! Apply normal contact stress to membrane
ESEL,S,ELEM,,1,(n-1)*r/a,1
SFE,ALL,1,PRES,0,s      ! Select elements to apply pressure
ESEL,ALL
SOLVE

! Post processing
/POST1
SHELL,MID               ! Specify location on membrane to store in
                        element table (BOT,MID,TOP)
*GET,UY,NODE,1,U,Y      ! Get max displacement
ETABLE,STRAINX,EPEL,X   ! Get strain in x (radial) direction

PLETAB,STRAINX,NOAV     ! Plot strain in x direction
ETABLE,STRAINZ,EPEL,Z   ! Get strain in z (theta) direction

*STATUS,PARM            ! Output parameters
```

Appendix B: MATLAB code to create a binary image of an aspirated liposome

```
% This code is to be used before 'AfterPaint' to enhance the quality of
% the image of the aspirated liposome.  After running this code on the
% original image, the resulting image should be saved as a .bmp, and
% areas of the image not representing the liposome should be removed in
% Paint Shop Pro.  The code 'AfterPaint' can then be run on the cleaned
% up image.

clc
clear all
close all
imtool close all

I = imread('Lip2_Out-6.tif');
imshow(I)

% crop image so that only liposome is included
I1 = imcrop;

% create grayscale image
I2 = rgb2gray(I1);

% enhance image contrast
I3 = histeq(I2);
se = strel('disk',5);
I4 = imsubtract(imadd(I3,imtophat(I3,se)),imbothat(I3,se));
figure, imshow(I4)

% create binary image
level = 0.3
bw = im2bw(I4,level);
bw = bwselect;
figure, imshow(bw)
```

Appendix C: MATLAB code to determine diameter and length of an aspirated liposome from the binary image of the liposome

```
% This code is to be used with 'ProcessImage' to determine the
% diameter an aspirated liposome and the length of the aspirated
% liposome inside the holding pipette.  The input image is a
% binary image of the aspirated liposome after it has been cleaned
% using Paint Shop Pro.

clc
clear all
close all
imtool close all

I = imread('Lip2_Out-6_PostProcess.bmp');
imshow(I)

% determine the size of the image
[rows, columns] = size(I)

% determine the distances between the outermost edges of the liposome
top=rows;
bottom=1;
left=columns;
right=1;

for r = 1:rows
    for c = 1:columns
        if (I(r,c)~=255)
            if(r<top)
                top=r;
            end
            if(r>bottom)
                bottom=r;
            end
            if(c<left)
                left=c;
            end
            if(c>right)
                right=c;
            end
        end
    end
end

% determine the diameter of liposome and length of liposome inside the
% pipette
D = right-left
L = bottom-top-D

% convert pixels to microns (40x objective)
D_micron = D*(200/1128)
L_micron = L*(200/1128)
```

Appendix D: MATLAB code to determine the surface area and bending energy of the pre-probed and probed liposomes

```
% This code is to determine the surface area and bending energy of an
aspirated liposome before probing of the liposome with an injection
pipette.

clear all
clc

% fixed parameters
rp = 7.5e-6;              % inner radius of holding pipette (m)
t = 5e-9;                 % thickness of the bilayer (m)
pi = 3.1416;              % pi
Ka = 0.067;               % area expansion modulus of liposome (N/m)
Kr = Ka/4;                % relative expansivity between bilayers (N/m)
kb = (Ka*(t^2))/24;       % bending modulus of the bilayer (Nm)

% variable parameters
l = 7.10e-6;              % length of liposome inside pipette (m)
r = 21.99e-6;             % outer radius of liposome outside pipette (m)
q = acos(rp/l)/sqrt(1-(rp/l)^2);  % constant in determining surface
                                    area of spheroidal cap inside
                                    holding pipette

% compute surface area (SA) and bending energy (BE) of aspirated
liposome before manipulation with injection pipette

if l > rp

% SA of outer surface of spherical portion outside pipette
SAso = (4*pi*r^2);
% SA of inner surface of spherical portion outside pipette
SAsi = (4*pi*(r-t)^2);
% SA of neutral surface of spherical portion outside pipette
SAsn = (4*pi*(r-(t/2))^2);


% SA of outer surface of cylindrical portion inside pipette
SAco = (2*pi*rp*l);
% SA of inner surface of cylindrical portion inside pipette
SAci = (2*pi*(rp-t)*l);
% SA of neurtal surface of cylindrical portion inside pipette
SAcn = (2*pi*(rp-(t/2))*l);

% SA of outer surface of spherical cap inside pipette
SAscapo = (2*pi*rp^2);
% SA of inner surface of spherical cap inside pipette
SAscapi = (2*pi*(rp-t)^2);
% SA of neutral surface of spherical cap inside pipette
SAscapn = (2*pi*(rp-(t/2))^2);
```

```
% SA of entrance to holding pipette
SAst = pi*(rp^2);
% SA of neutral surface of liposome
SAn = SAsn + SAcn + SAscapn - SAst

% BE of spherical portion outside pipette
BEs = ((Kr*(SAso-SAsi)^2)/(2*SAsn))+ (8*pi*kb);

% BE of cylindrical portion inside pipette
BEc = ((Kr*(SAco-SAci)^2)/(2*SAcn))+ ((kb*pi*l)/(rp-(t/2)));

% BE of spherical cap inside pipette
BEscap = ((Kr*(SAscapo-SAscapi)^2)/(4*SAscapn))+ (4*pi*kb);


% BE of aspirated liposome
BE = BEs + BEc + BEscap

end

if l == rp

% SA of outer surface of spherical portion outside pipette
SAso = (4*pi*r^2);
% SA of inner surface of spherical portion outside pipette
SAsi = (4*pi*(r-t)^2);
% SA of neutral surface of spherical portion outside pipette
SAsn = (4*pi*(r-(t/2))^2);

% SA of outer surface of spherical cap inside pipette
SAscapo = (2*pi*rp^2);
% SA of inner surface of spherical cap inside pipette
SAscapi = (2*pi*(rp-t)^2);
% SA of neutral surface of spherical cap inside pipette
SAscapn = (2*pi*(rp-(t/2))^2);

% SA of entrance to holding pipette
SAst = pi*(rp^2);

% SA of neutral surface of liposome
SAn = SAsn + SAscapn -SAst

% BE of spherical portion outside pipette
BEs = ((Kr*(SAso-SAsi)^2)/(2*SAsn))+ (8*pi*kb);

% BE of spherical cap inside pipette
BEscap = ((Kr*(SAscapo-SAscapi)^2)/(4*SAscapn))+ (4*pi*kb);

% BE of aspirated liposome
BE = BEs + BEscap

end

if l < rp

% SA of outer surface of spherical portion outside pipette
SAso = (4*pi*r^2);
```

```
% SA of inner surface of spherical portion outside pipette
SAsi = (4*pi*(r-t)^2);
% SA of neutral surface of spherical portion outside pipette
SAsn = (4*pi*(r-(t/2))^2);


% SA of outer surface of spheroidal cap inside pipette
SAocapo = (pi*(rp^2+rp*l*q*(1-(((rp^2-rp^2)/6*rp^2)*q^2))*(1-
          ((3*rp^2+10*rp^2)/56*rp^2)*q)));
% SA of inner surface of spheroidal cap inside pipette
SAocapi = (pi*((rp-t)^2+(rp-t)*(l-t)*q*(1-((((rp-t)^2-(rp-
          t)^2)/6*(rp-t)^2)*q^2))*(1-((3*(rp-t)^2+10*(rp-
          t)^2)/56*(rp-t)^2)*q)));
% SA of neutral surface of spheroidal cap inside pipette
SAocapn = (pi*((rp-t/2)^2+(rp-t/2)*(l-t/2)*q*(1-((((rp-t/2)^2-(rp-
          t/2)^2)/6*(rp-t/2)^2)*q^2))*(1-((3*(rp-t/2)^2+10*(rp-
          t/2)^2)/56*(rp-t/2)^2)*q)));

% SA of entrance to holding pipette
SAst = pi*(rp^2);

% SA of neutral surface of liposome
SAn = SAsn + SAocapn - SAst

% BE of spherical portion outside pipette
BEs = ((Kr*(SAso-SAsi)^2)/(2*SAsn))+ (8*pi*kb);

% BE of spheroidal cap inside pipette
BEocap = ((Kr*(SAocapo-SAocapi)^2)/(2*SAocapn))+
         ((kb/2)*SAocapn*((1/rp)+(1/l))^2);

% BE of aspirated liposome
BE = BEs + BEocap

end
```

```
% This code is to determine the surface area and bending energy of an
aspirated liposome during probing of the liposome with an injection
pipette.

clear all
clc

% fixed parameters
rp = 7.5e-6;              % inner radius of holding pipette (m)
t = 5e-9;                 % thickness of the bilayer (m)
pi = 3.1416;              % pi
Ka = 0.067;               % area expansion modulus of liposome (N/m)
Kr = Ka/4;                % relative expansivity between bilayers (N/m)
kb = (Ka*(t^2))/24;       % bending modulus of the bilayer (Nm)
x1 = 436e-9;              % increase in radius or injection pipette at
                            li = 10e-6 (taper = 2.5 degrees) (m)
x2 = 872e-9;              % increase in radius or injection pipette at
                            li = 20e-6 (taper = 2.5 degrees) (m)

% variable parameters
ri1 = 100e-9;            % outer radius of injection pipette at tip (m)
ri2 = ri1+x2;            % outer radius of injection pipette at
                           insertion distance (m)
i = 3.605e-9;            % integral of curvature of injection pipette
                           over surface area (Mathematica) (m)
li = 20e-6;              % length injection pipette inserted into
                           membrane (m)
l = 4.25e-6;             % length of liposome in holding pipette (m)
w = 25.18e-6;            % width/2 of liposome outside pipette (m)
h = 23.41e-6;            % height/2 of liposome outside pipette (m)
p = acos(w/h)/sqrt(1-(w/h)^2);   % constant in determining surface area
                                   of spheroid outside holding pipette
q = acos(rp/l)/sqrt(1-(rp/l)^2); % constant in determining surface area
                                   of spheroidal cap in holding pipette


% compute surface area (SA) and bending energy (BE) of aspirated
liposome after it is poked with injection pipette

if l > rp

% SA of outer surface of spheroidal portion outside pipette
SAoblateo = (2*pi*(w^2+w*h*p*(1-(((w^2-w^2)/6*w^2)*p^2))*(1-
            ((3*w^2+10*w^2)/56*w^2)*p)));
% SA of inner surface of spheroidal portion outside pipette
SAoblatei = (2*pi*((w-t)^2+(w-t)*(h-t)*p*(1-((((w-t)^2-(w-t)^2)/6*(w-
             t)^2)*p^2))*(1-((3*(w-t)^2+10*(w-t)^2)/56*(w-t)^2)*p)));
% SA of neutral surface of spheroidal portion outside pipette
SAoblaten = (2*pi*((w-t/2)^2+(w-t/2)*(h-t/2)*p*(1-((((w-t/2)^2-(w-
            t/2)^2)/6*(w-t/2)^2)*p^2))*(1-((3*(w-t/2)^2+10*(w-
            t/2)^2)/56*(w-t/2)^2)*p)));
```

```
% SA of outer surface of cylindrical portion inside pipette
SAco = (2*pi*rp*l);
% SA of inner surface of cylindrical portion inside pipette
SAci = (2*pi*(rp-t)*l);
% SA of neurtal surface of cylindrical portion inside pipette
SAcn = (2*pi*(rp-(t/2))*l);

% SA of outer surface of spherical cap inside pipette
SAscapo = (2*pi*rp^2);
% SA of inner surface of spherical cap inside pipette
SAscapi = (2*pi*(rp-t)^2);
% SA of neutral surface of spherical cap inside pipette
SAscapn = (2*pi*(rp-(t/2))^2);

% SA of entrance to holding pipette
SAst = pi*(rp^2);

% SA at insertion distance along injection pipette
SAir2 = pi*ri2^2;

% SA of inner surface of conical indentation due to injection pipette
SAii = pi*((ri1+t)+(ri2+t))*sqrt(((ri1+t)-
      (ri2+t))^2+(li^2))+(pi*(ri1+t)^2);
% SA of outer surface of conical indentation due to injection pipette
SAio = pi*(ri1+ri2)*sqrt((ri1-ri2)^2+(li^2))+(pi*ri1^2);
% SA of neutral surface of conical indentation due to injection pipette
SAin = pi*((ri1+(t/2))+(ri2+(t/2)))*sqrt(((ri1+(t/2))-
      (ri2+(t/2)))^2+(li^2))+(pi*(ri1+(t/2))^2);

% SA of neutral surface of walls of injection pipette
SAwalls = pi*((ri1+(t/2))+(ri2+(t/2)))*sqrt(((ri1+(t/2))-
         (ri2+(t/2)))^2+(li^2));

% SA of neutral surface of liposome
SAn = SAoblaten + SAcn + SAscapn - SAst - SAir2 + SAin

% BE of spheroidal portion outside pipette
BEoblate = ((Kr*(SAoblateo-SAoblatei)^2)/(2*SAoblaten))+
           ((kb/2)*SAoblaten*((1/w)+(1/h))^2);

% BE of cylindrical portion inside pipette
BEc = ((Kr*(SAco-SAci)^2)/(2*SAcn))+ ((kb*pi*l)/(rp-(t/2)));

% BE of spherical cap inside pipette
BEscap = ((Kr*(SAscapo-SAscapi)^2)/(4*SAscapn))+ (4*pi*kb);

% BE of conical indentation due to injection pipette
BEi = ((Kr*(SAii-SAio)^2)/(2*SAin))+ (kb*pi*i);

% BE of probed liposome
BE = BEoblate + BEc + BEscap + BEi

end
```

```
if l == rp

% SA of outer surface of spheroidal portion outside pipette
SAoblateo = (2*pi*(w^2+w*h*p*(1-(((w^2-w^2)/6*w^2)*p^2))*(1-
            ((3*w^2+10*w^2)/56*w^2)*p)));
% SA of inner surface of spheroidal portion outside pipette
SAoblatei = (2*pi*((w-t)^2+(w-t)*(h-t)*p*(1-((((w-t)^2-(w-
             t)^2)/6*(w-t)^2)*p^2))*(1-((3*(w-t)^2+10*(w-
             t)^2)/56*(w-t)^2)*p)));
% SA of neutral surface of spheroidal portion outside pipette
SAoblaten = (2*pi*((w-t/2)^2+(w-t/2)*(h-t/2)*p*(1-((((w-t/2)^2-(w-
            t/2)^2)/6*(w-t/2)^2)*p^2))*(1-((3*(w-t/2)^2+10*(w-
            t/2)^2)/56*(w-t/2)^2)*p)));

% SA of outer surface of spherical cap inside pipette
SAscapo = (2*pi*rp^2);
% SA of inner surface of spherical cap inside pipette
SAscapi = (2*pi*(rp-t)^2);
% SA of neutral surface of spherical cap inside pipette
SAscapn = (2*pi*(rp-(t/2))^2);

% SA of entrance to holding pipette
SAst = pi*(rp^2);

% SA at insertion distance along injection pipette
SAir2 = pi*ri2^2;

% SA of inner surface of conical indentation due to injection pipette
SAii = pi*((ri1+t)+(ri2+t))*sqrt(((ri1+t)-
      (ri2+t))^2+(li^2))+(pi*(ri1+t)^2);
% SA of outer surface of conical indentation due to injection pipette
SAio = pi*(ri1+ri2)*sqrt((ri1-ri2)^2+(li^2))+(pi*ri1^2);
% SA of neutral surface of conical indentation due to injection pipette
SAin = pi*((ri1+(t/2))+(ri2+(t/2)))*sqrt(((ri1+(t/2))-
      (ri2+(t/2)))^2+(li^2))+(pi*(ri1+(t/2))^2);

% SA of neutral surface of walls of injection pipette
SAwalls = pi*((ri1+(t/2))+(ri2+(t/2)))*sqrt(((ri1+(t/2))-
         (ri2+(t/2)))^2+(li^2));

% SA of neutral surface of liposome
SAn = SAoblaten + SAscapn - SAst - SAir2 + SAin

% BE of spheroidal portion outside pipette
BEoblate = ((Kr*(SAoblateo-SAoblatei)^2)/(2*SAoblaten))+
           ((kb/2)*SAoblaten*((1/w)+(1/h))^2);

% BE of spherical cap inside pipette
BEscap = ((Kr*(SAscapo-SAscapi)^2)/(4*SAscapn))+ (4*pi*kb);

% BE of conical indentation due to injection pipette
BEi = ((Kr*(SAii-SAio)^2)/(2*SAin))+ (kb*pi*i);

% BE of poked liposome
BE = BEoblate + BEscap +BEi

end
```

```
if l < rp


% SA of outer surface of spheroidal portion outside pipette
SAoblateo = (2*pi*(w^2+w*h*p*(1-(((w^2-w^2)/6*w^2)*p^2))*(1-
            ((3*w^2+10*w^2)/56*w^2)*p)));
% SA of inner surface of spheroidal portion outside pipette
SAoblatei = (2*pi*((w-t)^2+(w-t)*(h-t)*p*(1-((((w-t)^2-(w-
             t)^2)/6*(w-t)^2)*p^2))*(1-((3*(w-t)^2+10*(w-
             t)^2)/56*(w-t)^2)*p)));
% SA of neutral surface of spheroidal portion outside pipette
SAoblaten = (2*pi*((w-t/2)^2+(w-t/2)*(h-t/2)*p*(1-((((w-t/2)^2-(w-
            t/2)^2)/6*(w-t/2)^2)*p^2))*(1-((3*(w-t/2)^2+10*(w-
            t/2)^2)/56*(w-t/2)^2)*p)));

% SA of outer surface of spheroidal cap inside pipette
SAocapo = (pi*(rp^2+rp*l*q*(1-(((rp^2-rp^2)/6*rp^2)*q^2))*(1-
          ((3*rp^2+10*rp^2)/56*rp^2)*q)));
% SA of inner surface of spheroidal cap inside pipette
SAocapi = (pi*((rp-t)^2+(rp-t)*(l-t)*q*(1-((((rp-t)^2-(rp-
          t)^2)/6*(rp-t)^2)*q^2))*(1-((3*(rp-t)^2+10*(rp-
          t)^2)/56*(rp-t)^2)*q)));
% SA of neutral surface of spheroidal cap inside pipette
SAocapn = (pi*((rp-t/2)^2+(rp-t/2)*(l-t/2)*q*(1-((((rp-t/2)^2-(rp-
          t/2)^2)/6*(rp-t/2)^2)*q^2))*(1-((3*(rp-t/2)^2+10*(rp-
          t/2)^2)/56*(rp-t/2)^2)*q)));

% SA of entrance to holding pipette
SAst = pi*(rp^2);

% SA at insertion distance along injection pipette
SAir2 = pi*ri2^2;

% SA of inner surface of conical indentation due to injection pipette
SAii = pi*((ri1+t)+(ri2+t))*sqrt(((ri1+t)-
      (ri2+t))^2+(li^2))+(pi*(ri1+t)^2);
% SA of outer surface of conical indentation due to injection pipette
SAio = pi*(ri1+ri2)*sqrt((ri1-ri2)^2+(li^2))+(pi*ri1^2);
% SA of neutral surface of conical indentation due to injection pipette
SAin = pi*((ri1+(t/2))+(ri2+(t/2)))*sqrt(((ri1+(t/2))-
      (ri2+(t/2)))^2+(li^2))+(pi*(ri1+(t/2))^2);

% SA of neutral surface of walls of injection pipette
SAwalls = pi*((ri1+(t/2))+(ri2+(t/2)))*sqrt(((ri1+(t/2))-
         (ri2+(t/2)))^2+(li^2));

% SA of neutral surface of liposome
SAn = SAoblaten + SAocapn - SAst - SAir2 + SAin

% BE of spheroidal portion outside pipette
BEoblate = ((Kr*(SAoblateo-SAoblatei)^2)/(2*SAoblaten))+
           ((kb/2)*SAoblaten*((1/w)+(1/h))^2);

% BE of spheroidal cap inside pipette
BEocap = ((Kr*(SAocapo-SAocapi)^2)/(2*SAocapn))+
         ((kb/2)*SAocapn*((1/rp)+(1/l))^2);
```

```
% BE of conical indentation due to injection pipette
BEi = ((Kr*(SAio-SAii)^2)/(2*SAin))+ (kb*pi*i);

% BE of aspirated liposome
BE = BEoblate + BEocap + BEi

end
```

Appendix E: ANSYS code to determine the deformation and strain in an aspirated, probed liposome

```
! This code calculates the deformation and strain of an aspirated
! liposome that is being acted on by a micro or nanopipette.
! The liposome and pipette geometries are entered by the user, and the
! force that is required for membrane penetration is estimated.  The
! "correct" penetration force results in a membrane areal strain of ~3-
! 4%.


/CLEAR,NOSTART

pi = 3.1416                          ! pi
n = 20000                            ! total number of nodes
rp = 7.5E-3                          ! radius of holding pipette (mm)
l = 45E-3                            ! length of liposome inside the
                                       holding pipette (mm)
r = 25E-3                            ! radius of liposome outside the
                                       holding pipette (mm)
t = 5E-6                             ! thickness of membrane (mm)
P = 0                                ! aspiration pressure (MPa)
f = 25E-12                           ! force of injection pipette (N)
ip = 1.000E-3                        ! inner radius of the injection
                                       pipette (mm)
op = 2.000E-3                        ! outer radius of the injection
                                       pipette (mm)
op_area = (pi*op*op)                 ! outer cross sectional area of
                                       injection pipette (mm2)
ip_area = (pi*ip*ip)                 ! inner cross sectional area of
                                       injection pipette (mm2)
tot_area = op_area-ip_area           ! cross sectional area of
                                       injection pipette (mm2)
s = f/tot_area                       ! contact stress acting against
                                       membrane (MPa)
yx = 15                              ! Young's modulus of membrane
                                       (in-plane) (MPa)
yz = 15                              ! Young's modulus of membrane
                                       (in-plane) (MPa)
yy = 15                              ! Young's modulus of membrane
                                       (through-plane) (MPa)
gxz = yx/100                         ! shear modulus (in-plane)(MPa)
gxy = yy/3                           ! shear modulus (through-plane)
                                      (MPa)
gyz = yz/3                           ! shear modulus (through-plane)
                                      (MPa)
vxz = 0.49                           ! Poisson's ratio (in-plane)
vxy = 0.49                           ! Poisson's ratio (in-plane
                                       with through-plane)
vyz = 0.49                           ! Poisson's ratio (in-plane
                                       with through-plane)
c = (rp*pi)/2                        ! length of curved section of
                                       liposome in pipette (mm)
```

```
d = l                                   ! length of liposome inside pipette
                                          (mm)
e = (r*pi)/2                            ! approximate length of half of the
                                          liposome outside pipette
g = c+d+e+e                             ! approximate total length of
                                          liposome

! set pre-processing parameters
/PREP7

! define element type
ET,1,SHELL208                 ! set element type, SHELL208
SECT,1,SHELL                  ! set element type, shell
SECD,t                        ! set liposome thickness
KEYOPT,1,8,2                  ! store data for each layer in membrane

! set material properties of liposome membrane
MP,EX,1,yx
MP,EZ,1,yz
MP,EY,1,yy
MP,NUXZ,1,vxz
MP,NUXY,1,vxy
MP,NUYZ,1,vyz
MP,GXZ,1,gxz
MP,GXY,1,gxy
MP,GYZ,1,gyz

! create ratios for equally spaced nodes
u = ((c/g)*n)/2
v = (c/g)*n
w = ((c+d)/g)*n
x = ((c+d+(e/2))/g)*n
y = ((c+d+e)/g)*n
z = ((c+d+e+(e/2))/g)*n

! create nodes in shape of aspirated liposome
N,1,0,h,0                                   ! node 1
N,u,rp*cos(pi/4),rp*sin(pi/4),0             ! node 2
N,v,rp,0,0                                  ! node 3
N,w,rp,-l,0                                 ! node 4
FILL
QUAD,1,u,v
N,w+1,0,-l,0                                ! node 5
N,x,r*cos(pi/4),-l-(r-r*sin(pi/4)),0        ! node 6
N,y,r,-l-r,0                                ! node 7
QUAD,w+1,x,y
NDELE,w+1,w+(w/5),1
N,w+((w/5)+1)/2,rp+(.01*rp),-l-(.03*l),0    ! node 8
QUAD,w,w+((w/5)+1)/2,w+(w/5)+1
N,z,r*cos(pi/4),-l-r-(r*sin(pi/4)),0        ! node 9
N,n,0,-l-2*r,0                              ! node 10
QUAD,y,z,n

! create elements between nodes
E,1,2
EGEN,n-1,1,1
```

```
! determine elements in which injection pipette acts
es = e/(n-y-1)          ! length of element
a = ip/es               ! number of elements within inner radius of
                          injection pipette
b = op/es               ! number of elements within inner radius of
                          injection pipette

! set parameters for analysis
/SOLU

SOLCONTROL,ON
CNVTOL,STAT
ANTYPE,STATIC                       ! static analysis
NLGEOM,ON                           ! include large-deflection effects
SSTIF,ON                            ! include stress stiffening option
NSEL,S,LOC,X,0                      ! activate nodes at x=0
DSYM,SYMM,X                         ! symmetric boundary conditions at
active nodes (x=0)
NSEL,ALL                            ! activate all nodes

! set boundary conditions
NSEL,S,NODE,,w+1,w+(w/5)+1
D,ALL,UY,0                  ! membrane in contact with outside of
                              holding pipette is constrained in the Y
                              direction
NSEL,ALL
NSEL,S,NODE,,v,w
D,ALL,UZ,0,,,UX,ROTY,ROTZ,ROTX      ! membrane inside holding pipette
                                      wall is fully constrained
NSEL,ALL

! apply aspiration pressure to liposome
NSEL,S,NODE,,1,v,1
SF,ALL,PRES,-P
NSEL,ALL

! apply normal contact stress to liposome
ESEL,S,ELEM,,n-b-1,n-a,1      ! select elements in which stress acts
SFE,ALL,1,PRES,0,s            ! apply stress to selected elements
ESEL,ALL

SOLVE                                   ! solve simulation

! set information to extract from analysis
/POST1

SHELL,TOP                   ! specify location on membrane to
                              store in element table

! get/plot elastic strains
ETABLE,STRAINX,EPEL,X         ! get strain in x (radial) direction
ETABLE,STRAINZ,EPEL,Z         ! get strain in z (theta) direction

PLETAB,STRAINX,NOAV           ! plot strain in x direction


FINISH
```

Appendix F: 1D Strain Calculation Showing Strain Independent of Coordinate System

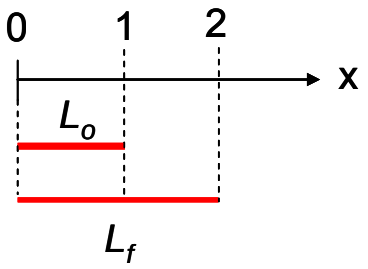

$$strain = \frac{L_f - L_o}{L_o}$$

tension

= +1

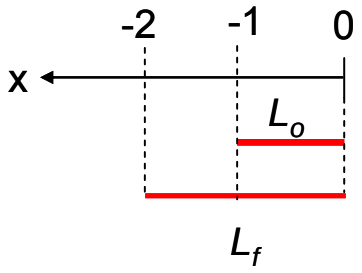

$$strain = \frac{L_f - L_o}{L_o}$$

tension

= +1

strain is independent of coordinate system

Vita

Educational Background:

Graduate:

Drexel University, Philadelphia, PA
- Anticipated date of graduation: Aug. 2008
- Degree: Ph.D. Mechanical Engineering

Undergraduate:

Drexel University, Philadelphia, PA
- Graduation date: June 2004
- Degree: B.S. Mechanical Engineering

Honors and Awards:
- National Science Foundation Graduate Research Fellow, Sept. 2005-Sept. 2008.
- Awarded Student Research Award at Drexel University's Honors Day, Feb. 2008.

Research Experiences*:*

Drexel University, Philadelphia, PA
Cell and Proteins Mechanics Laboratory
Advisor: Dr. Bradley Layton and Dr. Selcuk Guceri
Sept. 2004- Sept. 2008

National Nanotechnology Laboratories, Lecce, Italy
Soft Matter Nanotechnologies Laboratory
Advisor: Dr. Dario Pisignano
June 2007and July 2007

Baylor College of Medicine, Houston, TX
Department of Medicine
Advisor: Dr. Aladin Boriek
July 2004- Sept. 2004

Journal Papers*:*

K.B. Allen, Sasoglu F.M., Layton B.E., "Cytoskeleton-Membrane Interactions in Neuronal Growth Cones: A Finite Element Analysis Study*" in press ASME Journal of Biomechanics*.

K.B. Allen, Layton B.E., "Determination of the Mechanical Properties of Liposomes: A Precursor to the Numerical Quantification of the Forces Imposed by Micro and Nanopipettes during Liposome Manipulation*" in preparation for Biophysical Journal*.

K.B. Allen, Layton B.E., "Determination of the Forces Imposed by Micro and Nanopipettes during Liposome Manipulation*" in preparation for Biophysical Journal*.

K.B. Allen, Sasoglu F.M., Impagnatiello, T., Biasco A., Layton B.E., Pisignano D., Cingolani R., "Microcontact Printing of Fibronectin Channels for Biosensing Applications" *in preparation for Langmuir*.

B.E. Layton, Sullivan S., **Allen K.B**., Lynch B., Jamieson B, "Evaluation of Red Blood Cell Sorting with a Multi-Bed Microfabricated Filter" *submitted to Lab on a Chip*.

F.M. Sasoglu, Bohl A., **Allen K.B**., Layton B.E., "Parallel Nanonewton Force Measurement Using an Optical Microscope and Micromanipulator" *in press Computer Methods and Programs in Biomedicine*.

I. Chu, Fernandez C., **Allen K.B.**, Lopez M.A., Lu R., Hubmayr R.D., Boriek A.M., "Diaphragm Muscle Shortening Alters Kinematics, Surface Area and Volume Displacement of Lower Rib Cage in Dogs", *in preparation for the American Journal of Physiology*.